NORTHWESTERN UNIVERSITY

Regulation of Autonomous Pacemaking and High Frequency Firing in the Basal Ganglia

A DISSERTATION

SUBMITTED TO THE GRADUATE SCHOOL IN
PARTIAL FULFILLMENT OF THE REQUIREMENTS

for the degree

DOCTOR OF PHILOSOPHY

Field of Neuroscience

By

Jeffrey Neil Mercer

EVANSTON, ILLINOIS

December 2006

© Copyright by Jeffrey Neil Mercer 2006

All Rights Reserved

ABSTRACT

Regulation of autonomous pacemaking and high frequency firing in the basal ganglia

Jeffrey Neil Mercer

Following dopaminergic denervation in Parkinson's Disease, firing patterns in several basal ganglia neuron populations are pathologically altered. In the globus pallidus (GP), this manifests as a loss of autonomous, rhythmic, high–frequency pacemaking and an appearance of correlated, oscillatory bursting. This oscillatory bursting is best disrupted through high–frequency stimulation of affected nuclei in the basal ganglia. The goal of this research was to understand the intrinsic mechanisms by which the GP and other autonomous pacemakers establish their discharge patterns and how regulation of these mechanisms through electrical, pharmacological and genetic manipulations can alter firing properties. This was accomplished by integrating current–clamp recordings of activity patterns in pacemaking neurons with voltage–clamp recordings isolating important channel types.

By direct, high–frequency stimulation of GP neurons, we demonstrate that they are capable of sustaining high frequency firing during stimulation, suggesting that the therapeutic effect of this technique is a disruption of the pathological discharge pattern, not cessation of firing. Analysis of Na^+ channel biophysics in these neurons identifies a novel resurgent gating mode present only in channels of pacemaking neurons (GP neurons, striatal cholinergic interneurons and dopaminergic neurons). As a result of the unique properties underlying this gating mode, the Na^+ channels in autonomous pacemakers recover more rapidly from the previous spike, increasing availability during the interspike interval and increasing the depolarizing current that drives the membrane towards spike threshold. Without this gating mode, the ability of GP neurons to fire autonomously and at high frequencies is significantly reduced. Activation of D_2 receptors also affects channel availability

by increasing entry into the slow inactivated state, leading to a reduction in excitability of cholinergic interneurons.

Another channel important for autonomous spiking is the HCN channel, which is responsible for keeping the membrane depolarized enough for Na^+ channels to drive spiking. Following dopamine depletion, HCN channel density is reduced, leading to silencing of GP activity. This reduction in discharge from the GP can potentially have global effects on network connections throughout the basal ganglia.

Acknowledgements

NIH NINDS awards NS 34696, NS 047085, a Picower Foundation grant and the Morris K. Udall Center supported this work. These people made major contributions to the work: Salvador Hernandez–Lopez and C. Savio Chan did the slice recordings for the cholinergic interneuron paper, which were done prior to my training on the technique. Nico Maurice also contributed significantly to this work and the direction of the project. Tatiana Tkatch created all of the necessary primers for the scRT–PCR experiments and Yu Chen performed most of the molecular profiling. Corey McCoy helped with the maintenance of the numerous transgenic and reserpinized animals used during the experiments. Qing Ruan was also helpful in this respect, in addition to learning the sterotaxic surgeries and performing the 6–OHDA and rhodamine bead injections for our DA depletion studies. Sasha Ulrich and Karen Saporito were indispensable in more ways than I can express in this section, including many of the things already mentioned as well as much more. The largest contribution undoubtedly came from C Savio Chan, who not only assisted me with many of the slice experiments and collected his fair share of data along the way, but forced me to expand my understanding from Na^+ channels to the entire basal ganglia and pretty much everything I know about the brain. Without his help, this thesis would have taken 5 more years than it already did and would have been several hundred pages of information on Na^+ channels that nobody in their right mind would have read. I also am very grateful for the feedback I received from my thesis committee throughout my training — CJ Heckman, Mark Bevan and Nelson Spruston. And, of course, Jim Surmeier, who has been a great advisor for these five years and provided me with the necessary support and guidance to complete this training.

Terminology

General

AHP — after–hyperpolarization

AP — action potential

CNS — central nervous system

DBS — deep brain stimulation

F–I — plots of output frequency as a function of injected current

V–I — plots of output voltage as a function of injected current

I–V — plots of output current as a function of injected voltage

IC_{50} — concentration needed for 50% inhibition

PD — Parkinson's Disease

scRT–PCR — single–cell reverse–transcription polymerase chain reaction

Basal ganglia structures

The terminology applied to the divisions of the basal ganglia is particularly confusing because a) the nomenclature is based on the anatomical location and gross appearance of individual nuclei and b) differences in the gross anatomy of primate and rodent brains. For the purposes of this thesis, I will use the commonly used nomenclature for rodents: GP and EP for the external and internal globus pallidus of primates, respectively

CPu — Caudate & Putamen, also referred to as the striatum

MSN — medium spiny neuron

TAN/ChAT cell —tonically active neuron / choline acetyltransferase–expressing cholinergic interneuron

EP — entopeduncular nucleus (GPi in primates)

GP — globus pallidus (GPe in primates)

SNc — substantia nigra pars compacta

SNr — substantia nigra pars reticulata

STN — subthalamic nucleus

Channels

BK — big conductance Ca^{2+}–dependent K^+ channels

SK — small conductance Ca^{2+}–dependent K^+ channels

Cav — voltage–gated Ca^{2+} channel

Cav1.3–/– — neurons lacking Cav1.3 L–type Ca^{2+} channel

HCN — hyperpolarization activated, cyclic nucleotide–gated, nonselective cation channel

Nav — voltage–gated Na^+ channel

SCN8A — gene encoding the Nav1.6 α–subunit

med^{TG} — transgenic mutation of SCN8A, leads to motor endplate disease

Nav1.6–/– — neurons lacking Nav1.6 (*med*^{TG})

Kir/IRK — inward rectifying K^+ channel

Kv — voltage–gated K^+ channel

Signaling molecules/Drugs

6–OHDA — 6–hydroxydopamine, DA analog that kills DA neurons

αMT — α–methyl–tyrosine, inhibits tyrosine hydroxylase (enzyme that synthesizes DA)

calphostin C — PKC inhibitor

cBIMPS — Sp 5,6–DCl–cBIMPS, membrane–permeant cAMP analog.

ChAT — choline acetyltransferase

DA — dopamine, neuromodulator

D_1 family receptor — stimulatory DA receptor family (includes D_1 and D_5)

D_2 family receptor — inhibitory DA receptor family (includes D_2, D_3 and D4)

Quinpirole — selective D_2 receptor agonist

NPA — (r)–(–)–apomorphine hydrochloride, selective D_2 receptor agonist

Sulpiride — (s)–(–)–sulpiride, selective D_2 receptor antagonist

DAG — diacylglycerol

ENK — enkephalin, endogenous opioid

GABA — γ–amino butyric acid, inhibitory signaling molecule

- $GABA_A$ — ionotropic GABA receptor
- $GABA_B$ — metabotropic GABA receptor
- GAD_{67} — 67 kD form of glutamatic acid decarboxylase, synthesizes GABA

$G_{\beta\gamma}$ — inhibitory G–protein subunit

- βark–Cp — β–adrenergic receptor kinase 1 c–terminal peptide, scavenges $G_{\beta\gamma}$–subunits

IP_3 — inositol triphosphate

Mibefradil — modestly selective T–type Ca^{2+} channel blocker

*p*CPA — DL–*p*–chlorophenylalanine, selective serotonin depleting molecule

PKC — protein kinase C

- OAG — 1–oleoyl–2–acetyl–sn–glycerol, PKC activator

PKA — protein kinase A

PLC — phospholipase C

PV — parvalbumin, Ca^{2+} chelating protein

Reserpine — monoamine depleting molecule, used in models of PD

SR 95531 — gabazine, selective $GABA_A$ antogonist

TTX — tetrodotoxin, selective Na^+ channel blocker

Table of Contents

List of Figures

Chapter One

Introduction

Autonomous pacemakers — neurons capable of periodic spiking in the absence of synaptic input — are important participants in a wide array of neural networks in both vertebrates and invertebrates. The basal ganglia are particularly rife with spontaneously active neurons. This network is unique in the brain in that it is dominated by sequential tiers of GABAergic neurons (Oertel and Mugnaini, 1984). Initially, being the only excitatory element within the circuit, the autonomously active glutamatergic subthalamic nucleus (STN) was thought to drive this inhibitory network (Kitai and Kita, 1987), but we now know that the activity in all of the structures downstream of the striatum, namely the globus pallidus (GP), the entopeduncular nucleus (EP) and substantia nigra pars reticulata (SNr), is due to autonomous pacemaking. These output nuclei in turn send their GABAergic projections to the thalamus and premotor areas of the CNS critically involved in motor, associative, cognitive and mnemonic functions (Albin et al., 1989; Bolam et al., 2000).

In addition to the autonomous pacemakers populating the output structures of the basal ganglia, neurons of this type are strategically positioned in two major nuclei processing incoming neural signals. In the striatum, the giant cholinergic interneurons are autonomous pacemakers. Pauses in their activity are thought to generate a learning signal (dopamine, DA) in the striatum. The pause in cholinergic interneuron activity is generated by synaptically accelerated activity in another basal ganglia pacemaker; the DAergic neuron of the substantia nigra pars compacta (SNc) (Graybiel et al., 1994).

Within the basal ganglia, pacemakers can be divided into two broad categories formed upon the basis of the type of pacemaking they exhibit and their intrinsic properties. Principal neurons in the GP, STN and SNr are nominally fast–spiking pacemakers; they maintain high level of ambient

spiking in vivo and capable of discharge rates in excess of 200 Hz for sustained periods. In contrast, striatal cholinergic interneurons and DAergic neurons are slow spiking pacemakers, typically spiking at low frequencies (0.2–10 Hz) both in vitro and in vivo.

Fast–spiking pacemakers

Na^+ currents drive autonomous pacemaking

Autonomous pacemaking in GP and STN neurons relies upon voltage–dependent Na^+ channels (Beurrier et al., 2000; Cooper and Stanford, 2000; Do and Bean, 2003; Chan et al., 2004). That is, application of a Na^+ channel blocker (tetrodotoxin [TTX]) abolishes autonomous activity and subthreshold oscillations in membrane potential. In this respect, these basal ganglia neurons resemble cerebellar Purkinje neurons and deep cerebellar nuclei neurons (Raman et al., 2000; Afshari et al., 2004). Similar to these cerebellar cell types, the Na^+ currents in GP and STN neurons are unusual in that they exhibit 'resurgence' (Raman and Bean, 1997). Resurgent current develops from an open channel block at depolarized membrane potential. While spiking, channels block during the up–stroke and then unblock upon repolarization, leading to a late, inward, depolarizing current. Because blocked channels do not inactivate and recover faster and at more depolarized potentials, the addition of this voltage–dependent state has two effects relevant to autonomous fast spiking. The first effect is to reduce the amount of inactivation during a spike, increasing Na^+ channel availability for the next spiking cycle. The second effect is to reduce the 'depth' of the postspike after–hyperpolarization (AHP), shortening the depolarizing ramp to the next spike. The functional expression of resurgence during the inter–spike interval in GP or STN neurons (and in Purkinje neurons) is enhanced by their reliance upon very rapidly deactivating Kv3 channels for spike repolarization, therefore minimizing outward currents that would slow repolarization of the membrane toward spike threshold. Experimental and computational studies have shown that resurgent current increases excitability and promotes sustained, autonomous pacemaking (Khaliq et al., 2003). Direct examination of this gating mode of Na^+ channels has not been made in EP and SNr neurons; however, based on comparisons of the firing properties of these neurons to their

non–autonomous counterparts, the expression of resurgence is likely to be a general theme for autonomous pacemakers within the basal ganglia.

The molecular mechanism underlying resurgence is something of a mystery. Originally, it was thought to depend upon the Nav1.6 α–subunit because resurgence was largely lost in Purkinje neurons from mice lacking this subunit (Raman et al., 1997). GP and STN neurons express Nav1.6 subunits, in addition to Nav1.1 and Nav1.2 (see below). However, because many neurons that express Nav1.6 channels don't have resurgent current, and heterologously expressed Nav1.6 channels don't express resurgence, these subunits cannot be sufficient. Recent work in STN neurons has shown that Nav1.6 is not necessary either because resurgent current is intact in the mice originally used for the work with Purkinje neurons (Do and Bean, 2004). What else is involved? Although there have been several ideas generated, the most intriguing hypothesis is that the auxiliary β–subunit of the channel is involved (Grieco et al., 2005). Peptides mimicking the cytoplasmic C–terminus of Navβ4 restore a resurgent–like current to Purkinje neurons in which resurgent current has been eliminated by protease treatment, and introduce it in hippocampal pyramidal neurons that normally have no resurgent current. Although this hypothesis is compelling, there are bothersome parallels to the Nav1.6 story. Navβ4 is expressed in neurons that have no resurgence (e.g. striatal medium spiny neurons), and heterologous expression of this subunit with Nav1.2 subunits doesn't produce resurgence (Yu et al., 2003); this suggests that if Navβ4 is necessary, it isn't sufficient.

In most other respects, the Na^+ channel currents in GP and STN neurons are not unusual. The macroscopic voltage–dependence of activation and fast inactivation is similar to regular spiking neurons. The relative magnitude of the persistent current is similar to that found in neurons that aren't autonomously active (0.2–4% of the peak transient current) — which is contrary to the notion that Na^+ channel–dependent pacemaking neurons require an unusually large current of this type. Several lines of evidence suggest that the persistent Na^+ current does not arise from a channel different from the one generating the transient Na^+ current underlying the spike (coming up with an operational definition of the current does not make it 'a distinct entity') (Taddese and Bean,

2002). Simulations of GP neurons show that only a single Na^+ channel, displaying a normal level of persistent current, is necessary to mimic autonomous pacemaking (Chan et al., 2004). That said, both GP and STN neurons co–express several pore–forming α– subunits (Nav1.1, 1.2 and 1.6) and auxiliary β–subunits (Navβ1–4) (see section 1). Genetic deletion of Nav1.6 leads to a preferential loss of resurgent and persistent Na^+ current in STN and Purkinje neurons (Raman et al., 1997; Do and Bean, 2004). Nevertheless, spontaneous and driven activity of STN neurons lacking Nav1.6 is remarkably normal. It is possible that the similarity in discharge properties says as much about intrinsic homeostatic plasticity — that is, up or downregulation of channels that compensate for the loss of Nav1.6 channels — as it does about the normal role of Nav1.6 channels themselves.

Slow inactivation and autonomous pacemaking

Another mechanism by which Na^+ channel heterogeneity could play an important role in pacemaking is in the response to neuromodulators. Both Nav1.1 and Nav1.2 subunits are phosphorylated by both protein kinase A (PKA) and protein kinase C (PKC), leading to enhanced slow inactivation (Cantrell and Catterall, 2001; Carr et al., 2003), whereas Nav1.6 lacks a crucial PKA site, making it refractory to modulation by this protein kinase. Slow inactivation of Na^+ channels could be particularly important to GP and STN neurons, the in vivo discharge rates of which hover in the 50–90 Hz range. High frequency stimulation of STN neurons leads to significant elevations in Na^+ channel slow inactivation, reducing transient, persistent and resurgent currents (Do and Bean, 2003). Thus, enhancement of slow inactivation could compromise their ability to spike in the normal frequency range.

Subcellular localization of Na^+ channels

The roles of dendritic and initial segment or axonal Na^+ channels in pacemaking have yet to be defined. It is clear that channels near the soma (which are preserved when neurons are acutely isolated) are capable of sustaining pacemaking (Do and Bean, 2003). There are also indirect suggestions that the dendrites of GP neurons (and possibly STN neurons) also have a rich

investment of Na^+ channels that are capable of supporting spikes and integration of synaptic input (Goldberg et al., 2003; Hanson et al., 2004). Furthermore, as discussed below for slow–spiking pacemakers, the initial segment might contain a high concentration of Nav1.6 channels (Boiko et al., 2001; Boiko et al., 2003), making it a low–threshold point capable of driving pacemaking in intact neurons (Stuart and Hausser, 1994; Stuart et al., 1997). The absence of Nav1.6 in *med*^{TG} neurons significantly disrupts pacemaking in several neuron types, despite the introduction of Nav1.1 and 1.2 in the axon and initial segment to replace Nav1.6 (Van Wart and Matthews, 2006).

HCN and SK channels in pacemaking

Although Na^+ channel currents are necessary for autonomous activity in GP and STN neurons, several other channels contribute to the rate and regularity of discharge. Small conductance Ca^{2+}–dependent K^+ channels (SK class) slow and regularize the discharge of STN neurons (Hallworth et al., 2003). A similar dependence is found in GP neurons (unpublished observations). By contrast, hyperpolarization–activated, cyclic nucleotide–gated cation (HCN) channels are important for GP neuron pacemaking but not that of STN neurons (Do and Bean, 2003; Chan et al., 2004). In GP neurons, the mixture of HCN1 and HCN2 subunits endows these dendritic, hyperpolarization–activated cation channels with gating properties that enable their participation in pacemaking and in the integration of inhibitory synaptic input from the striatum. By activating HCN channels, this GABAergic input is capable of resetting the pacemaking cycle in individual neurons and generating synchronous discharge in neurons with temporally correlated input (Chan et al., 2004). GABAergic input to STN neurons from the GP has a similar effect, but the ionic mechanisms appear to depend more on the persistent Na^+ current (Bevan and Wilson, 1999; Bevan et al., 2002a; Baufreton et al., 2005). The basis for the differences between GP and STN neurons in this regard is not known yet. It might reflect differences in the gating properties of STN HCN channels (e.g. reliance upon HCN2 channels).

Kv3 channels are also common to GP and STN neurons, in addition to fast–spiking neurons elsewhere in the brain (Baranauskas et al., 1999; Wigmore and Lacey, 2000; Baranauskas et al.,

2003). They are thought to enable fast spiking by virtue of their ability to keep spikes brief (reducing Na^+ channel inactivation) and rapidly deactivate once the membrane has repolarized, thereby enabling the cell to rapidly depolarize to spike threshold again (Rudy and McBain, 2001). These channels are not necessary for ordinary pacemaking but might be important for sustained, high–frequency pacemaking. As mentioned above, the co–expression of Kv3 channels and Na^+ channels with resurgence creates a potent biophysical mechanism for high–frequency discharge (Akemann and Knopfel, 2006).

Fast spiking neurons in pathologic conditions

What is less clear is how important the capacity to spike at more than 100 Hz is to the functioning of the GP or STN. This capacity might be an evolutionary accident that can lead to pathophysiological consequences. For example, in parkinsonian humans and animal models at rest, GP and STN neurons often discharge in rhythmic, high frequency bursts (Bergman and Deuschl, 2002). Simulation studies have shown that this type of activity can arise in a reciprocally connected network of pacemakers such as that found between the GP and the STN (Terman et al., 2002). This aberrant activity is thought to be crucial to motor symptoms of the disease, because either GPi and/or STN lesioning or high frequency (90–150 Hz) electrical stimulation alleviates symptoms (Benabid et al., 2002).

Deep brain stimulation re–patterns aberrant high–frequency pacemakers

The nominal equivalence of lesioning and electrical stimulation is a bit of a puzzle. Recordings done in the STN suggest that deep brain stimulation (DBS) of the STN inhibits autonomous activity either through 'depolarization block' of Na^+ channels (Beurrier et al., 2001; Magarinos-Ascone et al., 2002; Tai et al., 2003), stimulation of GPe axons (Boraud et al., 1996; Wu et al., 2001) or a decrease in spontaneous activity during stimulation (Bevan and Wilson, 1999), making it functionally equivalent to lesioning (Bergman et al., 1990; Benazzouz et al., 1993; Limousin et al., 1995; Gill and Heywood, 1997). At the same time, stimulation of the STN leads to

increases in activity in GPe and GPi neurons (Jech et al., 2001; Hashimoto et al., 2003), as well as an increase in glutamate and GABA release in the GPi (Windels et al., 2003; Windels et al., 2005). One mechanism by which these apparently contradictory results could be explained is that DBS locally inhibits cell bodies within the STN while stimulating afferent fibers from the GPe and efferent fibers to the GPe and GPi (McIntyre et al., 2004a). The capacity of high frequency pacemakers to sustain this high frequency excitation remains to be elucidated. The ability to improve parkinsonian symptoms through lesioning or excitation suggests that the major disruption in PD is not the change in rate by the oscillatory burst pattern of activity. STN stimulation at 130 Hz should effectively eliminate the pathological activity and reset a more normal, rhythmic pattern that relies on the stimulation to drive the membrane potential to threshold instead of subthreshold Na^+ currents.

Slow–spiking pacemakers

Both striatal cholinergic interneurons and SNc DAergic neurons are slow spiking (0.1–10 Hz) autonomous pacemakers. Although similar in this respect, the ionic mechanisms underlying pacemaking in the two cells appear to be different.

Cholinergic pacemakers

Cholinergic interneurons display two pacemaking modes (Bennett et al., 2000). The most commonly encountered is the single spiking mode at 0.1–5 Hz. Blockade of voltage–dependent Na^+ channels with TTX eliminates this pacemaking mode and underlying membrane potential oscillations. Similar to fast–spiking pacemakers, interneurons express Nav1.1, 1.2 and 1.6 subunit mRNA, in addition to Navβ1– 4 (section 3.1). The normal range of persistent current (1–4% of peak transient current) is found in the somatodendritic membrane of these neurons but they do not manifest resurgent Na^+ current. The pacemaking rate in these neurons is tightly governed by the density of functional channels, because blocking even 10% of the channels with TTX slows pacemaking (section 3.2). In principle, pacemaking could be slowed or stopped transiently by any lowering of functional channel density. For example, excitatory synaptic input that increases

channel inactivation could induce a pause in activity (Reynolds et al., 2004). Activating G–protein coupled receptors linked to signaling cascades controlling the phosphorylation state of Na^+ channel α–subunits could accomplish the same result by increasing channel phosphorylation at sites that promote slow inactivation (Wilson, 2005). This mechanism could be important for DA signaling in the striatum and other areas of the basal ganglia, as DA is in the same class of catecholamines as serotonin and DA receptors activated G–protein pathways.

In addition to Na^+ channels, several other channels have pivotal roles in controlling interneuron single–spike pacemaking. HCN channels help to maintain the rate and regularity of discharge by providing a depolarizing current at the negative membrane potentials reached during the spike AHP. This AHP is largely mediated by Ca^{2+}–activated K^+ channels of the SK class (Bennett et al., 2000). Burst of APs also generate a long–lasting slow AHP, with properties similar to those found in cortical and hippocampal pyramidal neurons (Goldberg and Wilson, 2005).

Wilson (Wilson, 2005) has shown that the less common burst pacemaking mode can be triggered by hyperpolarization. The Na^+ channel independent oscillation appears to depend upon an interaction among Kir2 (IRK/KCNJ) channels, HCN channels and a leak conductance (e.g. TASK3). Kir2 channels are K^+ selective, inwardly rectifying channels possessing a negative slope conductance region above the potassium equilibrium potential. Hyperpolarization deactivates Na^+ channels and moves the membrane potential into a range dominated by the negative slope region of the Kir2 channels, producing a regenerative event that further hyperpolarizes the cell, driving it towards the K^+ equilibrium potential. This hyperpolarization activates the kinetically slower HCN channels and drives the membrane potential back toward –55 mV. Deactivation of the HCN channels returns the cell to the state dominated by the Kir2 channels and starts the cycle again. TASK3 channels have also found to be expressed at high level in these cells (Talley et al., 2001). The factors controlling the tendency to exhibit this slow oscillation have yet to be worked out but modulation of HCN, Na^+, Kir2 or TASK3 channels certainly could be important. Transient GABAergic inhibition appears not to be sufficient (Bennett and Wilson, 1998).

Dopaminergic neurons as Ca^{2+} pacemakers

Similar to cholinergic interneurons, DAergic neurons of the substantia nigra are slow–spiking pacemakers (Grace and Bunney, 1983b, a; Grillner and Mercuri, 2002). Although they exhibit burst or irregular firing in response to synaptic input, autonomous pacemaking is predominantly in the single–spike mode (0.2–10 Hz). The ionic mechanisms underlying autonomous activity in these neurons are debated. Membrane potential oscillations are reduced in amplitude and frequency by TTX, suggesting that spiking and Na^+ channel currents contribute to pacemaking (Wilson and Callaway, 2000). However, Na^+ currents are not necessary for oscillation. In the presence of TTX and in the absence of strong extrinsic Ca^{2+} buffers, DAergic neurons continue to oscillate at a low frequency. Moreover, blockade of Cav1/ L–type channels stops autonomous pacemaking without disrupting the responsiveness to extrinsic input (Harris et al., 1989; Nedergaard et al., 1993; Mercuri et al., 1994). This has posed some conceptual difficulties, because Cav1 channels are thought of as 'high–threshold', requiring spiking or strong depolarization for their activation. However, it appears that SNc DAergic neurons express a type of Cav1 channel (Cav1.3/class D) that begins to open in the appropriate, subthreshold voltage range (–50 mV) and inactivates slowly (Xu and Lipscombe, 2001; Olson et al., 2005). Immunocytochemical work has shown that SNc DA neurons robustly express Cav1.3 channels in the soma and dendrites, whereas Cav1.2/class C L–type and Cav2.2/ N–type channels are found at much lower densities (Takada et al., 2001). The hyperpolarizing phase of the subthreshold oscillation seen in TTX is disrupted by Ca^{2+} chelation or blockade of apamin–sensitive Ca^{2+}–dependent K^+ channels (Ping and Shepard, 1996). These channels appear to be composed largely of SK3 subunits (Wolfart et al., 2001). Thus, it would seem that two channels — Cav1.3 and SK3 — are all that is necessary for the oscillations underlying autonomous pacemaking in SNc DA neurons.

Is this plausible? Recent work suggests that it is (Amini et al., 1999; Wilson and Callaway, 2000). The work by Wilson and Callaway thoughtfully blends computational, imaging and electrophysiological approaches to show how the oscillations might arise. An important insight

is that the natural oscillation frequency that this type of mechanism produces is dependent upon the surface area–volume ratio of a cellular compartment. This means that smaller dendrites have a higher natural frequency than do larger dendrites or the soma. Their model predicts that normally pacemaking is driven by Ca^{2+} oscillations in proximal dendrites. Voltage–dependent Na^{+} channel currents amplify the Ca^{2+} channel–driven oscillation in the subthreshold voltage range and generate spikes that terminate the oscillatory cycle. Their 'coupled oscillator' model provides a means of explaining regular, single spike pacemaking and other activity patterns (irregular or burst firing) that are normally thought to depend upon synaptic input.

One of the controversies that has arisen in the field involves selective coupling of SK channels to Ca^{2+} channels. The Wilson and Callaway model builds a mechanistic foundation for the long held belief that Cav1.3 channels carry the flux that activates SK channels underlying the oscillation. Their work suggests that diffuse changes in Ca^{2+} concentration are crucial to the kinetics of the oscillation, something that would be difficult to achieve with tight spatial coupling between Ca^{2+} and SK channels. Work by Wolfart and Roeper (Wolfart and Roeper, 2002) challenges this view, arguing that Cav3/T–type—not Cav1 or Cav2 — channels carry the Ca^{2+} necessary for SK gating. The case is made largely on pharmacological grounds, using nickel and mibefradil to differentiate Cav3 channels from the others. The readily apparent chink in Roeper's armor is the reliance upon ligands that are not strongly selective for Cav3 channels. Better pharmacological tools or genetic approaches will be required to unequivocally resolve the controversy.

As noted above, HCN channels have been implicated in pacemaking in several cell types. HCN channels are robustly expressed in both SNc and ventral tegmental area (VTA) DA neurons. Neuhoff et al. (Neuhoff et al., 2002) have used an elegant combination of single cell reverse transcriptase– polymerase chain reaction (RT–PCR), electrophysiology and anatomy to make the case that the functional expression of HCN channels is negatively correlated with the expression of the Ca^{2+}–binding protein calbindin in DA neurons. In the SNc, the majority of DA neurons do not have detectable calbindin mRNA, and have a relatively high density of slow HCN (HCN2–4)

channels (Franz et al., 2000). In these neurons, blockade of HCN channels significantly slows pacemaking. However, eliminating HCN channels has little effect on pacemaking in the small population of SNc DA neurons that have high calbindin expression (and low HCN density) or in VTA DA neurons, both of which have lower HCN density. These results can be reconciled with the Wilson and Callaway model by simply assuming that HCN channel currents accelerate the depolarizing phase of the Cav1.3 and SK3–driven oscillatory cycle in most SNc DA neurons, as do Na^+ channels.

Disease states

A wide variety of neurological disorders can be traced to altered function of the basal ganglia. Parkinson's disease, Huntington's disease, dystonia, Tourette's syndrome, attention deficit hyperperactivity disorder (ADHD) and schizophrenia are among the most prominent neurological diseases with strong links with the basal ganglia. Clear links between these diseases and alterations in pacemaking have not been made, but there are few or no data to refer to. In Parkinson's disease, the most dramatic pathophysiology is found in the fast–spiking pacemakers of the GP and STN, where synchronous, rhythmic bursting emerges (Bevan et al., 2002b). How this arises is not clear. As mentioned above, the alterations in behavior can be simulated without modifications in pacemaking. But experimental data on this point are still lacking. Certainly, the channels underlying pacemaking in all of the involved structures are subject to modulation by G protein receptor signaling cascades, similar to those used by DA.

Is it possible that sustained activity can lead to premature death? There is no reason to believe that spiking per se is stressful. The only basal ganglia pacemaker that appears to be living on the edge is the principal DA neuron in the SNc. This cell type appears to be particularly vulnerable to environmental stress and genetic mutations that affect mitochondria or protein processing (Liang et al., 1996; Dawson and Dawson, 2003). Death of these neurons is the cause of Parkinson's disease and altered function is connected to many of the other basal ganglia diseases. Is there a link to pacemaking? This neuron is the only Ca^{2+}–dependent pacemaker in the group. Elevated intracellular

Ca^{2+} interferes with mitochondrial function and protein folding. Could the conjunction of these two stressors be what pushes DAergic neurons over the edge?

Organization of the dissertation

While Na^+ channels are clearly important in the pacemaking properties of some neurons, like fast–spiking GP neurons and slow–pacemaking striatal cholinergic interneurons, but not others, like Ca^{2+} pacemaking nigral DAergic neurons and quiescent striatal medium spiny neurons, no direct and systematic comparisons have been made analyzing the biophysical properties of these different classes of neurons. Specific interest was placed on mechanisms that would shape channel availability in neurons that rely on Na^+ channels during the interspike interval to drive pacemaking, such as voltage dependence of fast inactivation, kinetics of fast inactivation, development of slow inactivation and presence of the resurgent current (**section 3.1**). Once a thorough understanding of the biophysical properties was complete, I investigated the impact reduction in Na^+ channel availability by DAergic modulation has on spontaneous activity. This addressed whether modest modulation of Na^+ channels can have significant impacts on firing properties of autonomous pacemakers (**section 3.2**). I then delved further into the mechanisms of resurgent current and its role in the high frequency activity of GP neurons. Studies on the effectiveness of DBS in treating PD were focused around whether GP neurons are able to maintain activity during high frequency stimulation or if they are silenced because of accumulation of Na^+ channel inactivation and depolarization block. This research addressed this by directly stimulating GP neurons at high frequencies and observing the firing properties that emerged (**section 3.3**). This high frequency firing in the GP is adapted to its specific role in the basal ganglia as a central nucleus that has connections with all other nuclei. In PD, this firing pattern is severely disrupted and the GP transitions into a "burst–pause" mode of firing, that potentially entrains intranuclear correlated activity and oscillatory behavior with other neurons in the basal ganglia (Bergman et al., 1998; Raz et al., 2000; Raz et al., 2001; Bar-Gad et al., 2004). It is unclear whether this transition is from alterations in intrinsic membrane properties or a downstream result of increased synaptic activity from other nuclei. I addressed this issue by

creating different DA depletion models and studying the firing properties of GP neurons from tissue slice using cell–attached, current and voltage clamp recording in conjunction with pharmacological manipulations. The role and adaptation of HCN channels in pacemaking of GP neurons after DA depletion was also explored (**section 3.4**).

Chapter 2

Methods and Methods

Animals. Two– to four–week old Male C57Bl/6 mice (Charles River, Wilmington, MA) were used in the present study. C57Bl/6 mice with the *med*^{TG} mutation (Nav1.6–/–) were obtained from the Meisler Laboratory at the University of Michigan (Kohrman et al., 1995). BAC D_2 EGFP mice were acquired from the Heintz Laboratory at Rockefeller University (Gong et al., 2003). Cav1.3–/– mice were obtained from Joerg Striessnig (Institut für Biochemische Pharmakologie, Innsbruck, Austria) (Platzer et al., 2000), rederived and backcrossed onto a C57Bl/6 background in the Northwestern University barrier facility. The acute dopamine depletions were produced in C57BL/6 mice (17–25 day old) by administering reserpine (5 mg kg^{-1}) intraperitoneally (i.p.) for 5 successive days. The mice were decapitated for experiments 2–4 h after the final injection. Partial dopamine depletion was achieved with α–Methyl–DL–tyrosine methyl ester hydrochloride (α–MT) with three daily injections of 100 mg kg^{-1} (Lydiard et al., 1975). The serotonin depletions were produced in mice of the same age with three daily injections of 300 mg kg^{-1} DL–*p*–chlorophenylalanine methyl ester (*p*CPA) (Koe and Weissman, 1966; Steigrad et al., 1978; Steinman et al., 1987; Tohyama et al., 1988; Datla and Curzon, 1996). These mice were killed for experiments 24 h after the final *p*CPA injection. Saline–injected controls were prepared in the same conditions. To achieve unilateral lesions of the nigrostriatal system, C57BL/6 mice were anaesthetized using ketamine/xylazine anesthesia and place into a stereotaxic frame (David Kopf Instruments, Tujunga, CA) with an adaptor specially fitted for mice (Cunningham Mouse Adaptor, Harvard Apparatus, USA). 6–OHDA (Sigma) was dissolved at a concentration of 4 μg/μl saline with 02mg/ml ascorbic acid and injected in final dosages of 4–6 μg. The lesion was performed using a glass pipette at the following coordinates: AP: –0.4mm (from Bregma); ML: +1.6mm (from midline); DV: +3.3mm (from surface of skull). The

injection was conducted at a rate of 1 μl/30 min and the pipette was left in place for another 30 min after the injection before it was slowly retrieved. Experiments were performed 4–6 days postsurgery. The handling of mice and all procedures performed on them were approved by the Northwestern University's Animal Care and Use Committee and were in accordance with the *National Institutes of Health Guide to the Care and Use of Laboratory Animals* and Society for Neuroscience guidelines. All efforts were made to minimize the number of animals used and the suffering of those killed.

Tissue preparation. Animals were anesthetized with a mixture of ketamine and xylazine and transcardially perfused with ice–cold artificial cerebral spinal fluid (ACSF) containing (in mM): 125 NaCl, 2.5 KCl, 1 $MgCl_2$, 2 $CaCl_2$, 1.25 NaH_2PO_4, 13 glucose, and 25 $NaHCO_3$, bubbled continuously with carbogen (95% O2 and 5% CO2) (slice experiments) or isoflurane (acute experiments), followed by decapitation. Brains were removed rapidly and placed immediately in ice–cold aCSF (slice experiments) or ice–cold sucrose solution containing (in mM): 250 sucrose, 11 glucose, 15 HEPES, 4 $MgSO_4$, 1 NaH_2PO_4, 2.5 KCl, 1 kynurenic acid, 0.1 N–nitro–L–arginine and 0.005 glutathione, pH 7.4, 300–305 mOsm/L bubbled continuously with oxygen (acute experiments). Thin coronal or parasagittal slices (250–350 μm) containing GP, striatum or SNc were made using a vibrating microtome (VT1000s; Leica Instrument, Leitz, Nussloch, Germany) and equilibrated in fresh aCSF at 34°C for 30 min, followed by room temperature for 0.5–4 hrs (slice experiments) or sodium bicarbonate–buffered Earle's balanced salt solution (EBSS) bubbled with carbogen (acute experiments). EBSS also contained the following (in mM): 23 glucose, 1 kynurenic acid, 0.1 *N*–nitro–L–arginine, and 0.005 glutathione.

For the acute preparation, individual slices were transferred to a low–Ca^{2+} buffer containing (in mM) 140 Na isethionate, 23 glucose, 15 HEPES, 2 KCl, 4 $MgCl_2$, 0.2 $CaCl_2$, 1 kynurenic acid, 0.1 *N*–nitro–L–arginine, and 0.005 glutathione, pH 7.4, 300–305 mOsm/L, the GP was dissected and incubated at 30°C for 25 min in oxygenated Hanks' buffered salt solution (HBSS) containing (in mM): 11 HEPES, 4 $MgCl_2$, 1 $CaCl_2$, 1 pyruvic acid, 1 kynurenic acid, 0.1 N–nitro–L–arginine, 0.005 glutathione and 1 mg/ml protease XIV, pH 7.4 300–305 mOsm/L, bubbled with O_2.

Although protease treatment may partially degrade surface proteins, reducing the responsiveness of G–protein coupled receptors, there is no viable alternative to extracting cholinergic interneurons from tissue slices. There is no evidence that protease alters the properties of Na^+ channels. After enzyme incubation, the tissue was transferred to the low–Ca^{2+} HEPES–buffered saline, rinsed and mechanically dissociated using fire–polished Pasteur pipettes. The resulting cell suspension was plated onto a 35 mm Petri dish mounted onto an inverted microscope. During the course of the experiment, non–recorded cells were constantly perfused with a background solution containing (in mM): 140 NaCl, 23 glucose, 15 HEPES, 2 KCl, 2 $MgCl_2$ and 1 $CaCl_2$, pH 7.4, 300–305 mOsm/L.

Whole–cell and cell–attached recording in slices. Slices were transferred to a small–volume (<0.5 ml) recording chamber that was mounted on a fixed–stage, upright microscope (BX51; Olympus America, Melville, NY) equipped with IR–DIC [0.9 numerical aperture (NA)] with de Sénarmont compensation (Olympus). Experiments were performed at 34 °C ± 1 unless specified otherwise. Recording chamber was superfused with carbogen–saturated ACSF with a flow rate of 2–3 ml/min. Neuronal somata and proximal dendrites were visualized by videomicroscopy at high magnification (60x, 0.9 NA water immersion objective; Olympus) with a back–thinned, frame–transfer cooled–CCD camera (Micromax EBFT512; Roper Scientific, Trenton, NJ) aided by a contrast enhancement system (Argus–20; Hamamatsu Photonics, Bridgewater, NJ).

Conventional tight–seal (>3 GΩ) whole–cell patch–clamp and cell–attached recordings were made on visually identified, GP neurons, based on size and somatodendritic morphology. Only neurons in the rostral to midlevel GP were studied (Shammah–Lagnado et al., 1996). GP neurons were further identified by their physiological features (Chan et al., 2004), including resting level of discharge (~12 Hz during cell–attached recording) and a prominent voltage–sag during hyperpolarizing current injection.

Patch electrodes (1.5 mm outer diameter) were fabricated from filamented, thick–wall borosilicate–glass (Sutter Instruments, Novato, CA) pulled on a Flaming–Brown puller (P–97; Sutter) and fire polished immediately before use. Pipette resistance was typically ~3–6 MΩ when

filled with recording solution. The recording internal solution consisted of (in mM): 140 $KMeSO_4$, 5 KCl, 10 Na–phosphocreatine, 0.025–0.05 EGTA, 2.0 Mg–ATP, 0.4 Na_3–GTP, 10 HEPES, pH 7.25–7.30, 280 mOsm/L. The liquid junction potential in our slice recordings was ~7 mV and not corrected for. Somatic whole–cell patch–clamp recordings were obtained via a MultiClamp 700B amplifier (Molecular Devices, Union City, CA) interfaced to a Pentium–based PC running pClamp9 (Molecular Devices). The signal was filtered at 1–4 kHz and digitized at 5–20 kHz with a Digidata 1322A (Molecular Devices). For current–clamp recordings, the amplifier bridge circuit was adjusted to compensate for electrode resistance and monitored. Electrode capacitance was also compensated. If series resistance increased >20% during recording, the data were discarded. All experiments were done at 22°C except for DA neurons, which were done at 34°C.

Whole–cell recording in the acutely dissociated preparation: Voltage clamp recordings were performed using electrodes pulled from Corning (Corning, NY) 7052 glass, coated with R–6101 (Corning) and fire polished immediately before use. Electrodes were typically 2–3 MΩ in the bath. Recordings were obtained via an Axopatch 200B amplifier (Axon Instruments, Foster City, CA) interfaced to a Macintosh computer running Pulse software (HEKA, Lambrecht, Germany) through an ITC–16 (Instrutech, Port Washington, NY). After the gΩ seal was formed and the cell membrane was ruptured, series resistance was compensated (75–80%) and frequently monitored. The intracellular recording solution contained (in mM): 60 mM N–methyl–D–glutamine, 20 HEPES, 50 Cs_2SO_4, 2 $MgCl_2$, 0.5 Na_2SO_4, 22 phosphocreatine, 3 mM Mg–ATP, 0.7 Na_2–GTP and 0.1 leupeptin, pH 7.25 (with H_2SO_4), 265–270 mOsm/L. During recording, cells were bathed in extracellular solutions applied via a gravity–fed capillary perfusion array positioned several hundred micrometers away from the cell under study. Bathing solutions were changed by adjusting the position of the array using a DC actuator (Newport, Irving, CA). Solution changes were complete within <1 sec. For recording transient Na^+ currents, the external solution contained (in mM): 10 NaCl, 110 tetraethylammonium (TEA) chloride, 10 HEPES, 10 CsCl, 0.3 $CdCl_2$, 1 $MgCl_2$ and 2 $BaCl_2$, pH 7.4, 300–305 mOsm/L. For recording subthreshold Na^+ currents, the external solution contained (in mM): 115 NaCl,

45 TEA–Cl, 10 HEPES, 0.3 $CdCl_2$, 1 $MgCl_2$ and 2 $BaCl_2$, pH 7.4, 300–305 mOsm/L. Protocols were repeated in external solution plus 300 nM TTX, and these recordings were subtracted from the control records to isolate TTX–sensitive sodium current. The liquid junction potential for the acute preparation (~1 mV) was not compensated for. Unless noted otherwise, all chemicals were obtained from Sigma (St. Louis, MO). All recordings were performed at room temperature (22°C).

To ensure adequate voltage control, several steps were taken. Only cells with relatively short (25–50 µm) processes were selected for recording; after entering whole–cell mode, often the processes retracted, making cells nearly spherical. In each cell, current activation plots were generated, and any evidence of loss of voltage control (discontinuities in the current–voltage relationship that would yield slope factors <5 mV) resulted in the cell being discarded. Also, variation in the activation kinetics of test pulse currents evoked in inactivation protocols was taken for evidence of bad space clamp. In several experiments, reversal potentials were examined. These invariably fell within a few mV of the prediction based upon the Goldman–Hodgkin–Katz equation; suggesting that the transmembrane voltage was adequately controlled. In the ramp experiments, where external Na^+ was near physiological levels, discontinuities in the rising phase of the currents were taken as evidence of bad control; in the worst case, this was manifested as spiking. In the ramp experiments where external Na^+ was near physiological levels, discontinuities in the rising phase of the currents was taken as evidence as bad control in the worst case, this was manifested as spiking. In some cases, particularly with the larger cholinergic interneurons and DA neurons, control was achieved by reducing the Na^+ current driving force and the experiments were repeated.

Solutions and pharmacology: $KMeSO_4$ was purchased from MP Biomedicals (Solon, OH); SR95531 were purchased from Tocris Cookson (Ballwin, MO); TTX from Alomone Laboratories (Jerusalem, Israel). Calphostin C and 1–oleoyl–2–acetyl–sn–glycerol (OAG) were obtained from Calbiochem (San Diego, CA). Drugs were dissolved as stock solutions in either water or DMSO, aliquoted and frozen at –30°C before use. Each drug was diluted in the perfusate immediately before the experiment. When used, the final concentration of DMSO was always <0.1%. Stock solutions were

dissolved in 0.1% sodium metabisulfite to prevent oxidation. When drugs were dissolved in DMSO or sodium metabisulfite, equivalent amounts were added to all internal or external solutions as controls. BAPTA was obtained from Molecular Probes, (Eugene, OR). βARK–C peptide (βARK–Cp) is comprised of residues 548–671 of the rat homologue of βARK. βARK–Cp (4.9 mg/mL) was dialyzed against the recording internal solution by Dr. Heidi Hamm. This solution was diluted in the recording internal solution for a final concentration of 1 mg/ml. All other drugs were purchased from Sigma (St. Louis, MO).

Histology for light microscopy. Some cells were recorded with 0.1% biocytin for later morphological identification. Following recording, pallidal slices containing labeled neurons were fixed for 48 h at 4°C in 2–4% paraformaldehyde and 15% picric acid in 0.1 M phosphate buffer (pH 7.3–7.4). They were subsequently reacted in a 1:100 dilution of avidin–biotin complex conjugated to horseradish peroxidase (ABC Elite kit, Vector Laboratories, Burlingame, CA) overnight and incubated in 0.1 M Tris–buffered saline containing 0.025% 3–3–diaminobenzidine tetrahydrochloride (DAB, Sigma, St. Louis, MO), 0.05% nickel chloride, and 0.006% hydrogen peroxide. Slices were dehydrated through graded series of alcohol and xylene, coverslipped in DPX (Fluka), and permanently mounted for morphological examination.

Data analysis. Data were plotted and analyzed with IgorPro (Wavemetrics, Lake Oswego, OR) or Mathematica (Wolfram Research, Champaign, IL). Transient Na^+ currents evoked by depolarizing steps were fit with a modified Hodgkin–Huxley formalism of the form $g=g_{max}m^3(V,t)h(V,t)(V–V_{rev})$; where g is the conductance, g_{max} is the maximal conductance, V is transmembrane voltage, t is time, V_{rev} is the Na^+ reversal potential, $m(V,t)=\alpha(1–\exp(–t/\tau_m))$, $h(V,t)=\beta(\exp(–t/\tau_{h1}))+(1–\beta–\gamma)(\exp(–t/\tau_{h2}))+\gamma$, where α is a scalar, $0\leq\beta<1$ (the component of inactivation that decays with a τ_{h1} time constant), and γ is scalar representing the component of the current that is persistent (typically 0.01–0.05), τ_m is the activation time constant, τ_{h1} and τ_{h2} are the fast and slow inactivation time constants. The development of inactivation between –60 and –40 mV was estimated by stepping into this

voltage range for a variable period before delivering a test step to assay for de–inactivated channels. Inactivation kinetics were determined by fitting measurements of peak current as a function of prepulse duration. Deactivation kinetics were estimated by briefly depolarizing the membrane to open channels and then repolarizing to hyperpolarized membrane potentials. These tail currents were fit with simple mono– or bi–exponential functions. Nominally steady state conductance–voltage and inactivation–voltage curves were fit with a Boltzmann function of the form: $g(V) = 1/(1+\exp((V-V_{1/2})/ Vc))^C$ where $V_{1/2}$ is the half–activation or inactivation voltage and Vc is the slope factor. Activation data were fit with a third–order (c=3) and inactivation was fit with a first–order (c=1) Boltzmann function. Window current estimates and fits of persistent currents were generated assuming that the current was given by $\zeta(m^3(V,\infty)(h(V,\infty)+\gamma))(V-V_{rev})$. Driving force was estimated from the Nernst equation (as described above) or from the Goldman–Hodgkin–Katz equation (Hille, 2001); there were only small differences in the estimates of conductance or permeability (respectively) derived from these choices in driving force estimates with the ionic concentrations employed. Activation and deactivation time constants were plotted as a function of voltage and fit with an equation of the form: $c1+c2/(\alpha1\exp(-(V-\alpha2)/\alpha3)+\beta1\exp((V+\beta2)/\beta3))$, where V is transmembrane voltage and $\alpha1–3$, $\beta1–3$ and c1–2 are fitted constants. This equation is derived from the Hodgkin–Huxley formalism and assumes a single voltage–dependent state transition. Slow inactivation–voltage curves were fit with a modified Boltzmann equation of the form: $I/I_{max} = (1 - I_{resid})/((1+\exp(-(V-V_{1/2})/V_C))+I_{resid}$ where I_{resid} is the residual (non–inactivating) fraction of the current and V_C is the slope factor. Time constants for the entry into the slow inactivated state were reasonably fit with a single exponential function; exit from the slow inactivated state required a double exponential fit.

Statistical analyses were performed using Systat (SPSS, Chicago, IL). Sample statistics are given as mean ± SE or median if accompanied with a non–parametric box plot of data spread. In data presented as box plots, the central line represents the median, the edges of the box represents the interquartile range (25-75%) and the “whisker lines” show the extent of the overall distribution,

excluding outliers (points > 1.5 x interquartile range).

Interneuron computer simulation: Although the Hodgkin–Huxley (HH) formalism yielded accurate fits to the data generated by voltage steps, it does not account for a number of gating properties, including the voltage dependence of persistent Na^+ currents. Therefore, a Markov model of channel gating was fit to the data (Raman and Bean, 2001; Taddese and Bean, 2002; Carr et al., 2003) using *Neuron* (ver. 5.5) (Hines and Carnevale, 1997, 2001). Using the MultiRun Fitter in *Neuron*, the Markov model was constrained by the experimental data as abstracted by the HH description. To fit the bi–exponential decay of recorded currents, currents were modeled as the sum of two channels (this was consistent with the molecular profiling – see below); models were constructed with fast and slow kinetics (as well as slow inactivation (Carr et al., 2003)). The fast current had the following parameters: α=37exp((V–45)/40) ms^{-1}, β=10exp(–(V+50)/10) ms^{-1}, γ=40 ms^{-1}, δ=30 ms^{-1}, Con=0.001 ms^{-1}, Coff=0.1 ms^{-1}, Oon=1.6 ms^{-1}, Ooff=0.01 ms^{-1}. α=((Coff/Con)/(Ooff/Oon), αS1= 0.0025, αS2=0.0002, βS=0.00017; the slow channel parameters were: α=37exp((V–45)/40) ms^{-1}, β=10exp(–(V+50)/20) ms^{-1}, γ=40 ms^{-1}, δ=30 ms^{-1}, Con=0.001 ms^{-1}, Coff=0.1 ms^{-1}, Oon=0.7 ms^{-1}, Ooff=0.01 ms^{-1}. α=((Coff/Con)/(Ooff/Oon), Slow time constants. The ratio of the slow to fast channel density was adjusted to 0.4 to match macroscopic currents.

To simulate the pacemaking of cholinergic interneurons, a simplified model was constructed in *Neuron* using a spherical soma (30 μM) and two dendrites (200 μm long, 2 μm diameter) invested with ionic conductances known to participate in pacemaking based upon published (Song et al., 1998; Bennett et al., 2000) and unpublished studies. Membrane resistance was 1KΩcm^2, capacitance was 1 $\mu F/cm^2$ and axial resistivity was 70 Ωcm. In addition to the Na^+ channels described above, somatic currents included voltage–dependent K^+ channels (Kv4, Kv2, KCNQ), Ca^{2+}–dependent K^+ channels (BK, SK), voltage–dependent Ca^{2+} channels (Cav1.3, Cav2.1); these channels and voltage–dependent/cyclic AMP modulated cationic channels (HCN) also were placed in the dendrites, albeit at different densities. Intracellular Ca^{2+} handling and the model of SK currents was as described by Lazarewicz et al. and the model of BK channels was taken from Khaliq

et al. (Lazarewicz et al., 2002; Khaliq et al., 2003). Mod files for the other conductances (Kv4, Kv2, KCNQ, Cav1.3, Cav2.1, HCN1, HCN2) were generated from experimental data as described above for the Na^+ currents. The kinetic models for HCN1 and HCN2 channels were adapted from Wang et al. (Wang et al., 2001). Relative densities of the channels were adjusted to yield a pacemaking waveform and rate similar to that found in whole cell recordings from cholinergic interneurons in the slice (Bennett et al., 2000). The densities in the soma were (in mS/cm^2): fast Na 1.0, slow Na 0.4, Cav1.3 0.003, Cav2.1 0.05, Kv4 0.4, Kv2 0.1, KCNQ 0.002, BK 1, SK 0.003; in the dendrites: fast Na 0.25, slow Na 0.1, Cav1.3 0.003, Cav2.1 0, Kv4 0.4, Kv2 0.1, HCN1 0.01, HCN2 0.03, BK 1, SK 0.003. Copies of the mod files describing these channels are available upon request.

GP computer simulations. Experimentally recorded currents were modeled with *Neuron*, version 5.9 (Hines and Carnevale, 1997, 2001). All experimental data on TTX–sensitive sodium currents were obtained in this study and incorporated into a kinetic scheme based on previously derived models (Kuo and Bean, 1994; Raman and Bean, 2001; Taddese and Bean, 2002; Carr et al., 2003). The factor *a* from previous models was replaced with *m* and *n*, where *m*=((Oon/Ooff)/(Con/Coff))^(1/2), which preserves microcircuit reversibility, and *n*=2. Furthermore, the rates Oon, Ooff, ζ, αS_X (where x is either o, b or i, depending on the states between which the transition occurs) were made voltage dependent. The rates were calculated by Oon=Oon0*exp((v–hOon)/cOon), Ooff=Ooff0*exp((v–hOoff)/cOoff), ζ=exp(–(v–bvh)/bslope) and $\alpha S_X = S_X R * \exp((v - S_X H)/S_X C)$. The single slow inactivated states from Carr et al. were replaced with ten slow inactivated states (Fig. 3.8f). The values of all rate constants have been altered to more accurately fit the adjustments made to the model scheme. *Neuron* mod files containing these descriptions are available upon request. Na6 was modified from Na1 by increasing bl0 from 0.08 to 0.15 and decreasing Ooff0 from 3 to 0.77.

The model GP neuron was constructed of (in μm) a cylindrical soma (25x25), a conical axon hillock (L=10, D1=5, D2=1.4) initial segment (L=40, D=1.4) an axon (L=500, D=1.1) with five nodes (L=1, D=1.1) at 100 μm intervals and four tapering dendrites (L=500, D1=1.25). Axial resistivity between compartments were 200 Ω–cm. For wild–type simulations, Na1 was inserted

into the soma and hillock with a conductance density (Scm^{-2}) of 0.04 and into the dendrites with a conductance density of 0.02. It was not inserted into the nodes/initial segment. Na6 was inserted into the nodes/initial segment with a conductance density of 0.9, into the soma and hillock at 0.01. For Nav1.6–/– simulations, Na6 was eliminated and Na1 was adjusted to 0.9 in the nodes/initial segment. For the no–resurgent simulations, the densities were identical to the wild–type simulation, but ε was set to 1e–9 and Ooff for both channels was set to 3 to mimic the experimental data.

Also inserted into these compartments were channels known to be important to the spiking of GP neurons; mod files for HCN1, HCN2, BK, SK, Kv2, Kv3, Kv4, Kv7 (KNCQ) and Kir2 channels, as well as a Ca^{2+} buffering system were constrained by experimental data (Baranauskas et al., 1999; Tkatch et al., 2000; Baranauskas et al., 2003; Chan et al., 2004; Shen et al., 2005) or acquired from the *Neuron* database mod files from previous simulations (Migliore et al., 1995; Wang et al., 2002; Khaliq et al., 2003) and incorporated into the appropriate compartments. *Neuron* mod files providing a complete description of the model are available upon request. All experiments were done at 23°C and with an E_{Na} of 50 mV.

Tissue and single cell RT–PCR (scRT–PCR) analysis. These procedures were as previously described (Yan et al., 1997). Briefly, dissociated, individual cholinergic neurons were aspirated into sterile glass micropipettes containing diethyl pyrocarbonate (DEPC)–treated water and 1.5 U/µl SUPERase–In (Ambion, Austin, TX). The contents of the pipette were transferred to thin walled PCR tubes containing dNTPs (1 µl, 10mM), BSA (0.7 µl, 143 µg/µl), random hexamers or oligodT (2.6 µl, 50 ng/µl) and Superase–In (0.7 µl, 40U/µl). All RT reagents were obtained from Life Technologies. This mixture was heated to 65°C for 5 min to linearize mRNA and then placed on ice for 2 min. To each tube was added: 10x RT buffer (1 µl), $MgCl_2$ (2 µl, 25 mM), DTT (1 µl, 0.1 M), RNAse Out (0.5 µl), and 200U Superscript II reverse transcriptase. cDNA transcription was performed by heating the reaction mixture to 25°C for 10 min and 42°C for 50 min. The reaction is terminated by incubation at 70°C for 15 min and then placed on ice. RNA was then removed by adding 0.5 µl RNAseH to each tube and

incubating for 20 min at 37°C. All reagents except Superase–IN (Ambion) were obtained from Invitrogen (Gaithersburg, MD). Single–cell cDNA was amplified using a conventional PCR approach with a programmable thermal cycler (MJ Research, Watertown, MA). Amplification cDNAs for glutamate decarboxylase (67 KD isoforms, GAD_{67}), choline acetyltransferase (ChAT), D_2 dopamine receptor, parvalbumin (PV), enkephalin (ENK) and Na^+ channel alpha subunit cDNA (Nav1.1, 1.2, 1.5 and 1.6) was performed as previously described (Surmeier et al., 1996; Yan et al., 1997; Song et al., 1998; Tkatch et al., 1998; Maurice et al., 2001). The PCR primers for Na^+ cannel beta subunits (Naβ1, Naβ2, Naβ3 and Navβ4) were developed from GenBank sequences using OLIGO software (National Biosciences, Plymouth, MN). The primers for Naβ1 cDNA (GenBank accession number M91808) were AGAAGGGCACAGAGGAATTTGTCA (position 401) and GACGCTGGTGTTGTGCTCGTAAT (position 611). The predicted product length was 233. The primers for Naβ2 cDNA (GenBank accession number U37026) were CTGCCCTGTACCTTCAACTCCTG (position 308) and CCATCCGTCTTGCCTTCCTC (position 764). The predicted product length was 476. The primers for Naβ3 cDNA (GenBank accession number AJ243395) were TGAGGGCGGTAAAGATTTCCTT (position 560) and CTTCGGCCTTAGAGACCTTTCTGT (position 904). The predicted product length was 368. The primers for Naβ4 cDNA (Gen–Bank accession number BK001031) were GGATCGTGAAGAACGATAAGT (position 245) and AGCCAGGATGATGAGAGTCACCG (position 482). The predicted product length was 260. After amplification, PCR products were labeled by ethidium bromide and separated by electrophoresis on agarose gels. Amplicons were of the expected size and sequence. Negative controls for extraneous and genomic DNA contamination were run for each experiment. To verify that genomic DNA was not being amplified, reverse transcriptase was omitted during the RT reaction and the resulting reaction mixture was processed for PCR amplification as described above. Extraneous contamination during the PCR amplification was examined by replacing the cDNA template with buffer solution. If either control was found to be positive, the material from that experiment was discarded.

Chapter Three

Results

Section 3.1: The ability to conduct a resurgent current distinguishes voltage dependent Na^+ channels of pacemaking neurons

Introduction

The dynamics of communication within neurons of the basal ganglia are unique in that they rely predominantly on high levels of spontaneous activity. This autonomous activity is important because, except for glutamatergic neurons of the subthalamic nucleus (STN) and dopaminergic neurons of the substantia nigra pars compacta (SNc), all projection neurons are GABAergic. Pacemaking ensures that information is transmitted through the basal ganglia and to downstream recipients even in the face of inhibitory GABAergic input. While the machinery behind autonomous activity in various subpopulations is unique (overviewed in **Chapter 1**), the basic principle rests on the balance of depolarizing and hyperpolarizing currents conducted by the neuron. Within the basal ganglia, there are three different classes of pacemaking neurons: fast–spiking neurons of the globus pallidus (GP), entopenduncular nucleus (EP), substantia nigra pars recticulata (SNr) and STN, slow–spiking cholinergic interneurons of the striatum and slow–spiking dopaminergic neurons of the SNc. The dopaminergic neurons are unique in that their pacemaking activity is driven by subthreshold Ca^{2+} oscillations, while the other two classes rely on voltage–gated Na^+ channels to drive pacemaking. A fourth class of neurons contains the one major cell population that is conspicuously silent, the striatal medium spiny neurons. These neurons typically sit near –80 mV and require

transition to a depolarized upstate before action potentials can be triggered.

While several voltage–gated channels have been implicated in the variability of excitability in these four types of neurons, recent research in Na^+ channel properties suggest that unique biophysical alterations in the functionality of Na^+ channels expressed on the different neuron types could account for these variations. In cerebellar Purkinje neurons, which are the classical fast–spiking Na^+ pacemakers (Llinas and Sugimori, 1980; Hausser and Clark, 1997; Raman et al., 1997; Raman and Bean, 1999), Na^+ channels possess an additional mechanism that competes with the fast–inactivation gate at the intracellular mouth of the pore during depolarization of the membrane. Due to its novel recovery kinetics whereby the blocking particle must be removed before deactivation can occur, a resurgent Na^+ current is conducted upon repolarization once the blocking particle is removed and deactivation or fast–inactivation can occur. When a similar protocol is performed on quiescent (non–spontaneous) hippocampal CA3 neurons, no resurgent current is conducted (Raman and Bean, 1997). Since it's initial discovery, the resurgent current has been identified in other fast–spiking pacemaker neurons and neurons that have bursting or high–frequency firing patterns upon stimulation (Do and Bean, 2003; Afshari et al., 2004; Enomoto et al., 2006; Magistretti et al., 2006). This resurgent activity is believed to assist in autonomous, high–frequency firing through two processes. First, by competing with the fast–inactivation gate and exhibiting faster, more depolarized recovery kinetics, blocked channels are potentially 'rescued' from inactivation and made available sooner for the subsequent spike. Second, the presence of a depolarizing current during the downstroke and after–hyperpolarization potential (AHP) of the action potential could potentially prevent further hyperpolarization and prolongation of the AHP and jumpstart the Na^+–current driven depolarizing ramp towards threshold. In addition to this, previous work in the hippocampus suggests that Na^+ channels in fast spiking cells have slower inactivation kinetics than do regular spiking neurons (Martina and Jonas, 1997). By slowing inactivation kinetics, fewer Na^+ channels would be fast–inactivated during a spike, allowing for more channels available for the following spike. Furthermore, the ambient membrane potential between spikes between –65 and –45 mV.

In this potential range, Na^+ channels undergo fast inactivation, resulting in an inability of Na^+ to pass through the channel with further depolarization (Hille, 2001). If the biophysical properties of Na^+ channels in autonomous pacemakers were similar to those in regular spiking neurons (e.g., hippocampal and cortical pyramidal neurons), then only 20% of the Na^+ channels would be available to participate in pacemaking because of high levels of 'resting' channel fast inactivation (Maurice et al., 2001). This would make Na^+ channel dependent pacemaking very inefficient. A positive shift in the half–inactivation voltage in pacemaking neurons would allow for more channel availability at these near threshold potentials.

In addition to fast–inactivation, Na^+ channels are also susceptible to a more prolonged form of inactivation that develops during long periods at depolarized potentials and long trains of action potentials (Colbert et al., 1997; Jung et al., 1997; Mickus et al., 1999; Carr et al., 2003). The removal of Na^+ channels from the available pool by slow inactivation is particularly important to Na^+–driven pacemaking neurons because of their increased demand for subthreshold Na^+ currents to drive activity (Do and Bean, 2003). In prefrontal cortex neurons, 20% of the channels are slow–inactivated at –60 mV. In autonomous pacemakers, this is in addition to the slow inactivation that would be generated as a result of activity. By reducing the amount of slow inactivation, Na^+ pacemakers could increase the availability of Na^+ channels and thus increase the amount of depolarizing Na^+ current conducted during the inter–spike interval.

By analyzing the biophysical properties of Na^+ channels in Na^+–driven fast spiking (GP), Na^+–driven slow spiking (striatal cholinergic interneurons), Ca^{2+}–driven slow spiking (DA neurons) and quiescent neurons (striatal medium spiny neurons), we sought to determine the attributes important for distinguishing the firing patterns present in each neuron type.

Results

Molecular composition and fast gating kinetics of Na^+ channels in GP neurons

To understand how Na^+ channels contribute to high frequency autonomous activity in GP neurons, their gating properties and molecular composition were studied following acute isolation

from tissue slices. This preparation allows Na^+ channel currents in the somatic and proximal dendritic membrane to be pharmacologically isolated and accurately voltage–clamped for biophysical analysis and also allows cellular mRNA to be efficiently harvested for molecular profiling with single cell RT–PCR (scRT–PCR). As mentioned above, cells located within the physical confines of the GP are heterogeneous. Three cell types were identified visually and with scRT–PCR: medium sized neurons that expressed the 67 kDa isoform of glutamatic acid decarboxylase (GAD_{67}) and either enkephalin (ENK) or parvalbumin (PV); large neurons that expressed choline acetyltransferase (ChAT) but low or undetectable levels of GAD_{67}, ENK or PV (Fig. 1.1a). These large cholinergic neurons were excluded from further study. Profiling for the GABAergic (GAD_{67}+) population was also performed for the most commonly expressed pore forming α–subunit mRNAs in the adult brain: Nav1.1, Nav1.2 and Nav1.6, as well as for the four β–subunit mRNAs (Navβ1–4) (Isom et al., 1992; Isom et al., 1995b; Isom et al., 1995a; Goldin, 1999; Yu et al., 2003). GP neurons express all three Na^+ channel α–subunits (particularly with high level of Nav1.1 and Nav1.6 α–subunit) and the four Navβ accessory subunits (Fig. 1.1b).

The transient current typically associated with Na^+ channels was elicited with voltage steps from a holding potential of –80 mV (Fig. 1.2a). For the purposes of description, currents were fit with a Hodgkin–Huxley (HH) formalism (Fig. 1.2a, inset). Plots of the peak conductance estimates from these fits as a function of step voltage were fit with a third order Boltzmann function (Fig. 1.2b). The median half–activation voltage of a sample of GP neurons was –38.8 mV and the slope factor (Vc) was 7.3 mV (n=15) (data is summarized in non–parametric format in Figure 1.2b).

Deactivation of Na^+ channels was examined by activating them with a brief step to –20 mV and then stepping to more hyperpolarized membrane potentials (Fig 1.2c). Currents deactivated mono–exponentially at all potentials (at more depolarized potentials, inactivation accounted for the slower component of the bi–exponential decay seen in the traces). Time constants obtained by fitting these deactivation currents were plotted together with those obtained from the HH fits described above (Fig. 1.2d).

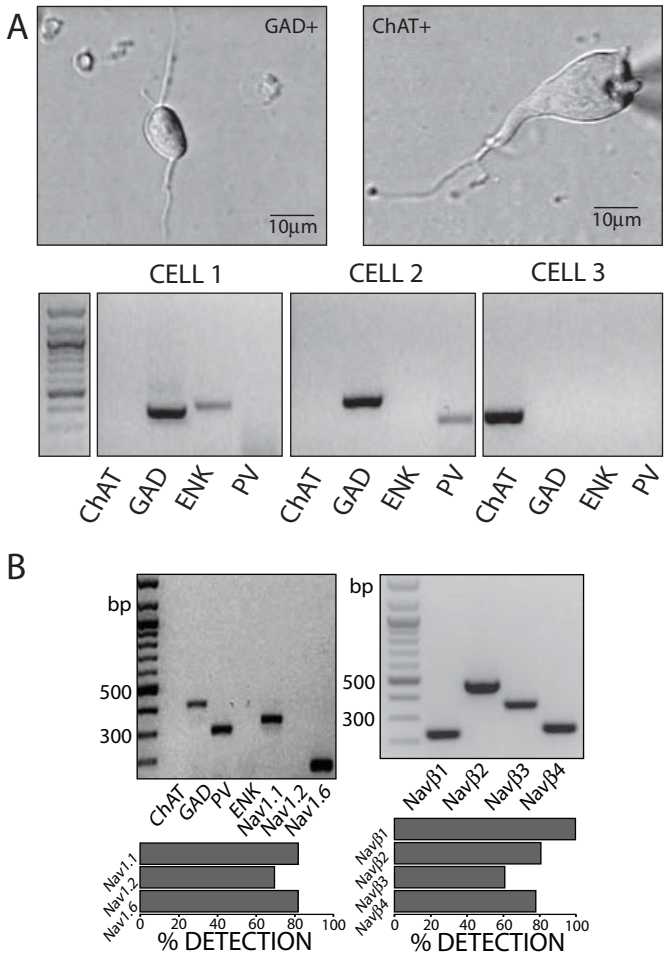

Figure 1.1. Morphological and molecular identification of GP neurons.

a. Light micrographs of two neuron types and mRNA expression from scRT–PCR of representative GP neurons. The GABAergic projection neuron on the left is roughly 10µm in diameter and expresses glutamic acid decarboxylase–67 (GAD) and enkephalin (ENK) or parvalbumin (PV) (cells 1 and 2). The larger cell on the right is a cholinergic basal forebrain neuron – it is roughly twice the diameter of GP projection neurons and expresses choline–acetyltransferase (ChAT).

b. Molecular phenotyping of GP neurons. GP neurons show high levels of expression of Nav1.1, 1.2 and 1.6, as well Navβ1, 2, 3 and 4.

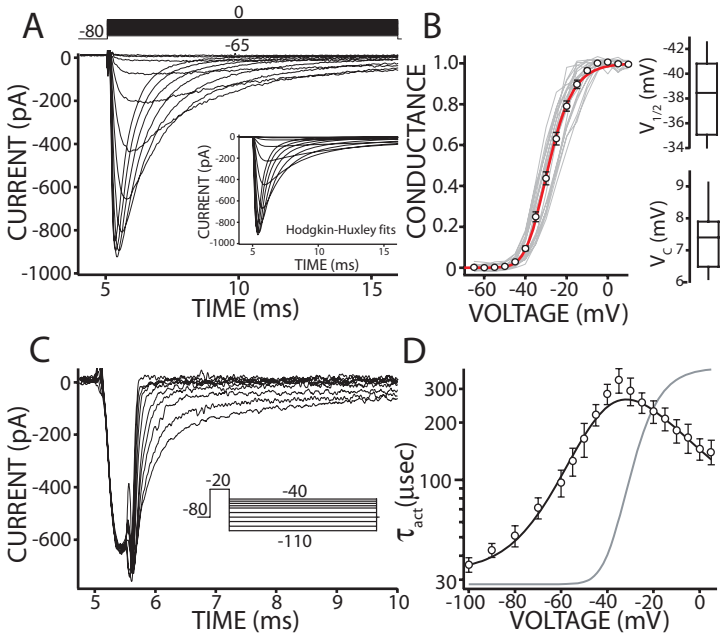

Figure 1.2. The kinetics of activation can be accurately measured in the dissociated, voltage–clamped GP neuron.

a. Transient currents measured by depolarizing steps from –80 mV can be accurately fit with a Hodgkin–Huxley formalism (inset).
b. The peak conductances as a function of step voltage are fit with a third order Boltzmann equation with a median half activation voltage (Vh) of –38.8 mV and slope factor (Vc) of 7.3 mV. Grayed lines are from individual neurons.
c. Deactivation is measured by brief steps to –20 mV and then repolarization of the membrane. The curve can accurately be fit with either a double exponential (if inactivation is occurring at that potential) or a single exponential (just deactivation).
d. Time constants of activation and deactivation can be compiled into a curve that predicts the kinetics of the activation gate at a given potential.

To characterize the steady–state voltage dependence of fast inactivation, the membrane potential was stepped to voltages between –110 and –30 mV for a period sufficient to allow this process to equilibrate (250 ms) and then a test pulse was given (Fig. 1.3a). Plots of the peak current evoked by the test pulse as a function of pre–pulse voltage were accurately described by a first–order Boltzmann function (Fig. 1.3b). The half–inactivation voltage$_{(median)}$ and slope factor$_{(median)}$ were V_h =–53 mV and V_c=5, respectively (data is summarized in non–parametric format in Figure 1.3b, n=21).

The kinetics of inactivation were determined using three different protocols. At depolarized potentials, the time constant for development of inactivation was determined from the Hodgkin–Huxley fits to the currents evoked in response to step depolarization (Fig. 1.2a, inset). Plotting currents evoked by steps to –30 mV and 0 mV on a log scale revealed two exponentials in the decay of the Na^+ current (Fig. 1.3e). Least squares analysis of the HH fits agreed with this inference, as the error of the curve fits reduced significantly with the addition of a second exponential component (at –30mV, $\chi^2_{(median)}=1.39x10^{-19}$ and $9.5x10^{-20}$ for single and double exponential fits, respectively; $p<0.05$ Wilcoxon signed rank test). Adding a third exponent did not significantly improve the fit over the double exponential ($\chi^2_{(median)}=9.4x10^{-20}$; $p>0.05$ Wilcoxon signed rank test). The development and recovery of inactivation near the foot of the activation curve were determined using standard multistep conditioning protocols. Plots of test step current as a function of time and voltage were best fit with bi–exponential equations (Figs. 1.3c,d). The fast and slow time constants from protocols were compiled into a single plot (Fig. 1.3f) and fit with a two state model derived from the HH formalism. The relative amplitude of the fast and slow time constants varied only modestly with membrane voltage (Fig. 1.3f, inset).

Properties of Na^+ channels in striatal cholinergic interneurons support pacemaking

Acutely isolated murine striatal cholinergic interneurons were identified by their relatively large somatic diameter (Fig. 1.4a). As in previous studies (Yan et al., 1997), scRT–PCR profiling of these neurons revealed that they express choline acetyltransferase (ChAT) and D_2 receptor

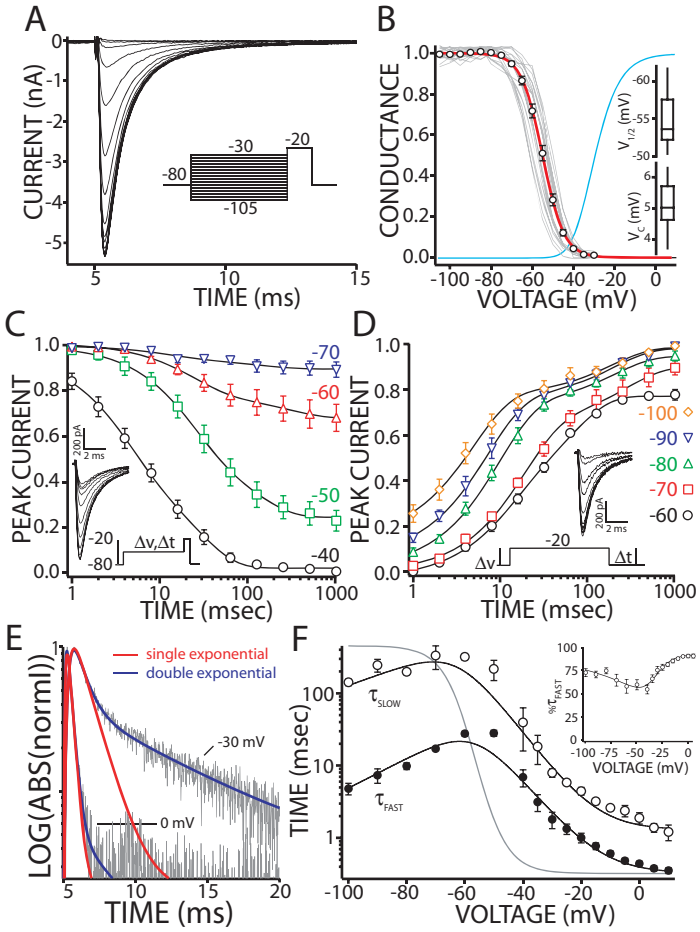
A
CURRENT (nA)
TIME (ms)
-30
-20
-80
-105
B
CONDUCTANCE
VOLTAGE (mV)
C
PEAK CURRENT
TIME (msec)
-70
-60
-50
-40
Δv,Δt
D
PEAK CURRENT
TIME (msec)
-100
-90
-80
-70
-60
Δv
Δt
E
LOG(ABS(normI))
single exponential
double exponential
-30 mV
0 mV
TIME (ms)
F
TIME (msec)
VOLTAGE (mV)

Figure 1.3. The fast inactivation kinetics of GP Na^+ channels are best described with two time constants.

a. The voltage dependence of inactivation was measured by 250 ms voltage steps, followed by a test pulse to –20 mV to measure peak amplitude.
b. The peak amplitude as a function of voltage is plotted and fit with a first order Boltzmann function. The half–inactivation voltage (Vh) was –53.7 mV and the slope factor (Vc) was 5.0 mV. Grayed lines are from individual neurons.
c. The development of inactivation at subthreshold potentials was measured by voltage steps of increasing length and fit with double exponential equations (–70 mV: blue triangles. –60 mV: red triangles. –50 mV: green squares. –40 mV: black circles).
d. The recovery of inactivation is measured by hyperpolarizing steps of increasing length, followed by a test pulse to –20 mV. Peak amplitudes as a function of time are best fit with a double exponential (–100 mV: orange diamonds. –90 mV: blue triangles. –80 mV: green triangles. –70 mV: red squares. –60 mV: black circles).
e. The decay of the sodium current generated by a step to –30 mV is most accurately fit with a double exponential fit (top trace, blue line). Decay at 0 mV could more accurately be fit with a single exponential than the step to –30 mV (bottom trace, red line), but was still better fit with a double exponential (blue line).
f. The fast and slow time constants (closed and open circles, respectively) for inactivation (measured from fits in fig. 1.2a inset and fig. 1.3c,d) are plotted as a function of voltage. The relative abundance of the fast time constant at each voltage is plotted in the inset.

mRNAs but not mRNA for 67kD isoform of glutamic acid decarboxylase (GAD_{67}) (Fig. 1.4b). To determine the molecular identity of the Na^+ channel subunits expressed by cholinergic interneurons, single neurons were profiled for mRNAs contributing to Na^+ channels. ScRT–PCR profiling was performed for the four β subunit mRNAs (Navβ1–4, n=10) — all four were consistently co–expressed in cholinergic interneurons (Fig. 1.4e,f, 1.9a)— and the three commonly expressed pore forming α–subunit mRNAs: Nav1.1, Nav1.2 and Nav1.6, as well as Nav1.5 (Goldin, 1999). Nav1.1 mRNA was detected in all cholinergic interneurons examined (n=16); Nav1.6 mRNA was detected in a large subset of the sample (12/16) whereas Nav1.2 mRNA was detected in only half (8/16) and Nav1.5 was rarely detected (1/6) (Fig. 1.4c,d). This detection profile differs from that previously reported in cortical pyramidal neurons only in the frequency of Nav1.2 mRNA detection (Maurice et al., 2001). The most parsimonious interpretation of these results is that cholinergic interneurons co–express significant levels of Nav1.1, 1.2 and 1.6 α subunit mRNAs, but that Nav1.2 mRNA abundance is relatively low. The relatively high level of Nav1.6 subunits in cholinergic interneurons may lead to relatively larger persistent Na^+ currents and an enhancement of pacemaking capacity (Raman et al., 1997; Maurice et al., 2001).

To determine if there was a high level of Na^+ channel inactivation during cholinergic interneuron pacemaking, whole–cell voltage clamp experiments were performed. To obtain an accurate biophysical characterization of the transient current, Na^+ currents were kept small by recording in a low (10 mM) external Na^+ concentration and with the internal Na^+ concentration near 4 mM. This modest concentration gradient ensured good voltage control and minimized series resistance errors. TTX–sensitive currents evoked by depolarizing voltage steps of increasing amplitude had kinetic features that were voltage dependent (Fig. 1.5a). These currents were fit with a modified Hodgkin–Huxley model (see Materials and Methods) to generate estimates of maximum conductance as a function of membrane voltage (Fig. 1.5c). These conductance estimates were well–fit with a third order Boltzmann function having a half–activation voltage near –40 mV (mean=–39.8 ± 0.8 mV, n=8) and a slope factor near 8 mV (7.6±0.2 mV) (Fig. 1.5d). As can be

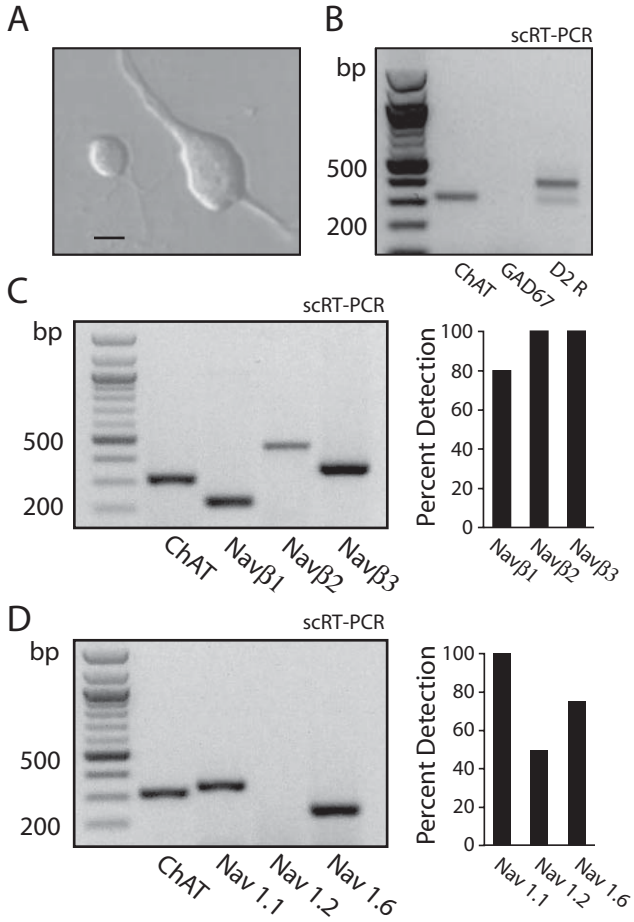

Figure 1.4. Identified cholinergic interneurons co–express Na^+ channel α– and β–subunit mRNAs.

a. Photomicrograph of an acutely isolated cholinergic interneuron and a neuron with an appearance resembling that of a medium spiny neuron. Scale bar is 8 μm.
b. Gel showing scRT–PCR amplicons for ChAT, GAD_{67} and D_2 receptor mRNAs. Note the neuron expressed ChAT and D_2 receptor mRNAs but not GAD_{67}.
c. Gel showing scRT–PCR amplicons from a ChAT–expressing neuron. The neuron co–expressed Navβ1–3 mRNAs. At the right is a summary from 10 neurons.
d. Gel showing scRT–PCR amplicons from a ChAT–expressing neuron. Both Nav1.1 and Nav1.6 mRNAs were detected. At the right is a detection summary for Nav1.1, 1.2 and 1.6 mRNAs in a sample of 16 neurons.

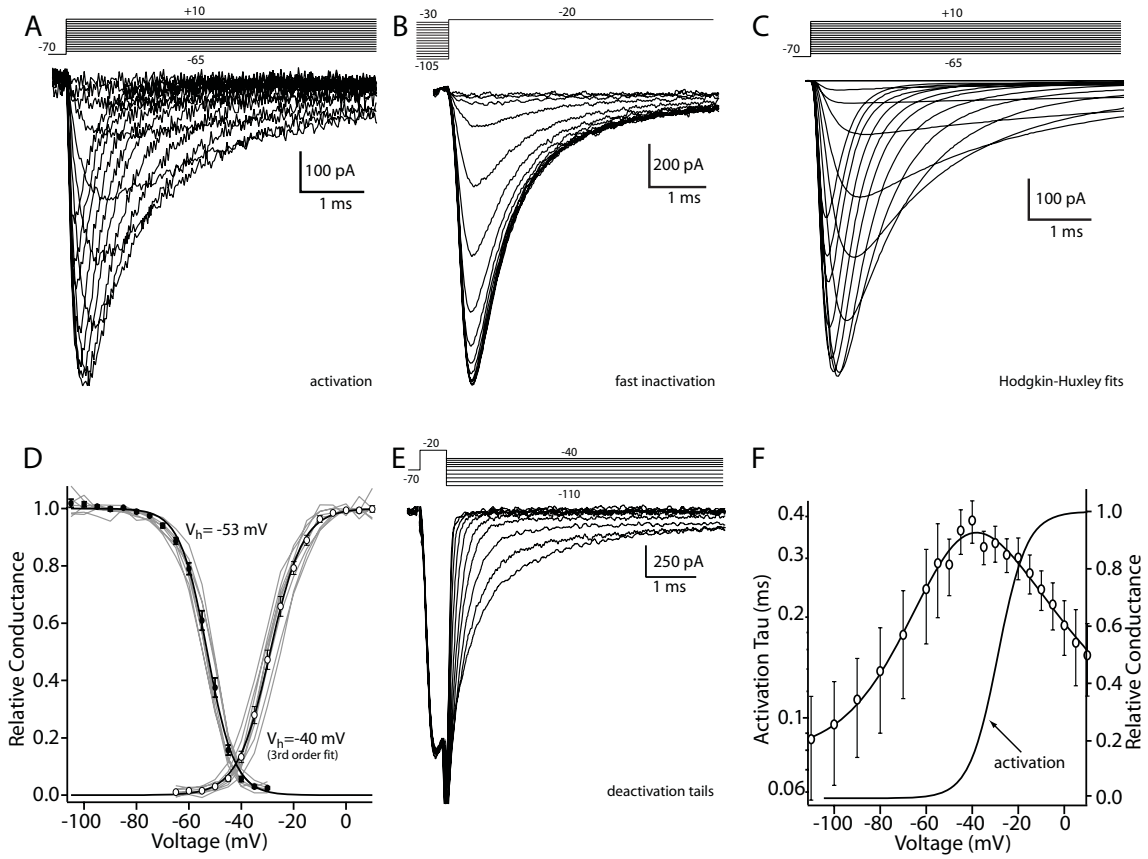

Figure 1.5. Activation properties of Na^+ channels in cholinergic interneurons.

a. Currents evoked in a cholinergic interneuron by a series of depolarizing steps from –65 mV to +10 mV from a holding potential of –70 mV.
b. Current evoked by a test step to –20 mV from increasingly more depolarized prepulse potentials. Prepulse was 200 ms and the holding potential was –70 mV.
c. Hodgkin–Huxley model fits to the data shown in *a*. Maximum conductance estimates from these fits were used to generate the activation plot in *d*.
d. Steady–state inactivation and activation data from a sample of neurons (n=8) are plotted and fit with Boltzmann functions of either first order (inactivation) or third order (activation). Grayed lines are from individual neurons. Also shown is the steady state inactivation plot derived from a sample of cortical pyramidal neurons.
e. Deactivation tail currents generated by briefly stepping to –20 mV and then repolarizing to potentials between –110 and –40 mV.
f. Plot of activation (n=8) and deactivation (n=4) time constants for a sample of neurons. Data were fit with a function of the form: (7.8e–5)+(6.1e–3)/((2.9e–6)exp(–(V–204.6)/16.4)+(4 .9e2)exp((V–63.9)/28.6)) and V is membrane voltage. Also shown is the fit of steady–state activation conductance from panel *d*.

seen by inspection of this plot, the macroscopic conductance was half maximal at about –30 mV. These parameters are similar to those obtained from a variety of other neurons from this study (Fig. 1.13a), including those that lack pacemaking ability and are regular spiking (Magistretti and Alonso, 1999; Maurice et al., 2001). Activation kinetics at depolarized potentials (>–40 mV) were extracted from Hodgkin–Huxley fits to the currents shown. Deactivation (the reversal of activation) kinetics were estimated by briefly depolarizing the membrane to activate channels and then repolarizing the membrane quickly to generate deactivation tail currents (Fig. 1.5e). These tail currents were well fit with a double exponential function; the fast component was taken as deactivation whereas the slow component was attributable to inactivation development (as slow time constant was identical to that reported in Fig. 1.6a). Pooled kinetic estimates were plotted and fit with a function derived from the Hodgkin–Huxley formalism assuming a single voltage–dependent state transition (Fig. 1.5f, See Materials and Methods).

The voltage dependence of Na^+ channel fast inactivation in cholinergic interneurons was studied with a combination of approaches. Using conditioning pulses of sufficient duration to reach equilibrium (250 ms), the voltage dependence of fast inactivation gating was extracted from the amplitude of currents evoked by a test voltage step to –20 mV (Fig. 1.5b). The amplitude of the current evoked by the test step was plotted as a function of conditioning voltage and fit with a first–order Boltzmann function (Fig. 1.5d). Half–inactivation voltages were near –55 mV (V_h=–52.9 ± 1.8 mV, n=8) and slope factors were near 5 mV (Vc = 5.1 ± 0.2 mV).

The development of fast inactivation at depolarized potentials (>–30 mV) was taken from the modified HH fits to currents activated by voltage steps, as shown above. In this potential range, current inactivation was voltage–dependent and invariably bi–exponential (see semi–log plot in Fig. 1.6a), with the fast component being the dominant component (although this fraction varied as a function of membrane potential – see inset Fig. 1.6a). At membrane potentials near threshold (–70 mV to –40 mV), inactivation rates were measured with a prepulse protocol (Fig. 1.6b). De–inactivation of Na^+ channels was measured by hyperpolarizing the membrane for variable durations

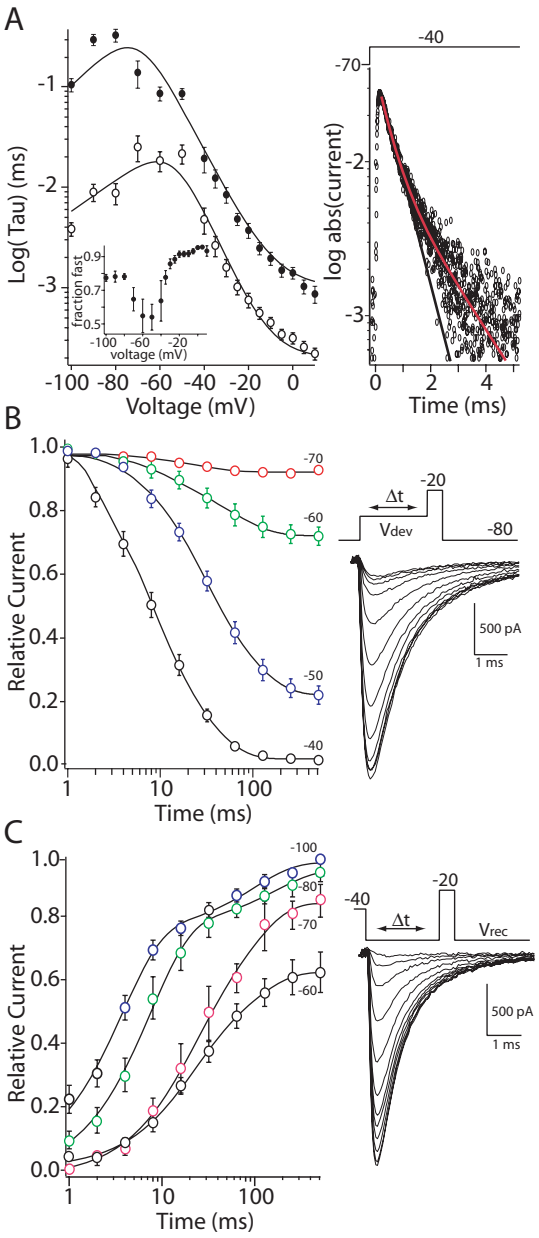
A
Log(Tau) (ms)
-1
-2
-3
-100 -80 -60 -40 -20 0
Voltage (mV)
fraction fast
0.9
0.7
0.5
-100 -60 -20
voltage (mV)
-40
-70
log abs(current)
-2
-3
0 2 4
Time (ms)
B
Relative Current
1.0
0.8
0.6
0.4
0.2
0.0
1 10 100
Time (ms)
-70
-60
-50
-40
Δt
-20
Vdev
-80
500 pA
1 ms
C
Relative Current
1.0
0.8
0.6
0.4
0.2
0.0
1 10 100
Time (ms)
-100
-80
-70
-60
-40
Δt
-20
Vrec
500 pA
1 ms

Figure 1.6. Inactivation kinetics of Na^+ currents in cholinergic interneurons are bi–exponential and voltage–dependent.

a. Summary showing fast inactivation development and recovery kinetics over a range of membrane potentials between +10 and –100 mV. Data points above –40 mV were derived from HH fits to currents evoked by depolarizing steps (see Fig. 1.5). The decay of these currents was typically bi–exponential as shown in the semi–log plot at the right. Here, currents evoked by a step to –40 mV are plotted after conversion to absolute values. Data were fit with a function as in 1.5f: fast time constant: (2e–3)+(5.5e–3)/((1e–6)exp(–(V–180)/20)+(4e3)exp((V–40)/10)); slow time constant: (7e–4)+(5.5e–3)/((6e–8)exp(–(V–140)/18)+(4e4)exp((V–90)/11)). Inset is a plot of the relative amplitude of the fast component as a function of membrane potential.

b. The development of fast inactivation at potentials between –70 and –40 mV was estimated by plotting the amplitude of the current evoked by a test step to –20 mV that followed a pre–pulse of variable duration (n=8). Data points were fit with a bi–exponential function.

c. The recovery from fast inactivation at potentials between –60 and –100 mV was determined by using a similar strategy to that shown in *b*. Peak current plots for a sample of neurons are shown along with bi–exponential fits (n=11). The parameters derived from *b* and *c* are plotted in panel *a*.

after a depolarizing step (Fig. 1.6c). Data derived from these protocols were well–fit only with a bi–exponential function, as with inactivation development. Data from all three protocols were pooled and then fit using a single state transition model (Fig. 1.6a).

Slow inactivation of Na^+ channels is governed by a power law

In addition to fast inactivation, another mechanism that reduces the availability of Na^+ channels is slow inactivation. Although relatively little is known about the molecular mechanisms of slow inactivation, channels are capable of entering this state from either the open or fast–inactivated states (Jung et al., 1997; Mickus et al., 1999; Carr et al., 2003; Chen et al., 2006). Thus, slow inactivation could be particularly important for GP neurons that, like their neighbors in the STN, spike autonomously at high rates and rarely hyperpolarize more than –65mV in a slice preparation (Do and Bean, 2003).

Entry of channels into the slow inactivated state from the fast–inactivated state was studied using long depolarizing steps, while entry from the open state was demonstrated with trains of short pulses (5 msec step to –20 mV at 20 Hz). Occupancy in the slow inactivated states is estimated by measuring channel availability after a one second step to –80 mV, a sufficient time to allow full recovery from fast inactivation. During pulse trains, entry of channels into the slow inactivated state from the open state occurs with a time constant of 4.5±1.0 seconds, and plateaus at 25% within 15 seconds. With prolonged steps to –20 mV, the entry into the slow inactivated state was comparable, at 4.0±0.5 seconds, but steps inactivated significantly more Na^+ channels after 15 seconds and inactivation continued to grow (Fig. 1.7a). However, if one accounts for the difference in time spent at the depolarized potential where the transition to the slow inactivated state is occurring (one tenth of the time during the 20 Hz train), the time constant of entry appears to be 10 times faster from the open state than from the fast inactivated state. So, while entry is faster, there is less overall entry from the open state during a pulse train for several reasons. First, because the channels spend so little time in the open state, there is insufficient time to accumulate. Second, recovery can occur between pulses, reducing accumulation. Third, though not tested here, it is possible that recovery into the

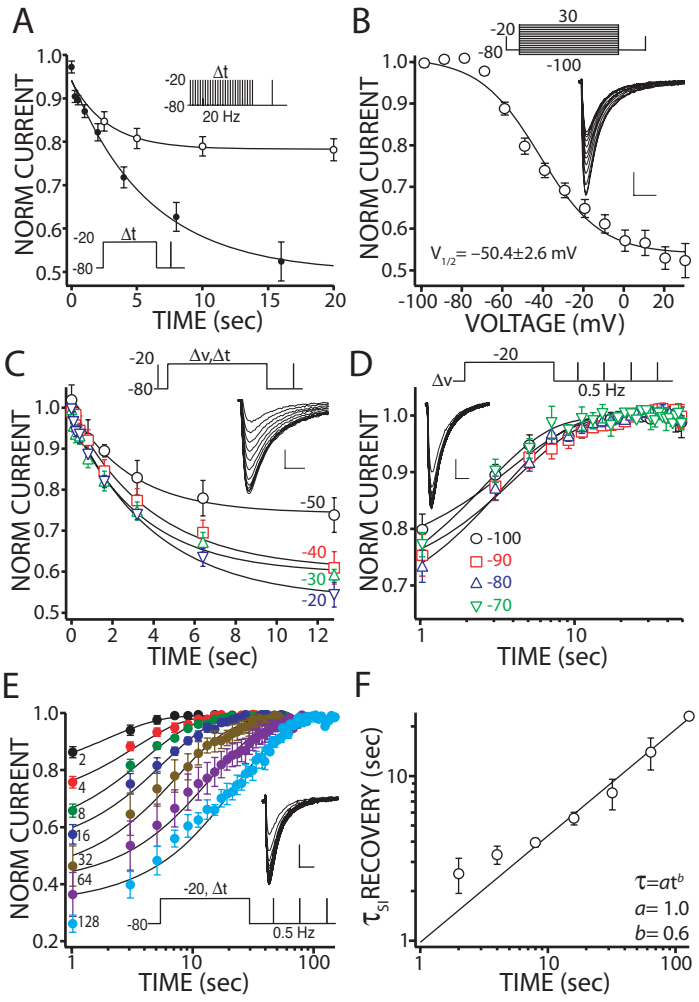
A
B
C
D
E
F
NORM CURRENT
TIME (sec)
VOLTAGE (mV)
Δt
20 Hz
30
-20
-80
-100
V1/2= −50.4±2.6 mV
ΔvΔt
Δv
0.5 Hz
-50
-40
-30
-20
-100
-90
-80
-70
2
4
8
16
32
64
128
-20, Δt
τSI RECOVERY (sec)
τ=atb
a= 1.0
b= 0.6

Figure 1.7. GP Na^+ channels undergo slow inactivation during extended periods at depolarizing potentials or long trains of depolarizing pulses.

a. Slow inactivation can be generated both by prolonged steps to depolarized potentials (closed circles) and trains of brief pulses (open circles), as measured by test pulses after increasing lengths of pulses or trains. The time constants for development during the pulse trains and steps are 4.5±1sec and 4.0±0.5sec, respectively.
b. The pseudo–steady state of slow inactivation after 5 seconds is measured by a test pulse one second after an inactivating step. The peak current is plotted as a function of voltage and fit with a first order Boltzmann equation. The half–inactivation voltage at this time point is –50.4±2.6 mV, with a slope factor of 20±2 mV. Scale bars for traces (inset) are 200 pA and 2 ms.
c. The kinetics of entry into the slow inactivated state are not voltage dependent (–50 mV: 4.0±2.1 sec. –40 mV: 4.3±0.7 sec. –30 mV: 3.7±0.5 sec. –20 mV: 4.0±0.5 sec [n=5]). seccale bar sec for trace sec (in secet) are 200 pA and 2 m sec.
d. The kinetic sec of recovery from seclow inactivation are not voltage dependent (–100 mV: 4.0±0.6 sec. –90 mV: –3.9±0.7 sec. –80 mV: 3.7±0.5 sec. –70 mV: 3.2±0.7 sec [n=5]). seccale bar sec for trace sec (in secet) are 200 pA and 2 m sec.
e. The recovery from slow inactivation is measured by test pulses every 2 seconds after increasing lengths of inactivating steps to –20 mV (2 sec: black. 4 sec: red. 8 sec: green. 16 sec: navy blue. 32 sec: brown. 64 sec: purple. 128 sec: sky blue). Scale bars for traces (inset) are 200 pA and 2 ms.
f. The time constants for recovery as a function of time at inactivating voltage obeyed a power law with $\tau=t^{0.6}$, where t is the length of the step to –20 mV.

open state is accelerated as well.

Estimating the voltage dependence of Na^+ channel availability at depolarized potentials over long periods is problematic because dissociated neurons do not tolerate prolonged depolarization well, but a quasi–steady state can be calculated by using 5 sec conditioning steps. These data were reasonably fit with a single Boltzmann function having a half–inactivation voltage of –50.4±2.6 mV and a slope factor of 20±2 mV (Fig. 1.7b).

While the amount of slow inactivation appears to show a dependence on voltage, the kinetics of entry and recovery from this state do not. Unlike fast inactivation, where entry into the fast–inactivated state is faster at more depolarized potentials and recovery is faster at more hyperpolarized potentials, the kinetics of slow inactivation are constant throughout the voltage range. With a step to –20 mV, slow inactivation developed with a time constant of 4.0±0.5 sec, while at –50 mV, the time constant of development is 4.0±0.6 sec (Fig. 1.7c). At –80 mV, the rate of recovery from a 5 second step is 3.7±0.5 sec, and at –100mV it is 4.0±0.6 sec (Fig. 1.7d).

In hippocampal dentate granule cells, the recovery from slow inactivation is dependent on the length of step used to produce inactivation. The longer the time spent at a depolarized potential, the slower the recovery kinetics (Ellerkmann et al., 2001). Recovery from slow inactivation in pallidal neurons is also dependent on the length of inactivating step. Plotting the time constant of recovery as a function of pre–pulse duration revealed a power law relationship of the form $\tau=t^{0.6}$, where t is the length of the inactivating step to –20mV (Fig. 1.7d,e). The deviation from the power law function at short pre–pulse durations is probably a measurement artifact, as there is a mixture of recovery from fast– and slow– inactivated states with shorter inactivating steps. This is not as crucial for longer inactivating steps because relatively little slow inactivation recovery occurs during the first second.

Persistent and Resurgent Na^+ currents in pacemaking neurons

Sub–threshold Na^+ currents have an important role in governing the excitability of neurons. Persistent Na^+ currents have well characterized roles in shaping excitability and action potential generation (Pennartz et al., 1997; Bevan and Wilson, 1999; Raman and Bean, 1999; Agrawal et al.,

2001; Taddese and Bean, 2002; Do and Bean, 2003). In addition to persistence, Na^+ channels in Purkinje and other fast spiking neurons display a gating mode that leads to a resurgent current upon repolarization after a spike (Raman and Bean, 1997; D'Angelo et al., 2001; Do and Bean, 2003; Afshari et al., 2004; Cummins et al., 2005; Enomoto et al., 2006; Magistretti et al., 2006).

Both sub–threshold persistent and resurgent Na^+ currents are present in GP neurons. The persistent current is present in the voltage range where activation of Na^+ channels has begun but inactivation is incomplete. During a four second ramp from –80 mV to 0 mV, persistent current is evident at potentials more depolarized than –65 mV and peaks at –40 mV with an amplitude of 55.3±6.4 pA in physiological external Na^+ concentration (Fig. 1.8e). This voltage range matches that between the trough of the AHP (–61±1mV) and the threshold for firing (–44±1mV) in GP neurons, suggesting that Na^+ channel currents play an important role in driving autonomous pacemaking.

Resurgence is thought to be created by removal of an open channel blocking particle as the membrane repolarizes (Raman and Bean, 1997). This blocking particle has been hypothesized to be the cytoplasmic tail region of the auxiliary β4 subunit (Grieco et al., 2005). As expected from their ability to spike at high frequencies and their expression of β4 subunit, GP neurons display a prominent resurgent Na^+ current (Fig. 1.8a). The kinetics of the current were similar to those described for Purkinje and STN neurons (Fig. 1.8b,c,d) (Raman and Bean, 1997; Do and Bean, 2003). As in STN neurons, slow inactivation reduced transient, persistent and resurgent Na^+ channel currents to similar extents, suggesting that the channels underlying these currents all were subject to this process (Fig. 1.8f).

The dependence of this gating mode on the β4 subunit is not clear in the basal ganglia. Immunocytochemistry studies show that β4 subunit is highly expressed in the striatum and not in the substantia nigra pars compacta (SNc) (Yu et al., 2003). Single cell RT–PCR confirmed that medium spiny neurons and cholinergic interneurons of the striatum express β4 mRNA and SNc neurons do not (Fig. 1.9a). However, electrophysiological study of dissociated neurons revealed that medium spiny neurons had no discernible resurgent current, while cholinergic interneurons and SNc

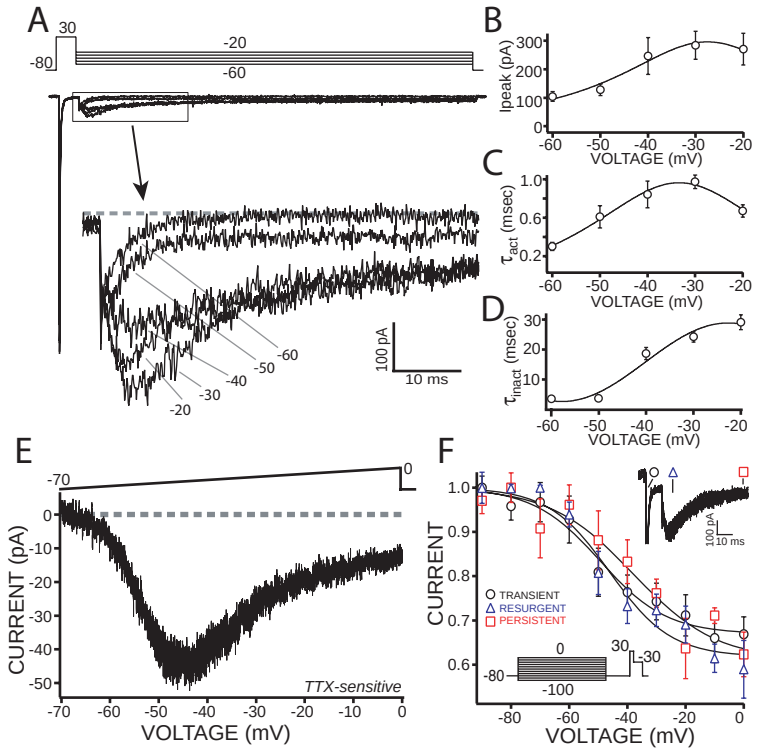

Figure 1.8. Na^+ channels in the GP conduct both persistent and resurgent currents.

a. Upon repolarization of the membrane from depolarized potentials, a 'resurgent' Na^+ current is conducted by channels that are transitioning from the blocked state to the inactive or closed states.

b. The amplitude of the resurgent current peaks near –30 mV at 260 pA (median, see Fig. 3.3b for boxplot).

c. The time constant of activation is plotted against repolarization potential. The activation kinetics are roughly five times slower than the activation kinetics of the transient current.

d. The time constant of decay of the resurgent current as a function of repolarization potential. The kinetics are in the range of the slow time constant for fast inactivation.

e. The persistent current is generated by a 4 second ramp from –80 mV to 0 mV. The conductance peaks at –40 mV with an amplitude of 55.3±6.4 pA.

f. Slow inactivation of transient (black circles, measured at depolarizing step to +30 mV), resurgent (blue triangles, peak current upon repolarization to –30 mV) and persistent (red squares, steady state current measured at end of repolarization step) are plotted as a function of prepulse potential and fit with a Boltzmann equation. The half inactivation for transient, resurgent and persistent currents were –49±3 mV, –45±5 mV, –51±2 mV, respectively, and the slope factors were 7±2 mV, 8±3 mV and 6±1 mV.

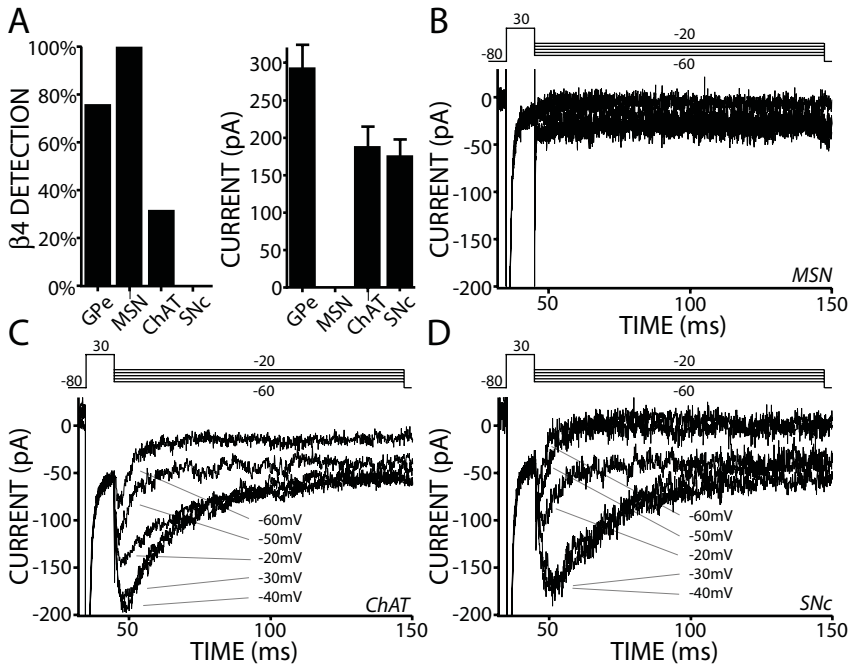

Figure 1.9. Comparisons of molecular profiling and resurgent current amplitudes of a subset of basal ganglia neurons.

a. Left, neurons from the GP and striatum (medium spiny neurons (MS) and cholinergic interneurons (ChAT)) express β4 while DA neurons of the SNc do not contain mRNA for the β4 protein (GP: 19 of 25 neurons, MSN: 9 of 9, ChAT: 3 of 10, SNc 0 of 20). Right, GP, ChAT and SNc neurons all exhibit resurgence, while MSNs do not (n=25 [GP], 5 [MSN], 6 [ChAT], 10 [SNc]).

b. Representative traces of resurgent current elicited by repolarizing the membrane from a depolarized potential in medium spiny neurons.

c. Representative traces of resurgent current elicited by repolarizing the membrane from a depolarized potential in cholinergic interneurons.

d. Representative traces of resurgent current elicited by repolarizing the membrane from a depolarized potential in DA neurons of the SNc.

neurons had prominent resurgent currents (Fig. 1.9b,c,d). The lack of resurgent current in medium spiny neurons could be a reflection of the restricted sampling of the somatodendritic membrane and not the axon, but it is more difficult to reconcile the inability to detect signs of the β4 subunit in SNc neurons with the prominence of the resurgent gating mode. This suggests that β4 in medium spiny neurons is not sufficient, nor necessary in SNc neurons, to produce the resurgent current. Regardless, the presence of resurgence in all three spontaneously active neurons and absence of it in quiescent neurons suggest an important role of resurgence in autonomous activity. This issue will be further addressed in the section 3.3.

Striatal projecting neurons have similar properties to the GP neuron population

Morphological and electrophysiological studies performed in rodents and primates are in agreement that there is one predominant cell type within the GP (DeLong, 1971; Bergstrom and Walters, 1981; Iwahori and Mizuno, 1981; Difiglia et al., 1982; Nambu and Llinas, 1994, 1997; Cooper and Stanford, 2000). These GP neurons express GAD_{67} and parvalbumin, have discoidally arborizing dendrites, and project an axon to the subthalamic nucleus (STN) (Kita, 1994; Kita and Kitai, 1994; Yelnik et al., 1996; Hoover and Marshall, 1999; Parent et al., 2000; Kita and Kita, 2001; Hoover and Marshall, 2002; Chan et al., 2004). This population of GP neurons is intermixed with ENK–expressing GABAergic neurons that predominantly project back to the striatum (Ruskin and Marshall, 1997; Hoover and Marshall, 1999; Voorn et al., 1999; Kita and Kita, 2001; Marshall et al., 2001; Hoover and Marshall, 2002). Throughout the course of random sampling of GP neurons, this subpopulation was occasionally encountered, as revealed by the biocytin visualization procedure, in which the axon of striatal–projecting neurons were recovered within the confine of dorsal striatum (Fig. 1.10a). However, due to the inefficient sampling of this population, studying the physiology of this subgroup of neurons with random sampling proved too inefficient. To better understand whether this subgroup of GP neurons exhibit membrane properties (i.e. Na^+ channels) with unique biophysical properties, these neurons were retrogradely labeled with intrastriatal injection of rhodamine microspheres. 3 days were then allowed for retrograde transport

of rhodamine microspheres back to the somata of pallidostriatal neurons (Bevan et al., 1998). Through this technique, we were able to visually identify striatal–projecting GP neurons both in the slice and in the acutely dissociated preparation (Fig. 1.10b,c,e). Whole–cell current–clamp recordings demonstrate that the cellular physiology of these neurons is similar to those observed in the general population of typical pallidal neurons recorded previously (Fig. 1.10d). Voltage–clamp recordings of Na^+ currents in the acute preparation also showed similar biophysical properties and amplitudes to the general population of globus pallidus neurons (Fig. 1.10f,g). These neurons do not appear to be cholinergic basal forebrain neurons because these rhodamine–labeled neurons share obvious similarities in their morphological and biophysical properties to typical GP neurons. Neurons in this class were not subjected to molecular fingerprinting of phenotypic markers, as there is evidence that neither the projection target nor the neurochemical content of GP neurons are distinct. Our preliminary data as well as others have suggested that some PV–expressing neurons co–express ENK. Moreover, striatal–projecting GP neurons also send their axon downstream to STN and SNr (Bevan et al., 1998; Parent et al., 2000).

Na^+ currents are not enhanced in SNc Cav1.3–/– neurons despite transition to Na^+ pacemaking

Similar to striatal cholinergic interneurons, dopaminergic neurons of the substantia nigra are slow–spiking pacemakers (Grace and Bunney, 1983b, a; Yung et al., 1991; Grillner and Mercuri, 2002). Although they exhibit burst or irregular firing in response to synaptic input, autonomous pacemaking is predominantly in the single spike mode (0.2–10 Hz). The ionic mechanisms underlying autonomous activity in these neurons are debated. Membrane potential oscillations are reduced in amplitude and frequency by TTX, suggesting that spiking and Na^+ channel currents contribute to pacemaking (Yung et al., 1991; Wilson and Callaway, 2000). However, Na^+ currents are not necessary for subthreshold oscillations. DA neurons were identified in coronal slices of the mesencephalon that included the SNc (Fig. 1.11a,b) and their firing rates during pharmacological manipulation were measured. In the presence of TTX and in the absence of strong extrinsic Ca^{2+} buffers, dopaminergic neurons continue to oscillate at a low frequency (Fig. 1.11c). Moreover,

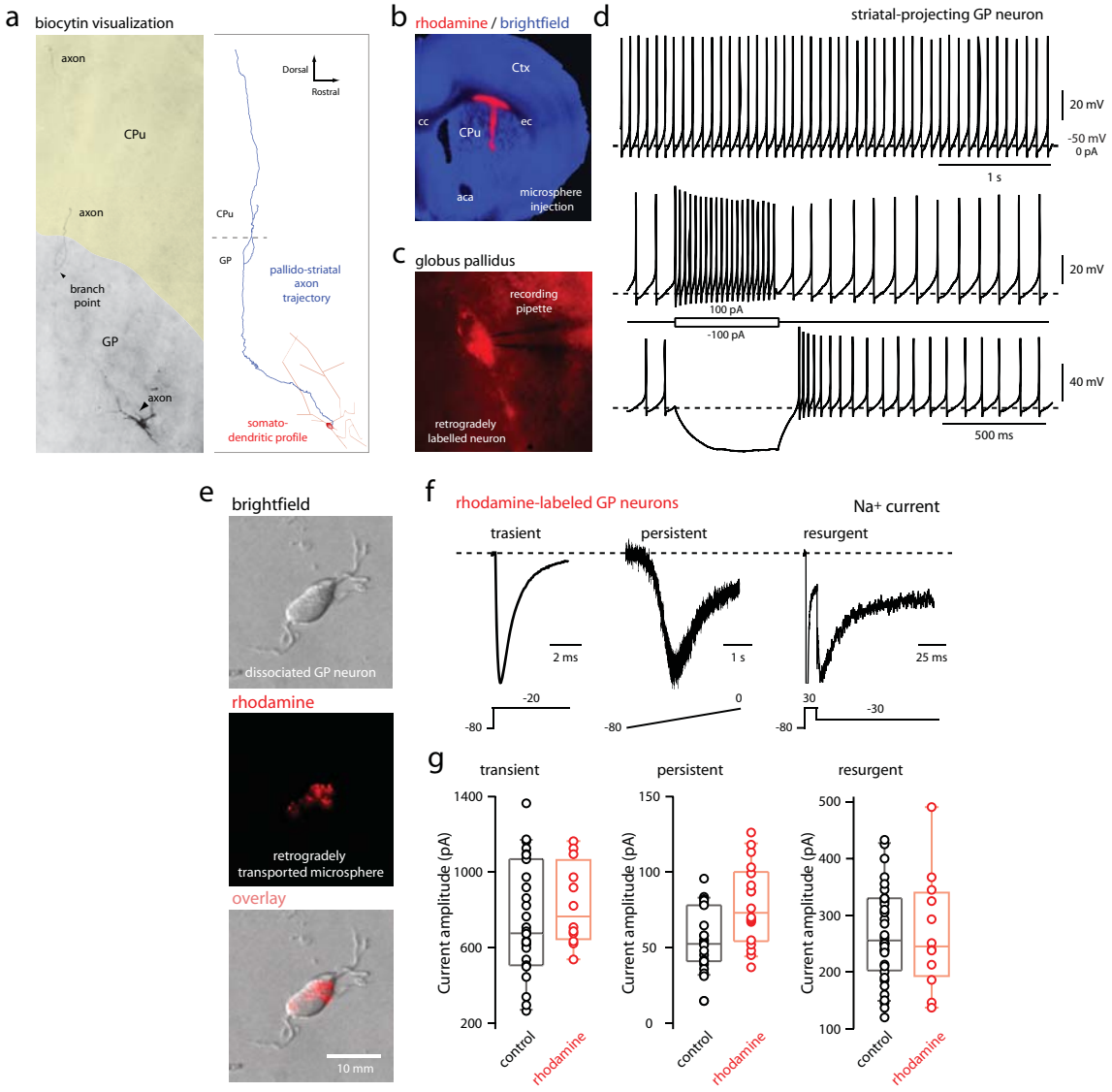
a
biocytin visualization
axon
CPu
axon
branch point
GP
axon
Dorsal
Rostral
CPu
GP
pallido-striatal axon trajectory
somato-dendritic profile
b
rhodamine / brightfield
Ctx
cc
CPu
ec
aca
microsphere injection
c
globus pallidus
recording pipette
retrogradely labelled neuron
d
striatal-projecting GP neuron
20 mV
-50 mV
0 pA
1 s
20 mV
100 pA
-100 pA
40 mV
500 ms
e
brightfield
dissociated GP neuron
rhodamine
retrogradely transported microsphere
overlay
10 mm
f
rhodamine-labeled GP neurons
Na+ current
trasient
persistent
resurgent
2 ms
1 s
25 ms
-20
-80
0
-80
30
-30
-80
g
transient
persistent
resurgent
Current amplitude (pA)
1400
1000
600
200
150
100
50
0
500
400
300
200
100
control
rhodamine

Figure 1.10. Anatomical and physiological features of pallido–striatal neurons.

a. Somatodendritic morphology (red) and axon trajectory (blue) of a typical mouse striatal–projecting GP neuron. Visualization of biocytin (injected via patch electrode) revealed Golgi–like labeling. This neuron emitted three aspiny, long, sparsely branched primary dendrites. The axon gave off two collaterals (a1, a2) that both extended into the caudate putamen. Inset represents the location of the neuron (red arrowhead). Inset shows location of cell with respect to other brain structures.

b. A light micrograph of a coronal mouse striatal slice showing the site (red) of rhodamine microsphere injection.

c. A retrogradely–labeled striatal–projecting GP neuron visualized with a Texas Red filer cube set.

d. Striatal–projecting neurons have physiological properties indistinguishable from other GABAergic projection neuron within the nucleus. Plotted are spontaneous autonomous pacemaking and membrane responses to current injection (+100 and –100 pA) of the neuron shown in *c*.

e. Identification of pallido–striatal neurons in the acute dissociation prep. Top, a light micrograph showing the morphology of a typical dissociated GP neuron under Hoffman modulation contrast. Middle, intrastriatal injection of rhodamine revealed retrograde transport of microspheres, as visualized with a Texas Red filter cube set. Bottom, overlay of brightfield and fluorescence images.

f. Voltage protocols (bottom) and representative traces (top) of transient, persistent and resurgent Na^+ currents recorded from typical rhodamine bead labeled GP neurons.

g. Population data on Na^+ current amplitudes from control and reserpine–treated animal groups. These parameters are not significantly different from their corresponding controls (p values > 0.05, Mann–Whitney Rank Sum Test). $Transient_{(median)}$: control=677 pA (n=31), rhodamine=831.5 pA (n=12). $Persistent_{(median)}$: control=52.1 pA (n=15), rhodamine=73.0 pA (n=15). $Resurgent_{(median)}$: control=255 pA (n=36), rhodamine=269.3 pA (n=12).

blockade of Cav1/L–type channels stops autonomous pacemaking (Fig. 1.11d). This termination of spontaneous and oscillatory behavior does not disrupt their responsiveness to extrinsic input (Harris et al., 1989; Nedergaard et al., 1993; Mercuri et al., 1994). The hyperpolarizing phase of the subthreshold oscillation seen in TTX is disrupted by Ca^{2+} chelation or blockade of apamin–sensitive Ca^{2+}–dependent K^+ channels (Ping and Shepard, 1996). These channels appear to be composed largely of SK3 subunits (Wolfart et al., 2001). Thus, it would seem that two channels — Cav1.3 and SK3 — are all that is necessary for the oscillations underlying autonomous pacemaking in SNc DA neurons.

This conclusion is supported by neurons from *med*^{TG} animals, which lack Nav1.6 subunits, which have been found to be important in the autonomous activity of Purkinje and GP neurons but not STN neurons (Khaliq et al., 2003; Do and Bean, 2004). Autonomous activity is only modestly reduced in Nav1.6–/– SNc neurons ($frequency_{(median)}$ of Nav1.6–/– neurons = 2.0 Hz, $frequency_{(median)}$ of wild–type = 2.5 at 34°C;$p<0.05$, Kruskal–Wallis), likely because there is a decreased demand for subthreshold Na^+ currents to drive spontaneous discharge (Fig 1.11e,f).

It would follow from acute pharmacologic studies where blockade of L–type Ca^{2+} channels terminates spontaneous activity that genetic deletion of this channel would have a similar result. However, Cav1.3–/– neurons do not show any reduction in their firing rates, still firing at a $frequency_{(median)}$ of 2.4 Hz (Fig 1.11e,f). One potential mechanism by which Cav1.3–/– DA neurons could compensate for a loss of Ca^{2+} channel activity is by increasing their Na^+ currents. Whole–cell voltage clamp studies show that Na^+ channels in these neurons possess all the attributes suggested to be necessary for autonomous activity in the Na^+ pacemakers. However, neither voltage dependence of gating or amplitudes of transient, persistent and resurgent currents are altered in the Cav1.3–/– neurons (Fig. 1.12b,c,d,f).

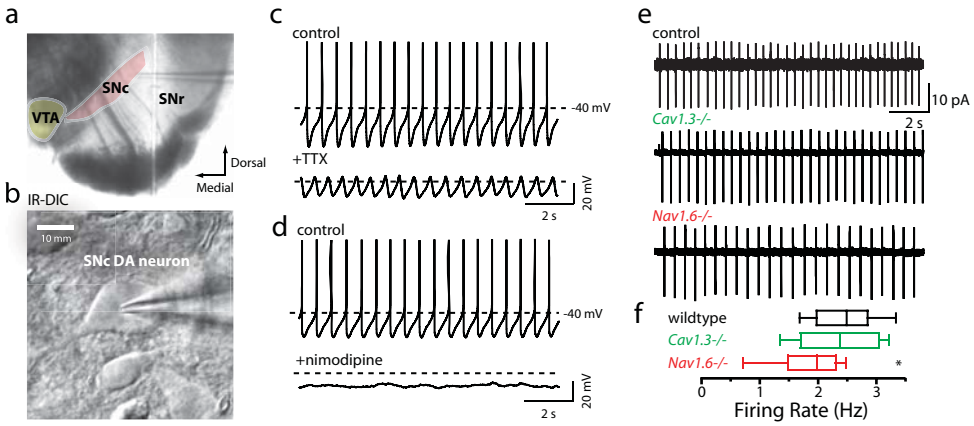

Figure 1.11. Pacemaking properties of SNc DA neurons from WT, Cav1.3–/– and Nav1.6–/– neurons.

a. Light micrograph showing the location of the substantia nigra pars compacta (SNc) and adjacent structures in mouse coronal slice. The SNc is situated dorsal to the substantia nigra pars reticulata (SNr) and medial to the ventral tegmental area (VTA).
b. Visualized whole–cell recordings from SNc DAergic neurons were made under IR–DIC videomicroscopy.
c. Under whole–cell configuration, application of saturating concentration of TTX (1 μM) abolishes spiking but leaves intact the Ca^{2+}–dependent pacemaker potentials.
d. Application of a Cav1/L–type Ca^{2+} blocker, nimodipine (10 μM), abolishes autonomous pacemaking in WT DA neurons.
e. Non–invasive, tight seal (>3 GΩ) cell–attached patch recordings showing a similar ($p>0.05$, Mann–Whitney Rank Sum Test) firing rate in WT (median=2.49 Hz, n=73) and Cav1.3–/– (median=2.39 Hz, n=42). A significant reduction in autonomous pacemaking rate is noted in Nav1.6–/– (median=1.99 Hz, n=15, $p<0.001$, Mann–Whitney Rank Sum Test).
f. Non–parametric summary of firing rates in control (top, black), Cav1.3–/– (middle, green) and Nav1.6–/– neurons (bottom, red).

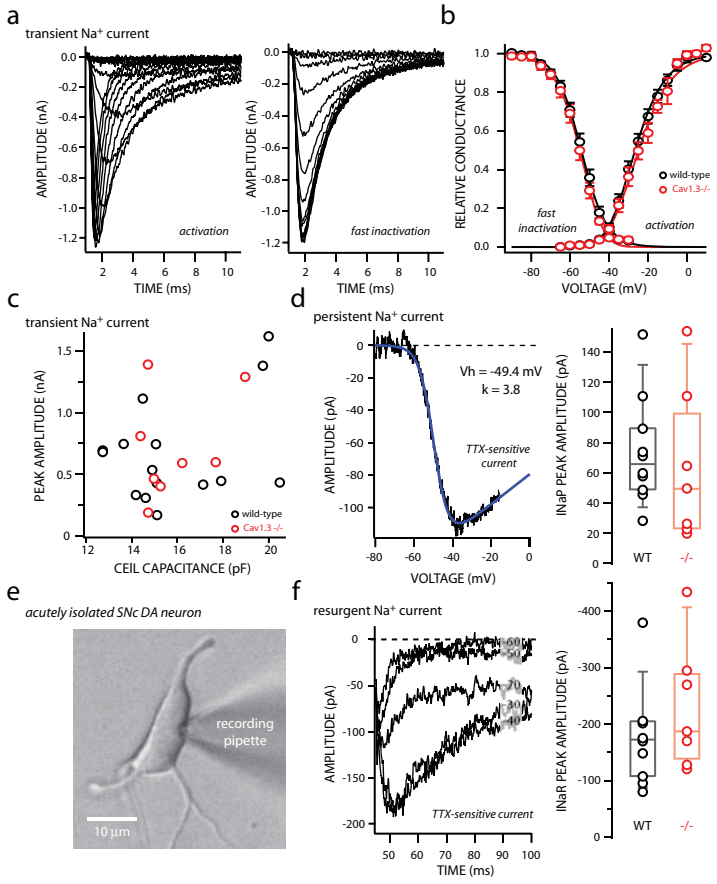
a
transient Na+ current
AMPLITUDE (nA)
activation
fast inactivation
TIME (ms)
b
RELATIVE CONDUCTANCE
wild-type
Cav1.3-/-
fast inactivation
activation
VOLTAGE (mV)
c
transient Na+ current
PEAK AMPLITUDE (nA)
wild-type
Cav1.3 -/-
CEIL CAPACITANCE (pF)
d
persistent Na+ current
Vh = -49.4 mV
k = 3.8
TTX-sensitive current
AMPLITUDE (pA)
VOLTAGE (mV)
INaP PEAK AMPLITUDE (pA)
WT
-/-
e
acutely isolated SNc DA neuron
recording pipette
10 µm
f
resurgent Na+ current
-50
-70
-90
-110
TTX-sensitive current
AMPLITUDE (pA)
TIME (ms)
INaR PEAK AMPLITUDE (pA)
WT
-/-

Figure 1.12. Biophysical properties of Na^+ channels are not altered in Cav1.3–/– SNc DAergic neurons.

a. Left, transient Na^+ currents evoked in a SNc neuron by a series of depolarizing steps from –65 to +10 mV from a holding potential of –70 mV. Right, current evoked by a test step to –20 mV from increasingly more depolarized prepulse potentials. Prepulse was 200 msec, and the holding potential was –70 mV.

b. Steady–state inactivation (WT: $Vh_{(median)}$ =–55.0 mV, Vc_{median}=5.7 mV, n=18; Cav1.3–/–: $Vh_{(median)}$ =–51.6 mV, $Vc_{(median)}$ =6.4, n=9) and activation (WT: $Vh_{(median)}$ =–39.4mV, $Vc_{(median)}$ =8.7 mV, n=18; $Ca_v1.3$–/–: $Vh_{(median)}$ =–35.2mV, $Vc_{(median)}$ =9.0 mV, n=9) data from WT (black) and Cav1.3–/– (red) are plotted and fit with Boltzmann functions of either first order (inactivation) or third order (activation), no significant difference was noted ($p>0.05$, Mann–Whitney Rank Sum Test).

c. Plotting peak transient current amplitude as a function of cell capacitance suggests adequate voltage control in our preparation, despite the relatively large somatic diameter of SNc. No systematic difference in the Na^+ channel density.

d. Left, ramping somatic potential from –80 to 0 mV revealed a TTX–sensitive persistent current. Blue line represents the best fitting to the current trace with an extended Boltzmann function as follows: $I=A\{[1+\exp[(Vm–Vh)/Vc]\}*(Vm–V_{Na})$, where V_{Na} is the reversal potential of sodium current. The fitting parameters are Vh=–49.4mV, k=3.8. No change ($p>0.05$, Mann–Whitney Rank Sum Test) in the peak amplitude of persistent currents was seen between WT ($amplitude_{median}$=–60 pA, n=11) and Cav1.3–/– ($amplitude_{(median)}$ =–50 pA, n=9).

e. A light micrograph showing the morphology of a typical dissociated SNc DAergic neuron under Hoffman modulation contrast.

f. TTX–sensitive resurgent currents were evoked from a holding potential evoked by a 20 msec step from –90 to +30 mV, after which the membrane was repolarized to voltages between –20 and –60 mV. No change ($p>0.05$, Mann–Whitney Rank Sum Test) in the peak amplitude of resurgent currents was seen between WT ($amplitude_{(median)}$ =–172.5 pA, n=10) and Cav1.3–/– ($amplitude_{(median)}$ =–187.0 pA, n=7).

Discussion

Properties of the transient and persistent Na^+ current are not significantly altered among the different neuron populations.

Contrary to initial predictions that the properties of Na^+ channels would be remarkably different between Na^+–pacemakers, Ca^{2+}–pacemakers and quiescent neurons, very few distinctions could be made between the transient currents of the various neuron groups. Perhaps most striking, the voltage dependence of the activation and inactivation gates were similar among neurons studied (Fig. 1.13a). It was previously reported that the half–inactivation voltage of another quiescent neuron population, prefrontal cortex neurons, was found to be 10 mV more hyperpolarized than reported here, at –65 mV (Carr et al., 2003). During the course of study, we observed that the half–inactivation voltage shifted considerably during the period of time patched onto the cell in whole–cell mode. Upon first patching onto the cell and allowing the cell to stabilize, the half–activation voltage was in the –55mV range. 20 minutes later, the half–inactivation voltage was roughly –70mV. Numerous unsuccessful efforts were taken to adjust the internal to prevent this drift, but no technique provided consistent improvement. This can be result of perturbation in the phosphorylation of Na^+ channel or dialysis of a critical cellular component (e.g. PIP_2) during whole–cell recording. As a result, all fast–inactivation protocols were taken as soon after breaking into the neuron as possible (after allowing ~ five minutes for the neuron and current to stabilize). It is possible that such measures were not taken previously, allowing for a different half–inactivation voltage to be reported. Regardless, the inclusion of several types of neurons with distinct firing properties in this study is sufficient to support the conclusion that the voltage dependence of activation and inactivation is not unique to any particular neuron group studied.

The only statistically significant values were increases in the slope factors of inactivation and activation for the DA neurons of the SNc, with conductance showing shallower voltage dependence ($p<0.05$, Kruskal –Wallis). This could be explained by the lack of Navβ4 expression in DA neurons. During expression profiling of the four neuron populations, all expressed the full complement

A

	ACTIVATION		INACTIVATION	
	Vh	Vc	Vh	Vc
GPe	-38.3±0.7	7.2±0.2	-55.5±3.6	5.0±0.2
MSN	-40.8±0.9	8.0±0.4	-56.0±2.3	5.4±0.2
ChAT	-39.8±0.8	7.6±0.2	-52.9±1.8	5.1±0.2
SNc	-40.1±0.8	8.4±0.3*	-54.3±1.2	5.7±0.1**

B

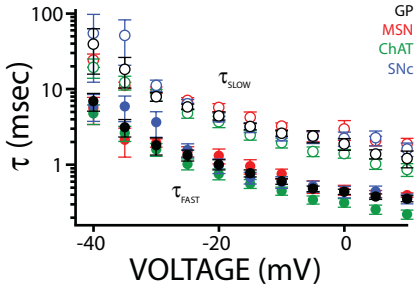

Figure 1.13. Comparison of activation and fast–inactivation properties in basal ganglia neurons.

a. The half–activation voltages and slope factors for globus pallidus neurons (GP), striatal medium spiny neurons (MSN), striatal cholinergic interneurons (ChAT) and nigral dopaminergic neurons (SNc), were calculated by a third order Boltzmann equation fit to conductance measurements of the transient current as a function of holding potential. The half–inactivation voltages and slope factors were calculated by a first–order Boltzmann equation fit to normalized peak amplitudes as a function of prepulse voltage. All values except the slope factors in SNc neurons*/** were not significantly different ($p>0.05$, Kruskal Wallis, $p<0.05$ for Vc of activation* and inactivation** of SNc neurons, Kruskal Wallis).

b. Fast (closed circles) and slow (open circles) time constants of inactivation, as calculated by Hodgkin–Huxley fits of transient currents generated by activation steps. All four neuron types, GP (black), MSN (red), ChAT (green) and SNc (blue) showed similar fast–inactivation kinetics.

of common brain Nav α–subunits as well as three of the four Navβ subunits (β1–3). The only subunit that was conspicuously missing was the β4 subunit in DA neurons (Fig. 1.9a). Because of the involvement of β subunits in fast–inactivation properties (Isom et al., 1992; Isom et al., 1995b; Tammaro et al., 2002), a lack of β4 could flatten the voltage–dependence of inactivation. This result is interesting, not only because of the lack of β4 in DA neurons, but because of the presence of β4 in MSN, where there is no sign of resurgent current. Previous studies on β4 have suggested a significant role in the generation of resurgent current. Introduction of a β4–like peptide introduces a resurgent current to Purkinje neurons that previously had the blocked state removed by trypsin treatment and CA3 neurons, which normally lack resurgent current (Grieco et al., 2005). Our results suggest that Navβ4 is neither sufficient in MSNs nor necessary in DA neurons to generate a resurgent current.

As with the steady–state voltage dependence, the kinetics of Na^+ channel activation and inactivation in pacemaking neurons were not distinctive, resembling those found in quiescent, non–pacemaking medium spiny neurons, striatal cholinergic interneurons and slow pacemaking substantia nigra neurons. Plots of fast and slow time constants (calculated by Hodgkin–Huxley fits of activation plots) as a function of step voltage for the four neurons show no significant differences (Fig. 1.13b).

At five–second voltage steps to –20 mV, 31±2% of the Na^+ channels are slow–inactivated in GP and MS neurons (n=25 and 10, respectively). Cholinergic interneurons have fewer channels impacted by this form of inactivation, as only 22±2% of the channels are slow inactivated (n=8, $p<0.05$, Kruskal–Wallis [between only GP and ChAT]). At –60 mV (near the modal membrane potential during single–spike pacemaking), less than 10% of the Na^+ channel population appears to be in the slow inactivated state and this proportion is likely to be smaller at physiological Na^+ concentrations (Townsend and Horn, 1997). This distinctive feature of cholinergic interneuronal Na^+ channels was not an obvious consequence of the rate of entry into the slow inactivated state or the voltage–dependence of the process. It may be that basal serine/threonine kinase phosphorylation of Na^+ channels in cholinergic interneurons is low (Carr et al., 2003). This could result from

relatively high levels of protein phosphatase activity targeting Na^+ channels or by reliance upon Na^+ channels that have a low probability of being phosphorylated by protein kinases responsible for setting the basal tone. Despite this, the similarity in GP and MSN slow inactivation properties suggest that autonomous pacemakers do not have less slow inactivation than quiescent neurons.

In many Na^+–pacemaking neurons, persistent currents are key determinants of the rate and regularity of spiking (Raman and Bean, 1999; Taddese and Bean, 2002). After spike repolarizing currents wane, these Na^+ currents provide the inward depolarizing force necessary to bring the membrane potential to spike threshold again. Because the slope of the current–voltage relationship in the sub–threshold voltage region becomes very shallow (Bennett et al., 2000), even small changes in the amplitude of the persistent Na^+ current can have profound effects on pacemaking rate. The importance of the persistent current would suggest an increase in amplitude for Na^+–pacemaking neurons. However, the persistent current in these four neuron types is strikingly similar. If the persistent current were defined as a window current by the overlap of the steady–state activation and inactivation curves (Maurice et al., 2001), this result would not be surprising because of the similarity of these neurons' voltage dependence parameters. The inactivity and hyperpolarized resting potential during the downstate of MSNs is likely not as much a result of altered Na^+ currents as it is the presence of increased Kir2 and TREK1 expression levels (Nisenbaum and Wilson, 1995; Talley et al., 2001), which keep the membrane potential out of the range where the Na^+ persistent current can depolarize the membrane towards spike threshold.

The resurgent current is important for the activity patterns of autonomous pacemakers

The significant result from the parametric analysis of these four neuron classes is the presence of the resurgent current in all autonomously active neurons and the absence of it in quiescent MSNs. Because blocked channels do not inactivate, the addition of this voltage–dependent state has two effects relevant to autonomous spiking. The first effect is to reduce the amount of inactivation during a spike, increasing Na^+ channel availability for the next spiking cycle. The second effect is to reduce the 'depth' of the postspike AHP, shortening the depolarizing ramp to the next spike. Experimental

and computational studies have shown that resurgent current increases excitability and promotes sustained, autonomous pacemaking (Khaliq et al., 2003).

Differences within the firing properties of the pacemakers are likely a result of varied expression levels of other channel types. The functional expression of resurgence during the inter–spike interval in fast spiking GP neurons, and in fast–spiking neurons elsewhere in the brain is enhanced by their reliance upon very rapidly deactivating Kv3 channels for spike repolarization, therefore minimizing outward currents that would slow repolarization of the membrane toward spike threshold (Baranauskas et al., 1999; Wigmore and Lacey, 2000; Rudy and McBain, 2001; Baranauskas et al., 2003). Kv3 are thought to enable fast–spiking by virtue of their ability to keep spikes brief (reducing Na^+ channel inactivation) and rapidly deactivate once the membrane has repolarized, thereby enabling the cell to rapidly depolarize to spike threshold again (Rudy and McBain, 2001). These channels are not necessary for slow pacemaking, as their absence in cholinergic interneurons and DA neurons demonstrates (Song et al., 1998), but might be important for sustained, high frequency pacemaking. As mentioned above, the co–expression of Kv3 channels and Na^+ channels with resurgence creates a potent biophysical mechanism for high frequency discharge (Akemann and Knopfel, 2006). Without the rapid repolarization of the membrane following the spike, the action potentials are significantly wider and result in more Na^+ channel inactivation per spike. Furthermore, the high level of Kv4 expression in cholinergic interneurons and DA neuron, relative to GP neurons, creates a larger A–type K^+ current that fights the subthreshold Na^+ currents and leads to a slower ramp towards threshold, so there are less Na^+ channels fighting a larger hyperpolarizing current, which slows the cell down significantly. DA neurons also have greater levels of Ca^{2+} activated channels of the SK class, which are responsible for the post–spike AHP and the hyperpolarization phase of the Ca^{2+} oscillations seen in TTX (Amini et al., 1999; Wilson and Callaway, 2000; Wolfart et al., 2001). The combination of high Kv4 and SK tone likely overpower the Na^+ channel machinery enough that it is unable to drive activity. With the elimination of the Ca^{2+} conductance through genetic deletion or prolonged pharmacological antagonism, SK channels

are sufficiently dampened and other depolarizing currents are activated (HCN channels) to push the membrane depolarized enough to initiate Na^+ pacemaking (our unpublished observation).

Conclusions

The gating properties of Na^+ channels in basal ganglia neurons are highly similar, despite their distinct firing properties. Neither the voltage dependence (for both activation and inactivation) nor fast– and slow–inactivation properties among these neurons are significantly different. Instead, the presence of the resurgent Na^+ current in all three autonomous pacemakers and its absence in the regular spiking neurons suggest it is important for autonomous pacemaking. However, the expression of β4 in MSNs and the lack in SNc DA neurons suggesting that β4 is neither sufficient in MSNs nor necessary in DA neurons in creating resurgence. Nevertheless, in the absence of resurgence, there is likely insufficient recovery from a spike to supply enough Na^+ channels during the interspike interval to create a large enough depolarizing current to drive the subsequent spike. Section 3.3 will further address these issues through the use of genetic mutations, high frequency protocols and computer simulations.

Section 3.2: D_2 dopamine receptor mediated modulation of voltage–dependent Na^+ channels contributes to the suppression of autonomous activity of striatal cholinergic interneurons

Introduction

Cholinergic interneurons are critical elements of the striatal circuitry controlling motor planning, movement and associative learning (Graybiel et al., 1994). Their central role was first inferred from clinical observations that striatal cholinergic tone was elevated in Parkinson's Disease (PD) and that the restoration of a balance with the dopaminergic afferent system was important in alleviating the motor symptoms of the disease (Hornykiewicz, 1976). Although they appear to receive a sparse dopaminergic innervation (Smith et al., 1994), cholinergic interneurons express both D_2 and D_5 dopamine receptors, making them responsive to volume–transmitted dopamine (Levey et al., 1993; Bergson et al., 1995; Yan et al., 1997). The best characterized effect of dopamine on cholinergic interneurons is mediated by activation of D_2 receptors, which inhibit N–type Ca^{2+} channel opening and the Ca^{2+}–dependent release of acetylcholine (Lehmann and Langer, 1983; Bertorelli et al., 1992; Stoof et al., 1992; DeBoer et al., 1993; Di Chiara et al., 1994; Yan et al., 1997).

There are reasons to believe that dopamine acts to shape cholinergic interneuron function in other ways as well. Perhaps the most intriguing evidence for additional mechanisms comes from studies of behaving monkeys. Unconditioned reinforcers that are known to activate dopaminergic neurons (Schultz, 2002) inhibit the activity of tonically active neurons (TANs) that have been identified as cholinergic interneurons (Aosaki et al., 1994; Graybiel et al., 1994; Bennett and Wilson, 1999). In associative learning paradigms, the activity of dopaminergic neurons – and the suppression of TAN activity – becomes bound to conditioned stimuli. Lesioning dopaminergic neurons disrupts conditioning and the linkage between TAN activity and behaviorally relevant stimuli (Aosaki et al.,

1994). These findings make a strong case that dopamine not only reduces the release of acetylcholine but also reduces cholinergic interneuron spiking, but how?

Electrophysiological studies of cholinergic interneurons in slices have shown that they are autonomous pacemakers – they are capable of maintained spike discharge in the absence of synaptic input (Bennett and Wilson, 1999). This finding argues that the pause in cholinergic interneuronal discharge must come from either synaptic inhibition or suppression of the intrinsic mechanisms underlying the autonomous activity. D_5 dopamine receptor activation does enhance cholinergic interneuronal $GABA_A$ receptor currents (Yan et al., 1997) and spike after–hyperpolarization (Bennett and Wilson, 1998), but studies *in vivo* suggest that the cholinergic interneuronal pause is dependent primarily upon D_2 receptors (Watanabe and Kimura, 1998). If this is the case, there are no known synaptic mechanisms involving ionotropic receptors by which dopamine could induce a pause.

Could D_2 receptors suppress the pacemaking mechanism? Pacemaking in cholinergic interneurons is dependent upon voltage–gated Na^+ channels (Bennett et al., 2000). Phosphorylation of Na^+ channel alpha subunits by protein kinase C (PKC) is a particularly potent means of reducing Na^+ channel currents (Cantrell and Catterall, 2001; Carr et al., 2003). As a consequence, G protein–coupled receptors that activate PKC are potential regulators of autonomous activity. As D_2 receptors fall into this class (Hernandez-Lopez et al., 2000), it is possible that they are capable of suppressing Na^+ channel currents and slowing autonomous activity in cholinergic interneurons. The studies reported here provide support for this view.

Results

D_2 receptor stimulation reduces evoked and autonomous spiking

Cholinergic interneurons were identified in tissue slices by their large somal diameter and spontaneous activity (Bennett and Wilson, 1999). D_2 receptor class agonist R(–)–propylnorapomorphine (NPA, 10 μM) consistently suppressed spiking evoked by somatic current injection in cholinergic interneurons recorded in tissue slices without changing resting membrane

potential (Fig. 2.1a,b). On average, NPA reduced the number of spikes evoked by near rheobase current injection by near half (Fig. 2.1c, n=4, $p<0.05$, Kruskal–Wallis). To gain a better idea of how this modulation would affect the relationship between discharge frequency and injected current, slow current ramps were delivered (Fig. 2.1d,e). NPA reduced discharge frequency across a range of current intensities. The frequency–intensity plots were shifted toward higher currents and down on the frequency scale (Fig. 2.1f). A similar alteration was seen in all of the cholinergic interneurons tested (n=3).

As discussed above, cholinergic interneurons are capable of sustained, autonomous pacemaking. In the tissue slice, this pacemaking is completely independent of synaptic input, being unaltered by blockade of either glutamatergic or GABAergic receptors (Bennett and Wilson, 1999). To determine if D_2 receptor stimulation could influence autonomous pacemaking, cholinergic interneurons were recorded in cell–attached patches in tissue slices. Bath application of the D_2 receptor–class agonist quinpirole (10 μM) slowed cholinergic interneuron discharge (Fig. 2.2a). The average behavior of our sample (n=6) can be seen in Figure 2.2b, where the discharge rates were normalized and the mean (across the sample) plotted as a function of time after quinpirole application. The median suppression of discharge rate was 43% (Fig. 2.2c, n=6, $p<0.05$, Kruskal–Wallis). As discharge rate slowed following receptor activation, the variability of the discharge also increased. One measure of irregularity in interspike intervals is the coefficient of variation; this measure increased significantly following receptor activation (Fig. 2.2d, n=6, $p<0.05$, Kruskal–Wallis). Because pacemaking is independent of synaptic activity and no other neuronal class in striatal slices is spontaneously active, D_2 receptor agonists are likely to be acting directly to suppress pacemaking. Single spike pacemaking in cholinergic interneurons is dependent upon voltage–dependent Na^+ channels (Bennett et al., 2000), suggesting that D_2 receptors may be acting to suppress these currents. As a first step toward testing this hypothesis, the properties of the Na^+ channels underlying pacemaking were studied.

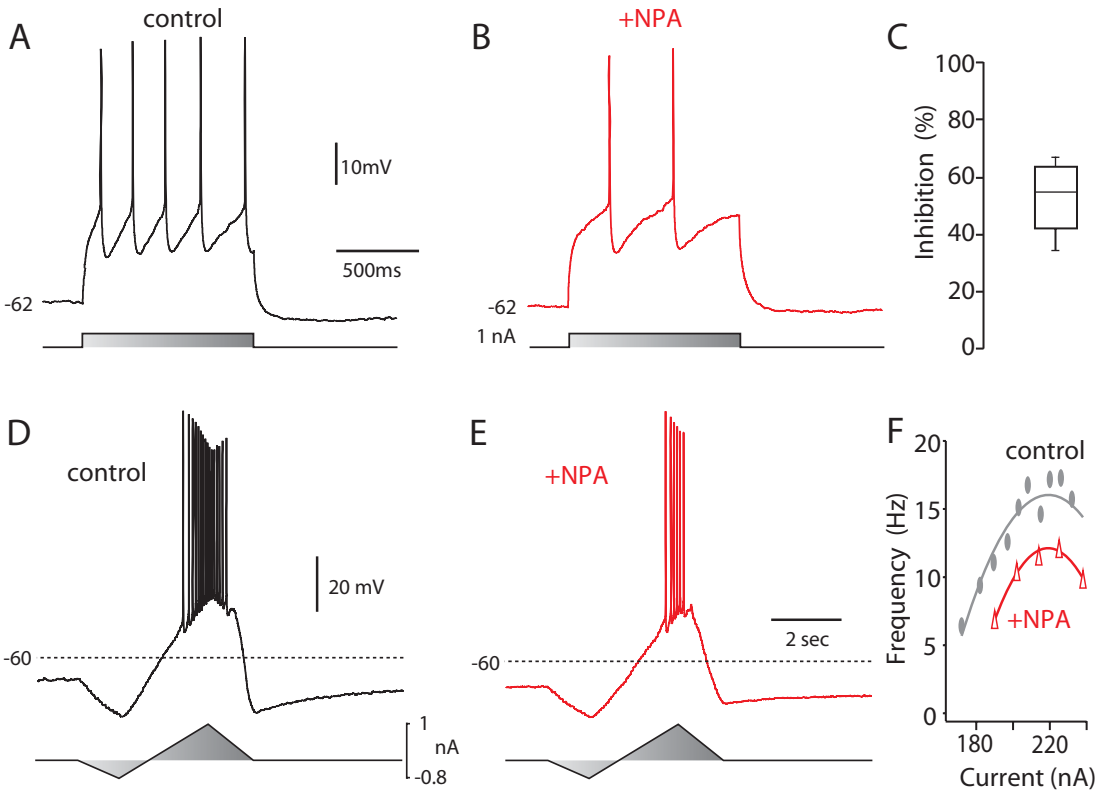

Figure 2.1. D_2 receptor activation suppresses evoked activity.

a. Repetitive spiking evoked in a cholinergic interneuron by intrasomatic current injection during a recording in a tissue slice.
b. The same neuron after bath application of NPA (10 μM). Note the reduction in evoked discharge.
c. Statistical summary of NPA induced reduction in evoked spiking.
d. Repetitive activity evoked by somatic injection of a current ramp.
e. The response to the same stimulus was reduced after application of NPA (10 μM).
f. Instantaneous discharge frequency–current injection plot for the neuron shown in *d, e*. Data were fit with a polynomial function; control: $-206.8+2.03i-0.0046i^2$; NPA: $-287.4+2.74i-0.0062i^2$, where I is current. Similar results were obtained in two other neurons tested.

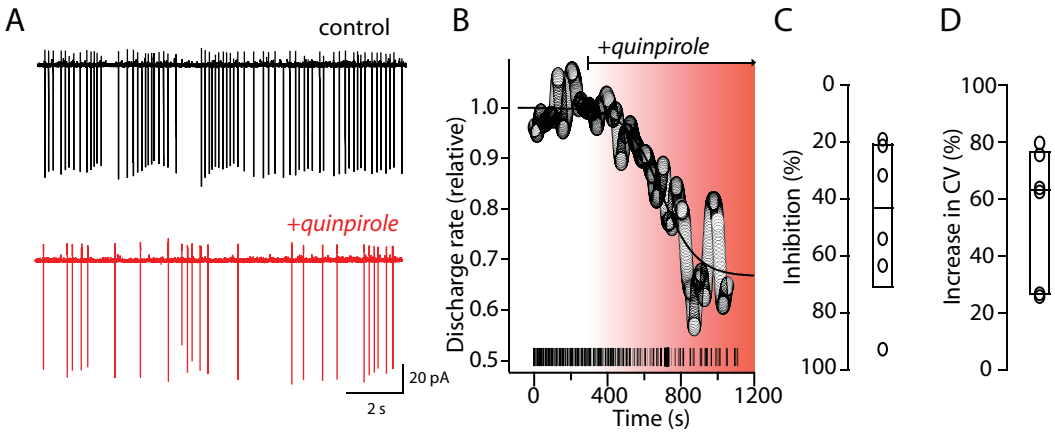

Figure 2.2. D_2 receptor activation suppresses autonomous spiking.

a. Somatic cell–attached recording of spontaneous action potential firing in a cholinergic interneuron under control conditions and in the presence of quinpirole (10 μM). The discharge rate was slowed (control = 4.7 Hz; quinpirole = 1.8 Hz) and discharge coefficient of variation was increased (control = 0.66; quinpirole =1.47).

b. An average time course of quinpirole's action on spontaneous firing rate of cholinergic interneurons. Inset represents the activity of the neuron that was shown in *a*.

c. A summary of the modulation in firing rate and coefficient of variation in six cholinergic interneurons.

D_2 receptor stimulation reduces Na^+ currents at depolarized potentials in cholinergic interneurons

As shown in the previous chapter, cholinergic interneurons express mRNA for the D_2 dopamine receptor. In most cholinergic interneurons tested (12/13), the application of the D_2–class receptor agonist NPA (10 μM) rapidly and reversibly suppressed the rapidly inactivating Na^+ currents evoked by a step from –70 mV (mean suppression=10.5±1.2%; n = 12, $p<0.05$, Kruskal–Wallis, Fig. 2.3a,e). The D_2–class receptor antagonist sulpiride (10 μM) significantly reduced this modulation (median suppression=2%; interquartile range: 0–5%, n=5, $p<0.05$ Kruskal–Wallis); lower concentrations of sulpiride (1 μM) gave partial block of the NPA (10 μM) modulation (n=3, range 20–80% block), possibly because of alterations in the receptor during enzymatic dissociation of the tissue. Because cholinergic interneurons do not express detectable levels of mRNA for other members of the D_2 receptor class (D_3, D_4) that bind NPA and sulpiride with high affinity (Yan et al., 1997), these results argue that the modulation observed is mediated by D_2 receptors. Dialysis with the $G_{\beta\gamma}$–subunit scavenger βark–Cp (Koch et al., 1994) also attenuated the modulation (median suppression=4%, interquartile range: 1–5%, n=4). In agreement with this inference that the signaling was mediated by $G_{\beta\gamma}$–subunits and the demonstration that striatal D_2 receptors couple though these subunits to phospholipase Cβ isoforms (Hernandez-Lopez et al., 2000), application of the protein kinase C (PKC) activator 1–oleoyl–2–acetyl–sn–glycerol (OAG, 2 μM) mimicked the effect of D_2 receptor agonists – rapidly and reversibly suppressing peak Na^+ currents evoked by a step from –70 mV (median suppression =16%; interquartile range: 13–20%, n = 7; $p<0.05$ Kruskal–Wallis, data not shown). Dialysis with the PKC inhibitor calphostin C (1 μM) eliminated the effects of D_2 receptor agonist application (median modulation=2%, interquartile range: 0–4%, n=4, $p>0.05$ Kruskal–Wallis, data not shown).

The D_2 receptor mediated modulation of Na^+ channel currents resulted in an apparent reduction in maximal conductance without prominently shifting the voltage dependence of fast inactivation (Fig. 2.3b,c) (control: V_h=– 55 mV, interquartile range: 53–56 mV, NPA: V_h=–56 mV, interquartile range: 54–58 mV, n = 6). Slope factors were unaltered by NPA as well (control: k=5.5

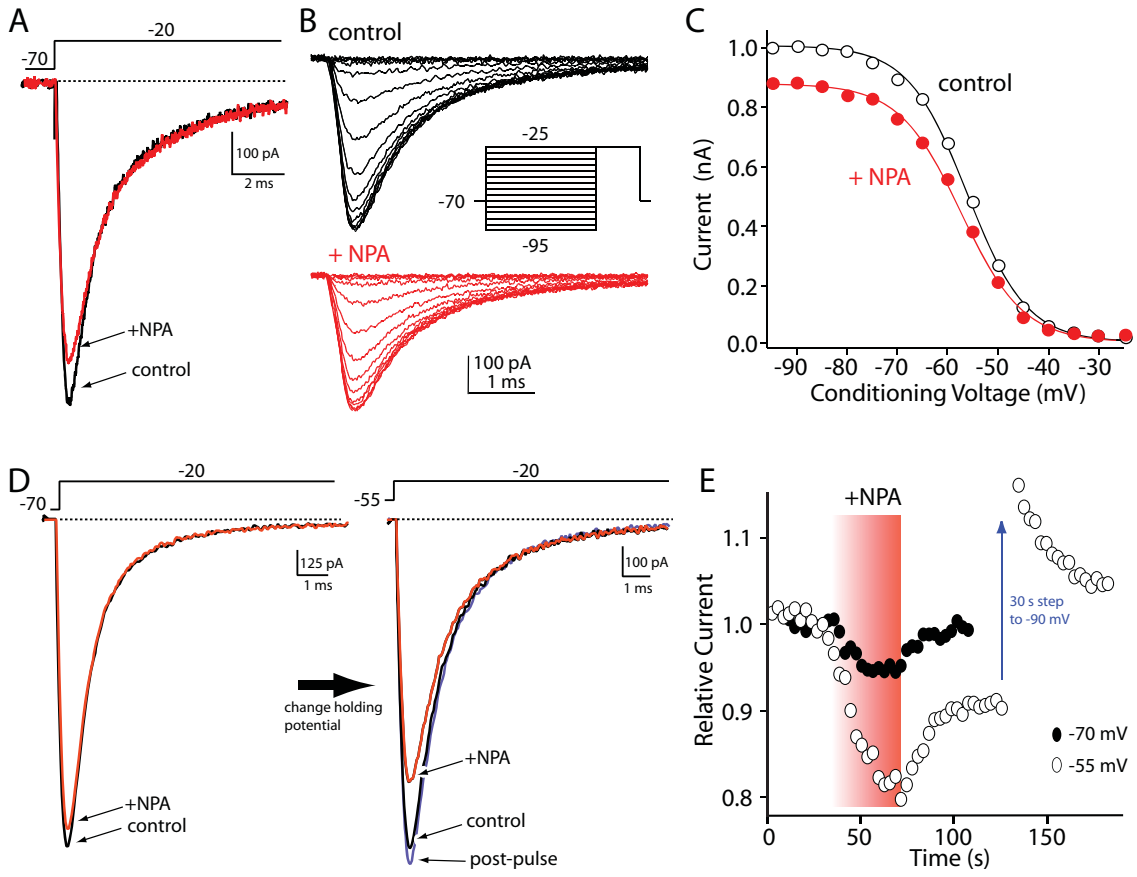

Figure 2.3. D_2 receptor activation suppresses Na^+ currents in a voltage–dependent fashion.

a. Application of the D_2 receptor class agonist NPA (10 μM) reversibly suppressed Na^+ currents evoked by a test step to –20 mV from a holding potential of –70 mV.

b. Currents evoked before and after application of NPA by a fast inactivation protocol. Peak current data derived from these traces are shown at the right.

c. Data were normalized to the peak current in control records and fit with Boltzmann functions (see text); although peak conductance was reduced there was no change in voltage dependence.

d. In another neuron, NPA had a smaller effect when holding at –70 mV; changing the holding potential to –55 mV increased the magnitude of the modulation.

e. Time course showing the increase in modulation at more positive holding potentials. This modulation reversed very slowly at positive potentials; however, the modulation was reversed by a brief step to –90 mV.

mV, interquartile range: 5.2–5.8 mV, NPA: V_h=5.8 mV, interquartile range: 5.4–6.1 mV, n = 6). Direct activation of PKC with OAG had very similar effects (control: V_h=– 54 mV, interquartile range: 52–55 mV, OAG: V_h=–56 mV, interquartile range: 54–58 mV, n = 6). Slope factors were unaltered by OAG (control: k=5.4 mV, interquartile range: 5.1–5.7 mV, OAG: V_h=5.4 mV, interquartile range: 5.3–5.6 mV, n = 6).

Although D_2 receptor stimulation consistently reduced Na^+ currents evoked from –70 mV, the magnitude of the modulation was modest. Holding the membrane potential at more negative membrane potentials (ca. –90 mV), further reduced the modulation of current amplitudes (data not shown). In contrast, when cholinergic interneurons were held at –55 mV (near their normal resting membrane potential) and the D_2 receptors activated, the reduction in current amplitude nearly doubled from that seen in the same cell at –70 mV (Fig. 2.3d,e). Similar results were obtained in every neuron examined (median increase in modulation at –55 mV = 342%, range 168–680%, n=18). However, at depolarized membrane potentials, unlike the situation at –70 mV, reversal of the modulation was typically very slow after washing off the agonist (Fig. 2.3e). To test whether this sustained reduction was due to a voltage–dependent, reversible process, neurons were hyperpolarized to –90 mV for 30 seconds after agonist application and then the membrane potential returned to –55 mV. In all of the neurons examined with this protocol (n=7), brief hyperpolarization reversed the modulation (Fig. 2.3e). The hyperpolarization was not accompanied by any discernible change in input or series resistance. As shown below, this reversal was presumably accomplished by promoting exit of Na^+ channels from a slow inactivated state.

D_2 receptor stimulation reduces persistent Na^+ currents

Activation of D_2 receptors on cholinergic interneurons with NPA (10 μM) also reversibly diminished persistent Na^+ currents evoked by a slow voltage ramp from –80 mV to 0 mV (8/10 neurons tested) (Fig. 2.4a). At –25 mV, the peak current was suppressed by around 30% (median=29%, interquartile range: 25–39, n=8). This was substantially larger than the reduction in transient Na^+ current seen even at a holding potential of –55 mV (see Fig. 2.3). This modulation

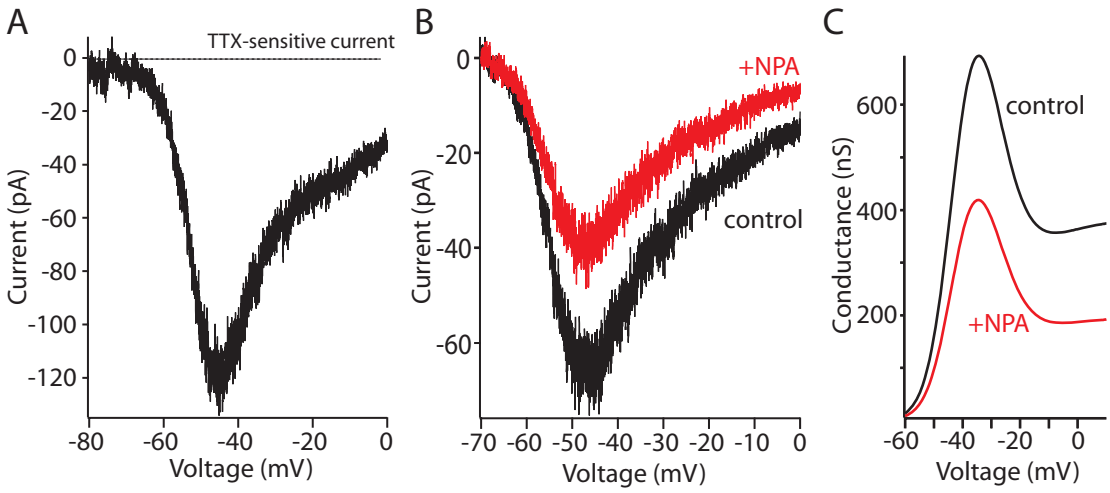

Figure 2.4. D_2 receptor activation suppresses persistent Na^+ currents.

a. Current–voltage plot of TTX–sensitive persistent Na^+ currents evoked by a slow voltage ramp (4 sec) from –80 mV to 0 mV in an acutely isolated cholinergic interneuron

b. NPA (10 μM) reversibly suppressed persistent Na^+ currents. The current–voltage relationship of the TTX–sensitive currents before and after NPA application.

c. Conversion of the current–voltage plots in *a* to conductance estimates were fit using an HH model.

was mimicked by application of OAG (2 μM), which reduced ramp currents at –25 mV by a similar amount (median=30%, interquartile range: 21–34, n=6). To estimate changes in conductance, currents were converted using the assumption that currents were ohmic and driving force was determined by the Nernst equation (Hille, 2001). The median reduction in the peak persistent conductance was larger than that for current, being near 41% (interquartile range: 28–62%, n=5).

D_2 receptor stimulation reduces Na^+ currents by enhancing a process resembling slow inactivation

What type of mechanism could explain the voltage dependence of the Na^+ channel modulation? Recent work has shown that PKC and protein kinase A (PKA) mediated modulation of Na^+ channel currents in cortical pyramidal neurons and heterologous expression systems is produced by enhancing channel entry into a slow inactivated state (Carr et al., 2003). To test whether a similar process was at work here, the voltage dependence and kinetics of slow inactivation were examined in the presence and absence of D_2 receptor class agonists. Na^+ channel currents in cholinergic interneurons exhibited slow inactivation, but the extent of slow inactivation was less than that seen in cortical pyramidal neurons (Carr et al., 2003). In pyramidal neurons, a 5 second depolarization to –20 mV forces roughly 60% of the Na^+ channels into a slow inactivated state, whereas the same protocol converted only about 20% of the cholinergic interneuronal channels into this state. In this protocol, channels are allowed to recover from fast inactivation by holding the membrane potential at –80 mV for 1 second before delivering a test pulse (see inset Fig. 2.5a). Any reduction in current amplitude with this protocol is attributable to slow inactivation. NPA (10 μM) significantly increased the extent of slow inactivation measured using 5 second voltage steps to –20 mV (mean control slow inactivation (SI) =19%$\pm$1% (sem), SI in NPA=30%$\pm$2%, n=18, $p<0.05$, Kruskal–Wallis). D_2 receptor activation did not discernibly change the voltage dependence of slow inactivation (Fig. 2.5a) or the rate of entry into the slow inactivated state produced by a voltage step to –20 mV (Fig. 2.5b). Entry in the SI state was mono–exponential in both cases with time constants equal to 5 seconds (Fig. 2.5b). D_2 receptor activation did not alter the rate of recovery from slow inactivation either (Fig. 2.5c); recovery was bi–exponential in both cases with a fast time

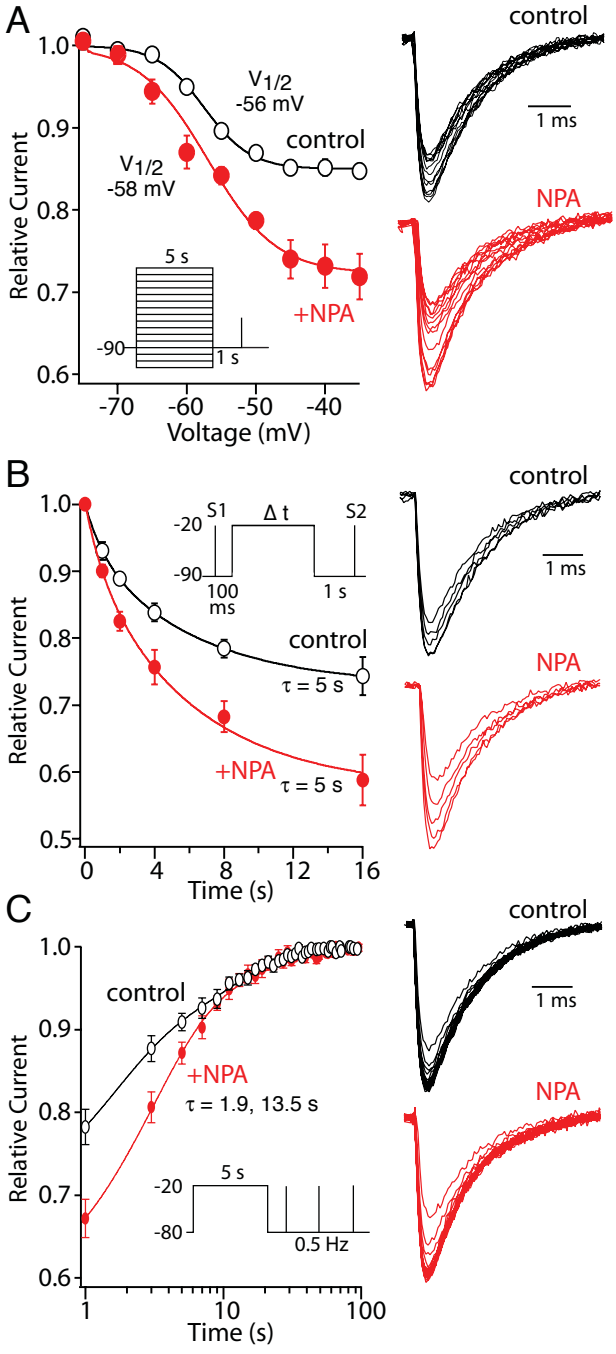
A
1.0
0.9
0.8
0.7
0.6
Relative Current
V1/2
-56 mV
control
V1/2
-58 mV
+NPA
5 s
-90
1 s
-70
-60
-50
-40
Voltage (mV)
control
1 ms
NPA
B
1.0
0.9
0.8
0.7
0.6
0.5
Relative Current
-20
-90
S1
Δ t
S2
100
ms
1 s
control
τ = 5 s
+NPA
τ = 5 s
0
4
8
12
16
Time (s)
control
1 ms
NPA
C
1.0
0.9
0.8
0.7
0.6
Relative Current
control
+NPA
τ = 1.9, 13.5 s
5 s
-20
-80
0.5 Hz
1
10
100
Time (s)
control
1 ms
NPA

Figure 2.5. D_2 receptor activation enhances slow inactivation of Na^+ currents.

a. NPA (10 μM) increased the extent of slow inactivation evoked by a 5 s voltage step to potentials between –35 mV and –60 mV but did not change the apparent voltage dependence of the process. Boltzmann fits to normalized data are shown for control (open circles) and NPA (filled circles) data (n=4). Representative current traces are shown at the right.

b. The rate of entry into the slow inactivated state was unchanged by NPA (10 μM). Single exponential fits to control (open circles) and NPA (filled circles) data are shown (n=5). Both data were well–fit with a single exponential having a time constant near 5 s. The extent of slow inactivation was greater in NPA however. Representative current traces are shown at the right. Protocol is shown inset.

c. NPA did not significantly alter the rate of recovery from slow inactivation at –80 mV. Double exponential fits to control (open circles) and NPA (filled circles) data are shown (n=8). Both data sets were well–fit with a double exponential having a time constant of 1.9 and 13.5 s. Representative current traces are shown at the right. Protocol is shown inset.

constant of 1.9 seconds and a slow time constant of 13.5 seconds. However, D_2 receptor activation modestly increased the fraction of the current that recovered rapidly (control: 63%; NPA: 72%; n=8, p>0.05, Kruskal–Wallis).

Similar effects of D_2 receptor activation are seen in GP and MS neurons

GP and MS neurons are different from cholinergic interneurons in that only a subpopulation of neurons express D_2 receptors (Surmeier et al., 1996; Ruskin and Marshall, 1997; Marshall et al., 2001). To identify neurons that could potentially be modulated by D_2 agonists, we utilized a strain of mice generated by the Heinz and Greengard labs that co–expressed GFP under the D_2 receptor promoter, which enabled us to easily identify neurons with the use of fluorescent filters (Gong et al., 2003). This method was readily utilized in the striatum, where D_2 receptor + medium spiny neurons were clearly fluorescent (Fig. 2.7c). However, despite scRT–PCR data showing expression of D_2 receptor mRNA in a population of GP neurons (Fig. 2.6a), fluorescence was not readily detectable in the acutely dissociated GP prep of D_2 BAC mice, so cells lacking any modulation by NPA were assumed to lack D_2 receptors and were eliminated from analysis.

Similar to the observations seen in cholinergic interneurons, transient Na^+ currents in GP and MS neurons were only modestly reduced by NPA (10 μM) at hyperpolarized potentials, but significantly reduced at more depolarized potentials (Figs. 2.6b, 2.7d,e). In GP neurons, NPA reduced transient Na^+ currents by 52±10% at –50 mV, 33±8% at –60 mV, 22±4% at –70 mV and only 11±1% at –80 mV (Fig. 2.6b, n=5). In MSNs, NPA reduced the transient current by 20% at –60mV and only 7% at –80 mV (Fig. 2.7d, n=8). This voltage dependence of modulation was more for the persistent current in MSNs, where NPA reduced the peak amplitude by 35% at –60 mV and 14% at –80 mV (Fig. 2.7e).

The mechanism of modulation is similar to that of cholinergic interneurons in that NPA increases entry into the slow inactivated state, thus blocking more channels at more depolarized potentials because of the increased amount of slow inactivation that occurs (Figs. 2.6c,d and 2.8a,b,c). For MSNs, this voltage dependence of modulation is important because of the state

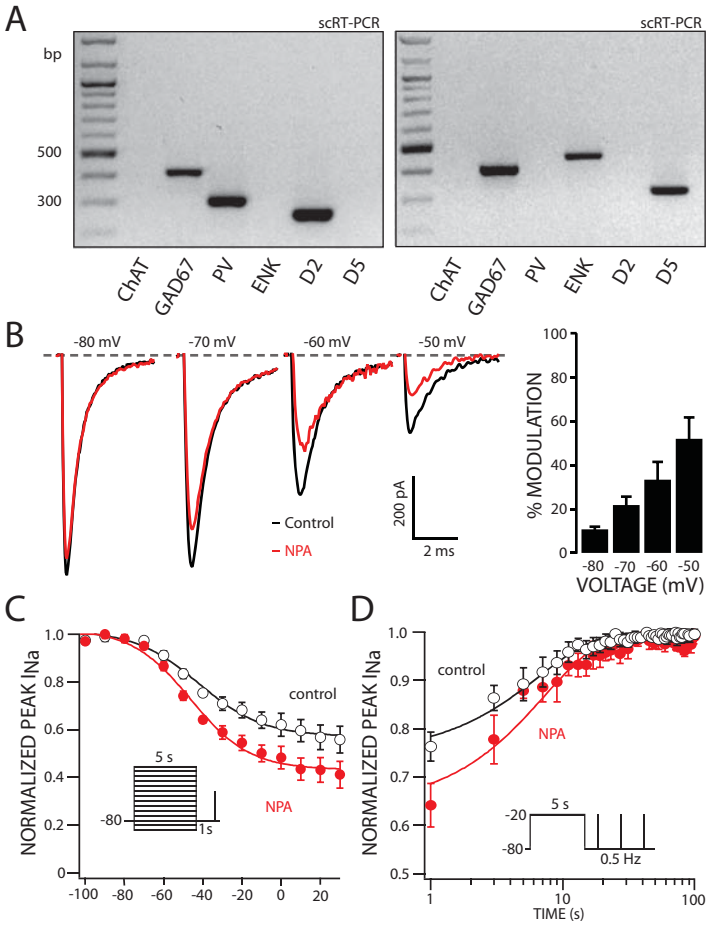

Figure 2.6. D_2 receptor activation suppresses Na^+ current in GP neurons by enhancing slow inactivation.

a. ScRT–PCR profiling of two representative neurons, showing that subpopulations of GP neurons express D_2 or D_5 receptors, PV, ENK and GAD_{67}. There was no significant correlation between PV and ENK expression and D_2 and D_5 receptors in the entire population.

b. NPA (10 μM) reduced Na^+ current by 52±10% at –50 mV, 33±8% at –60 mV, 22±4% at –70 mV and only 11±1% at –80 mV. Histogram showing the amount of modulation as a function of holding potential.

c. NPA does not appear to shift the half–inactivation voltage of slow inactivation. The pseudo–steady state V_h at 5 seconds is near –45 mV with and without NPA. The curves are the best fit to a modified Boltzmann equation control.

d. NPA did not significantly alter the rate of recovery from slow inactivation at –80 mV. Single exponential fits to control (open circles) and NPA (filled circles) data are shown. The time constant for recovery is 5.9±0.3 sec for control and 6.1±0.4 sec for NPA.

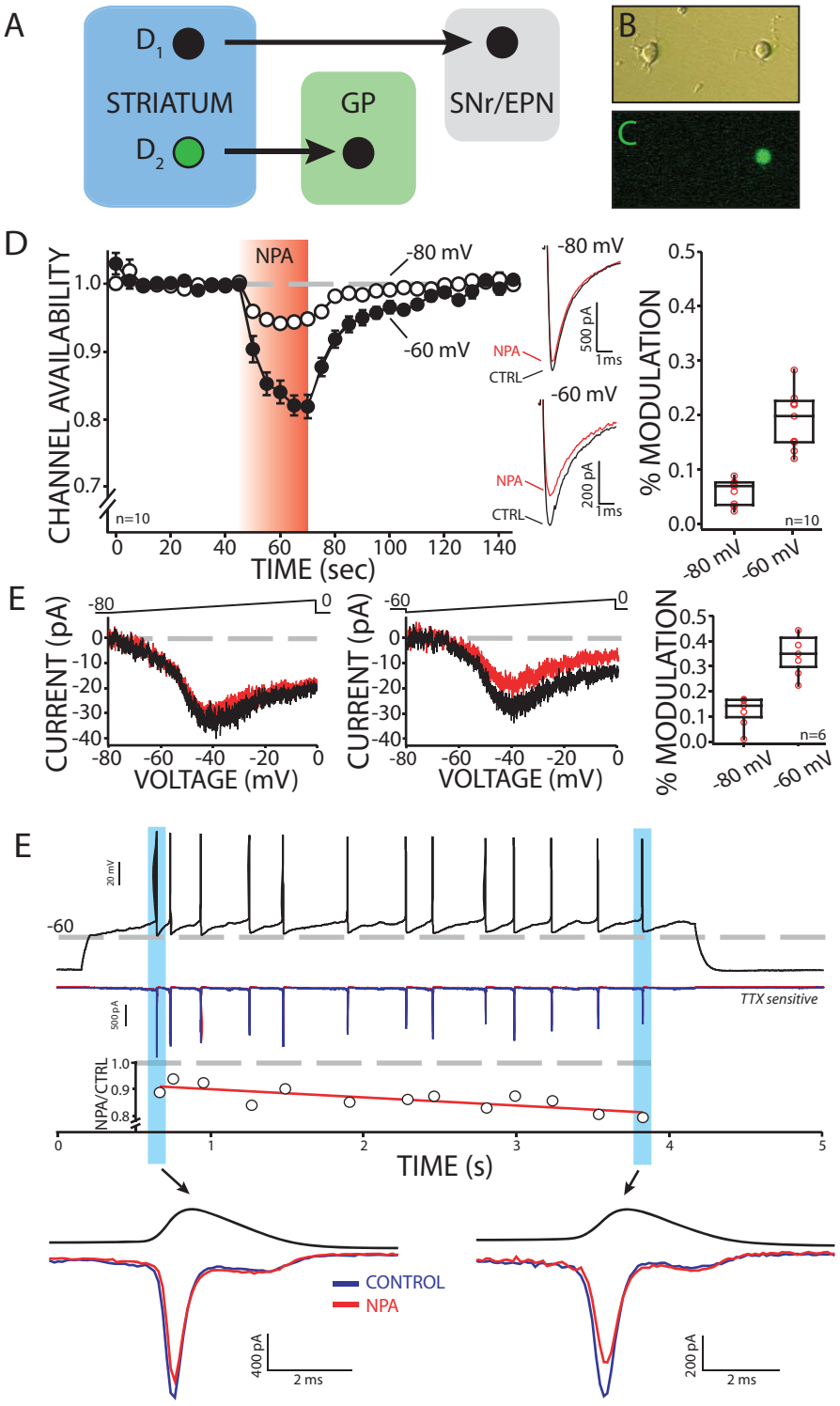
A
D1
STRIATUM
D2
GP
SNr/EPN
B
C
D
CHANNEL AVAILABILITY
NPA
-80 mV
-60 mV
n=10
TIME (sec)
-80 mV
NPA
CTRL
500 pA
1ms
-60 mV
NPA
CTRL
200 pA
1ms
% MODULATION
n=10
-80 mV
-60 mV
E
CURRENT (pA)
VOLTAGE (mV)
CURRENT (pA)
VOLTAGE (mV)
% MODULATION
n=6
-80 mV
-60 mV
E
-60
TTX sensitive
NPA/CTRL
TIME (s)
CONTROL
NPA
400 pA
2 ms
200 pA
2 ms

Figure 2.7. D_2 receptor activation reduces Na^+ channel availability in MS neurons is dependent on holding potential.

a. The striatum is composed of two groups of medium spiny neurons — those that express D_1 receptors and P and project to the substantia nigra, and those that express D_2 receptors and enkephalin and project to the pallidus. Using GFP under the control of the D_2 receptor promoter allows us to identify this latter group easily (Gong et al., 2003).
b. Brightfield image of two medium spiny neurons.
a. Same field viewed using fluorescence optics.
c. NPA (10 μM) reduced the peak amplitude of Na+ currents evoked by a step to –20 mV. At a holding potential of –80 mV, NPA only reduced the current by 6±1%, while at a holding potential of –60 mV the peak current was reduced by 19±2%.
d. Modulation of the persistent current, measured with a ramp protocol from –80 mV to –60 mV, showed a similar dependence on holding potential. The current was reduced by 11±2% at a holding potential of –80 mV and 33±3% at –60 mV.
e. An upstate created by a cell's response to current injection was fed back into a voltage–clamped cell as a voltage command. During the 4 seconds in the upstate, the peak amplitude of the Na^+ current during a spike was reduced more when D_2 receptors were activated by NPA, as measured by comparing the ratio of peak amplitude with and without NPA.

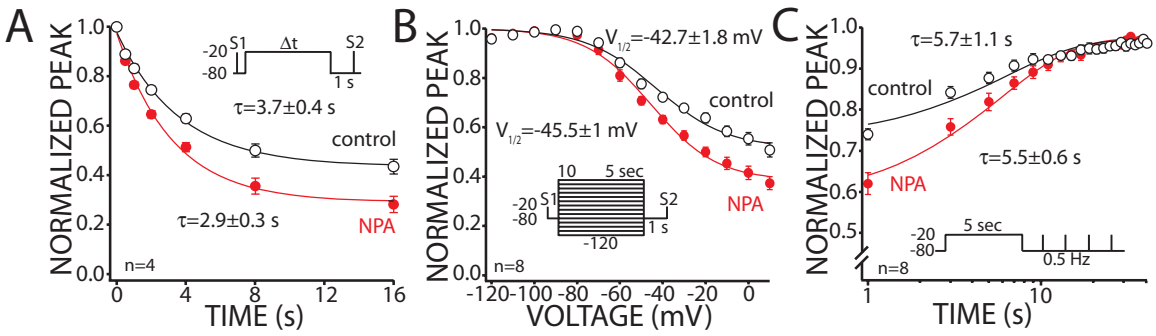

Figure 2.8. D_2 receptor activation reduces Na^+ channel availability in MS neurons through increased entry into the slow inactivated state.

a. 10 μM NPA (filled symbols) increases the reduction of Na^+ channel availability by accelerating entry into the slow inactivated state (τ=3.7±0.4 sec for control and 2.9±0.3 sec for NPA). The curves are the best fit to a single exponential equation (n=4).

b. NPA does not appear to shift the half–inactivation voltage of slow inactivation. The pseudo–steady state V_h at 5 seconds is near –45 mV with and without NPA ($p>0.05$, Kruskal–Wallis). The curves are the best fit to a modified Boltzmann equation (n=8).

c. NPA increases the fraction of Na^+ channels in the slow inactivated state, but did not significantly alter the time course of recovery kinetics. The curves are the best fit to a single exponential equation (n=8).

transitions that are inherent in the membrane properties of this neuron. Typically, MSNs sit in a down–state near –80 mV, where relatively little modulation is taking place. During activation, they transition to an upstate near –60 mV from which action potentials can be generated. Since significantly more D_2 receptor–mediated modulation occurs at –60 mV, D_2 acts in a state dependent manner in MSNs. To understand the increase in NPA modulation during the upstate, a trace of a 4 second stimulus–generated upstate with action potentials was used as a voltage command to measure transient Na^+ currents generated during the action potentials. When NPA was applied to the neuron, the reduction in peak Na^+ current amplitude of the last pulse was reduced more relative to the first pulse. Over the course of the upstate, the amount of modulation by NPA for transient currents generated by the action potential waveform was increased (Fig. 2.7e). This shows that D_2 receptor activation acts as a state dependent modulator of Na^+ channels, reducing activity in the upstate and having significantly less of an impact during the downstate.

Impact of NPA modulation on rebound spiking in cholinergic interneurons

Distinguishing features of the D_2 receptor modulation of Na^+ channels are slow kinetics and voltage dependence. Long–lasting but not short hyperpolarization of the membrane should reverse the modulation. To test this conjecture, the effect of D_2 receptor activation on 'post anode–break' spiking – like that triggered by termination of somatic GABAergic inhibitory input – was examined. This post anode–break depolarization is generated by slowly deactivating, hyperpolarization activated cation (HCN) channels in cholinergic interneurons (Bennett and Wilson, 1999). With strong enough HCN activation, the rebound depolarization is accompanied by spiking (Fig. 2.9a). NPA (10 μM) had no discernible effect on HCN channel activation, as judged by the sag in membrane potential with membrane hyperpolarization, but it did suppress spiking during the rebound depolarization. With a 1 second hyperpolarization to around –80 mV (Fig. 2.9b); similar results were obtained in other neurons (median reduction in rebound spike number=63%, n=5, $p<0.05$, Kruskal–Wallis, Fig. 2.9c). In the presence of TTX, the rebound depolarization produced by HCN activation was unaffected by NPA (data not shown, n=4). If the suppression of rebound discharge

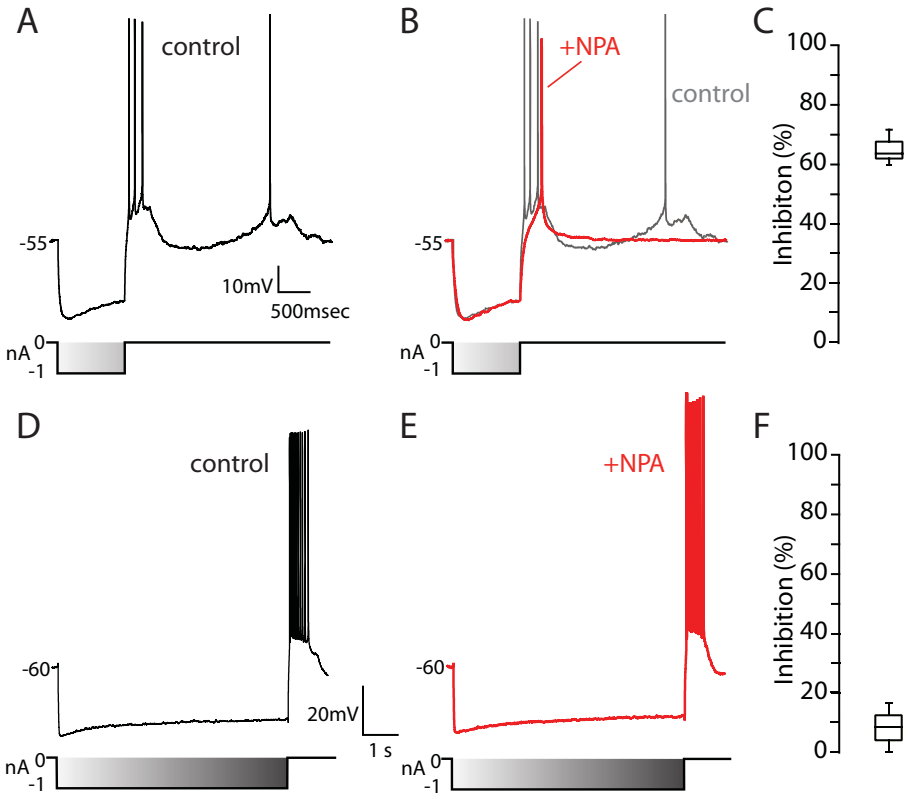

Figure 2.9. D_2 receptor activation suppresses rebound spiking.

a. Hyperpolarizing current pulse (1 s) induces rebound discharge in a cholinergic interneuron.
b. Application of the D_2 receptor agonist NPA reduces the rebound discharge (red line); control data from *a* is shown in background.
c. Statistical summary of the inhibition of rebound discharge following application of NPA (n=5).
d. Rebound discharge after a longer hyperpolarizing prepulse (10 sec).
e. NPA failed to noticeably alter the rebound discharge.
f. Statistical summary showing that NPA produced only a modest inhibition of discharge with the long prepulse, in contrast to the short prepulse (n=5).

was a consequence of enhanced slow inactivation of Na^+ channels, increasing the duration of the hyperpolarizing pulses should reverse the effects of NPA. To test this hypothesis, the current steps were lengthened to 10 seconds, a period that at 35 °C should de–inactivate roughly 90% of the Na^+ channel population. In this situation, NPA did not have a significant impact on rebound spiking (Fig. 2.9d,e,f; n=5, $p>0.05$, Kruskal–Wallis).

Is the D_2 receptor mediated suppression of pacemaking attributable to modulation of Na^+ channels?

The data presented are consistent with the hypothesis that the effects of D_2 receptor activation on evoked activity and pacemaking are attributable to an enhanced slow inactivation of voltage–dependent Na^+ channels. Is this plausible? The suppression in the transient Na^+ current produced by D_2 receptor activation was modest — 15–20%. The suppression of persistent Na^+ current was twice as large — 30–40%. But is this sufficient to explain the change in pacemaker rate? If so, then simply blocking 10–30% of the Na^+ channels with tetrodotoxin (TTX) should reproduce the effects of D_2 receptor agonists (recall that interneuron spiking in the slice is not affected by blocking synaptic input). To determine what concentration of TTX would suffice to test this hypothesis, the affinity of interneuron Na^+ channels for TTX was determined using whole cell voltage clamp recordings. The data were well fit with a Langmuir isotherm having an IC50 value of approximately 5 nM (Fig. 2.10a), a value very close to that found in other preparations (Goldin, 2001). This data suggests that the application of 1 nM TTX should block 10% of the interneuron Na^+ channels. Doing so slowed interneuronal discharge rate in the slice preparation by over 20%, on average (Fig. 2.10b,c). These data argue that even modest suppression of Na^+ channel currents can have significant effects on pacemaking.

To provide an additional test, a computational approach was used that allowed selective manipulation of Na^+ channels. A simple *Neuron* simulation was constructed using a soma, two dendrites (see Fig. 1.4a) and a complement of channels known to contribute to pacemaking and repetitive discharge in cholinergic interneurons (see Materials and Methods). To match the bi–exponential kinetic features of macroscopic currents, the Na^+ channel population was broken into

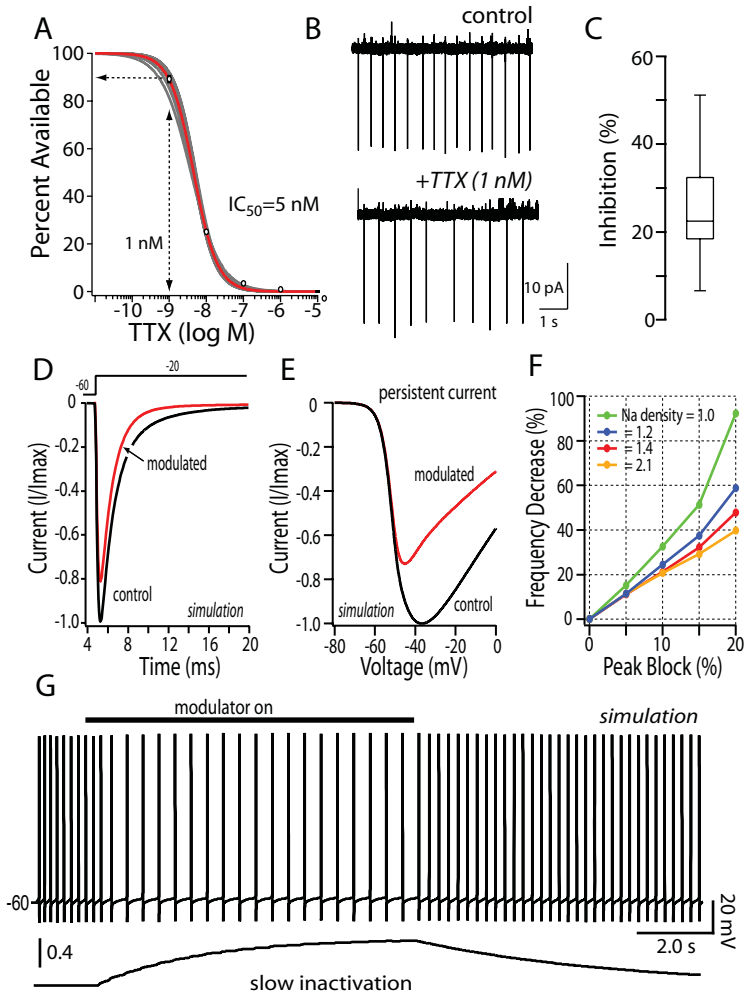
A
Percent Available
100
80
60
40
20
0
IC50=5 nM
1 nM
-10 -9 -8 -7 -6 -5
TTX (log M)
B
control
+TTX (1 nM)
10 pA
1 s
C
Inhibition (%)
60
40
20
0
D
-60
-20
0
-0.2
-0.4
-0.6
-0.8
-1.0
Current (I/Imax)
modulated
control
simulation
4 8 12 16 20
Time (ms)
E
persistent current
0
-0.2
-0.4
-0.6
-0.8
-1.0
Current (I/Imax)
modulated
simulation
control
-80 -60 -40 -20 0
Voltage (mV)
F
Frequency Decrease (%)
100
80
60
40
20
0
Na density = 3.0
= 1.2
= 1.4
= 2.1
0 10 20
Peak Block (%)
G
modulator on
simulation
-60
20 mV
2.0 s
0.4
slow inactivation

Figure 2.10. Modest suppression of Na^+ channel currents mimics D_2 receptor effects on pacemaking.

a. Dose response for relationship for TTX in acutely isolated cholinergic interneurons (n=5). Peak transient Na^+ current evoked by a step to –20 mV from a holding potential of –80 mV as a function of TTX dose were fit with a Langmuir isotherm having a slope of 1 and an IC50 of 5 nM.
b. Cell–attached patch recording in tissue slices before and after bath application of 1 nM TTX.
c. The median reduction in discharge rate was just greater than 20% (n=5), data are shown in box plot format.
d. Simulation of Na^+ channel currents evoked by a step to –20 mV before and after enhancing entry into the slow inactivated state from the fast inactivated state (Carr et al., 2003) ($\alpha S2$=0.0002 –> 0.005); the modulation was restricted to the kinetically slow current. Total (fast+slow) Na^+ current evoked by the step was reduced by 20% as in experimental observations.
e. The same change produced a larger reduction (~40%) in the total current evoked by a voltage ramp because of the relatively large contribution of the slower channel to these currents.
f. The reduction in autonomous discharge rate increased monotonically as the percent reduction in transient current was increased from 5–20%. Channel densities from 1.0 to 2.1 mS/cm^2 yielded qualitatively similar relationships.
g. In a simulation of pacemaking (Na^+ channel density of 1.4 mS/cm^2), mimicking the D_2 receptor modulation by selectively increasing Na^+ channel entry into a slow inactivated state (as in *d,e*) slowed the discharge rate by over 40%. Restoration of the control values for this rate constant restored the discharge rate. The bar depicts the onset and offset of the change in slow inactivation. At the bottom, the change in slow inactivation in the affected channel population is plotted.

fast and slow channel types, an assumption that was consistent with the molecular heterogeneity of Na^+ channel subunit expression (see above and Materials and Methods). The cell model accurately reproduced the autonomous discharge of interneurons and yielded membrane trajectories resembling those found in whole cell recordings (Fig. 2.10g). Enhancing entry of the slower channel population into the slow inactivated state (Carr et al., 2003) accurately reproduced the macroscopic modulation – decreasing peak transient current by 20% and persistent Na^+ current by 40% (Fig. 2.10d,e). This modulation led to an obvious slowing of autonomous discharge (Fig. 2.10g). Alteration in no other channel was necessary to produce this change in discharge rate. Grading the modulation to produce transient current reductions of 5–20% produced a graded reduction in pacemaker rate over a wide range of Na^+ channel densities (Fig. 2.10f). At lower channel densities, a modulation sufficient to produce a 20% suppression in transient Na^+ current almost completely stopped spiking, producing a greater than 90% reduction in spike rate. At intermediate channel densities, a modest suppression of Na^+ currents led to a suppression of discharge rates like that seen experimentally (~40%) with the application of D_2 receptor agonists. These findings, together with those derived from TTX application, provide direct support for the conclusion that modulation of Na^+ channel currents in cholinergic interneurons is a major component of the D_2 receptor mediated modulation of interneuron excitability and the reduction in autonomous spiking.

Discussion

D_2 receptor activation suppresses cholinergic interneuronal pacemaking

In associative learning paradigms, the ongoing, spontaneous activity of primate cholinergic interneurons (or TANs) is suppressed by presentation of unconditioned, positive stimuli and by learned, conditioned stimuli (Aosaki et al., 1994; Graybiel et al., 1994; Raz et al., 1996). In both cases, the suppression is dependent upon stimulus–linked elevations in dopamine cell activity and dopamine release in the striatum (Aosaki et al., 1994). Work *in vivo* has shown that the pause in cholinergic interneuronal discharge is primarily mediated by D_2 receptors (Watanabe and Kimura, 1998). In agreement with this conclusion, the application of D_2 receptor agonists to cholinergic

interneurons in the slice preparation suppressed autonomous spiking. In this preparation, activity is independent of synaptic connectivity (Bennett and Wilson, 1999), arguing that the D_2 receptors expressed by the cholinergic interneurons themselves are critical to the response. The experiments reported here provide a direct linkage between these interneuronal D_2 receptors and the ionic mechanism underlying their spontaneous activity.

D_2 receptor activation decreases Na^+ channel currents

In isolated neurons, activation of postsynaptic D_2 receptors reduced the Na^+ currents underlying pacemaking. The suppression did not depend upon an alteration in the voltage–dependence of channel opening or fast inactivation. Rather, the reduction in Na^+ channel current was brought about by an enhanced entry into a slow inactivated state (Carr et al., 2003). This endowed the modulation with profound voltage dependence. Holding the membrane potential at –55 mV, rather than –70 mV, tripled the magnitude of the modulation of peak Na^+ current, whereas holding at –90 mV virtually eliminated the development of the modulation or quickly reversed it. This feature should maximize the impact of the D_2 receptor modulation on pacemaking, where the modal membrane potential of cholinergic interneurons is near –55 mV. On the other hand, the modulation should have much less of an impact on rhythmic bursting where slow inactivation of Na^+ channels should be less prominent (Bennett and Wilson, 1999).

The D_2 receptor modulation appeared to be accomplished through a $G_{\beta\gamma}$–signaling pathway that activated PKC. This inference is based upon 1) the ability of a $G_{\beta\gamma}$ scavenger (βark–Cp) to reduce the modulation, 2) the mimicry of the modulation by PKC activators (OAG) and 3) the blockade of the modulation by intracellular dialysis with a PKC inhibitor (calphostin C). Although at variance with the conventional model of D_2 receptor coupling (Stoof et al., 1992), this signaling linkage aligns with several recent lines of study. For example, D_2 receptors have been shown to preferentially couple through $G_{\beta\gamma}$ subunits associated with $G_{o\alpha}$ to activate phospholipase C (PLC) isoforms (Hernandez-Lopez et al., 2000; Jiang et al., 2001). PKC activation is a well–characterized consequence of PLC stimulation, resulting from the generation of diacylglycerol (DAG) and

mobilization of Ca^{2+} from inositol trisphosphate (IP_3) sensitive intracellular stores. This linkage also is consistent with the recent demonstration that phosphorylation of Na^+ channels enhances entry into a slow inactivated state (Carr et al., 2003).

Is the suppression of Na^+ channel currents sufficient to explain D_2 receptor mediated changes in pacemaking?

Although it is clear that activation of D_2 receptors led to a suppression Na^+ channel currents, the modulation of transient Na^+ currents was modest. Although within the range reported in previous studies (Cantrell and Catterall, 2001), peak transient current at –55 mV was reduced by only about 15–20% by D_2 receptor agonists or PKC activators. The maximal persistent Na^+ conductance was more substantially reduced (~30–40%) by the same manipulations, but is this sufficient to account for the suppression in pacemaking seen in tissue slices? There are two lines of evidence that suggest so. First, application of the specific Na^+ channel blocker TTX a concentration adequate to block only 10% of the Na^+ channel population (with full penetration of the tissue) reduced pacemaking by over 20% on average. Since pacemaking is not dependent upon synaptic input (Bennett and Wilson, 1999), this reduction is directly attributable to blockade of the Na^+ channels underlying pacemaking. Second, computer simulation of the pacemaking process in cholinergic interneurons revealed that a modest enhancement of Na^+ channel slow inactivation – one sufficient to bring about reductions in transient and persistent current like those seen experimentally – had profound effects on pacemaking. At intermediate channel densities that gave discharge rates like that seen *in vivo* (3–6 Hz), suppression of the transient Na^+ channel current by 15% and the persistent current by about 30% brought about a 30–50% reduction in spiking rate. Given the likelihood that acute isolation and whole cell dialysis attenuates the D_2 receptor mediated modulation of Na^+ channels, the degree of agreement between the experimental results (where D_2 receptor agonists decreased the discharge rate by around 40%) and the simulation is remarkable. The simulations also showed that the relationship between channel inactivation and discharge rate was monotonic over a wide range, providing a potential readout of the intensity of D_2 receptor

stimulation. The sensitivity of pacemaking to Na^+ channel modulation isn't surprising given that the slope of the current–voltage relationship in cholinergic interneurons is very shallow in the voltage range were Na^+ channels begin to open (Bennett et al., 2000), allowing small changes in current to significantly change the trajectory of the membrane potential to the next spike. This appears to be a common feature of Na^+ channel dependent pacemakers (Raman and Bean, 1999; Taddese and Bean, 2002; Do and Bean, 2003).

There are undoubtedly collateral mechanisms by which dopamine acts to suppress the activity of cholinergic interneurons. The best characterized of these is the D_5 receptor–mediated augmentation of spike after–hyperpolarization, which should slow discharge (Bennett and Wilson, 1998). This modulation could account, in part, for conjectured involvement of D_1–class receptors in generation of the pause (Watanabe and Kimura, 1998). These alterations in intrinsic properties governing autonomous spiking complement the direct D_2 receptor mediated inhibition of acetylcholine release (Lehmann and Langer, 1983; Bertorelli et al., 1992; Stoof et al., 1992; Di Chiara et al., 1994; Yan et al., 1997), further reducing the impact of cholinergic interneurons on striatal circuitry.

Although dopamine acts directly on interneurons, it may also sculpt synaptic inputs to cholinergic interneurons that contribute to the generation of pauses during learning. Thalamic inputs carrying sensory information are important participants in the regulation of cholinergic interneuronal activity (Matsumoto et al., 2001). Although there are direct thalamic projections to cholinergic interneurons (Wilson et al., 1990; Lapper and Bolam, 1992), the most important synaptic linkage in this context may be through intrastriatal GABAergic interneurons. Thalamic activation of these neurons following presentation of a sensory cue could act to suppress cholinergic interneuron discharge. But, because thalamic activity does not appear to be contingent upon reward, this linkage would have to be gated by dopamine. This could be accomplished by dopaminergic enhancement of GABAergic interneuron activity (Bracci et al., 2002) and of cholinergic interneuron sensitivity to this input (Yan et al., 1997; Yan and Surmeier, 1997).

Conclusions

The studies reported here show that activation of D_2 dopamine receptors suppresses evoked activity and autonomous pacemaking in identified cholinergic interneurons. PKC– dependent enhancement of Na^+ channel slow inactivation appears to make a major contribution to this reduction in activity. The voltage dependence and kinetics of the change in Na^+ channel gating state create a novel form of short–term, activity–dependent plasticity that may contribute to striatal alterations in associative and instrumental learning paradigms.

Section 3.3: Resurgent Nav1.6 channel gating is critical to pacemaking and fast spiking in globus pallidus neurons

Introduction

The external segment of the globus pallidus (GP) is a key component of the basal ganglia circuitry controlling movement (Albin et al., 1989). Principal, GABAergic GP neurons normally exhibit sustained high frequency spiking that is interrupted by pauses that are associated with movement (DeLong, 1971; Wichmann and DeLong, 1999; Raz et al., 2000; Bevan et al., 2002b). In Parkinson's disease (PD), the activity of many GP neurons change. Rhythmic, high frequency bursts of spiking becomes the predominant firing pattern (Filion and Tremblay, 1991; Raz et al., 2000). Similar patterns of activity emerge in the synaptically coupled entopeduncular nucleus (EP) and the subthalamic nucleus (STN). This pathological pattern of spiking is thought to be responsible for motor symptoms as they are alleviated by lesioning or deep brain stimulation (DBS) of these nuclei (Wichmann and DeLong, 1999). The factors controlling the emergence of this pathological activity are not clear, but modeling studies have implicated interplay between the intrinsic properties of GP neurons and their synaptic interaction with STN neurons (Terman et al., 2002).

The intrinsic properties of GP neurons that contribute to the emergence of rhythmic burst firing in PD are not well understood. What is known is that these neurons are unusual in that they are fast spiking, autonomous pacemakers (Chan et al., 2004; Surmeier et al., 2005). In other cell types, voltage dependent Na^+ channels are primary determinants of these behaviors. In cerebellar Purkinje neurons for example, Nav1.6 Na^+ channels reopen during the falling phase of the spike, giving rise to a resurgent current that promotes high frequency spiking (Raman and Bean, 1997; Khaliq et al., 2003). This gating mode also is important for the maintenance of autonomous pacemaking in these cells. Although voltage–dependent Na^+ channels are critical to autonomous pacemaking in GP neurons (Kita and Kitai, 1991; Nambu and Llinas, 1994; Chan et al., 2004), it

is not known to what extent resurgent gating contributes to this capacity and that of fast spiking. In the neighboring subthalamic nucleus (STN), neurons are minimally affected by the loss of Nav1.6 subunits, unlike Purkinje neurons (Raman et al., 1997; Do and Bean, 2004).

Not only should Na^+ channels be primary determinants of rhythmic bursting in PD, but they should also be critical to how GP neurons respond to DBS. DBS was originally thought to functionally inactivate neurons by producing enough Na^+ channel inactivation to prevent the generation of a spike (depolarization block) (Benabid et al., 1998; Beurrier et al., 2001; Tai et al., 2003). Although more recent work has questioned this inference (Benabid et al., 2002; Lozano et al., 2002; Hashimoto et al., 2003; McIntyre et al., 2004b; McIntyre et al., 2004a; Vitek et al., 2004), the prevailing view remains that functional activity of targeted structures is suppressed by DBS. Direct electrophysiological examination of changes produced by high frequency stimulation revealed a substantial reduction in Na^+ channel availability in acutely isolated STN neurons, largely mediated by slow inactivation (Do and Bean, 2003). It is not clear whether this result can be generalized to other fast spiking basal ganglia neurons, like GP neurons.

The studies reported here employ electrophysiological, molecular and modeling approaches to characterize Na^+ channels in GP neurons that underlie fast spiking and pacemaking, as well as the response to DBS. Although similar in many respects to those found in regular spiking neurons, Na^+ channels in GP neurons were distinctive in the prominence of their resurgent gating mode. This gating mode was strongly, but not exclusively, dependent upon channels with a pore–forming Nav1.6 subunit. Nav1.6 channels with resurgent gating were critical to the ability of GP neurons to spike autonomously at normal frequencies and to respond to extrinsic stimulation with high frequency spiking for sustained periods. In their absence, GP neurons respond to DBS as originally envisioned, with depolarization block and cessation of spiking.

Results

Autonomous discharge rate in GP neurons grades with Na^+ Channel availability

In tissue slices held at room temperature (20–22°C), medium sized, GABAergic GP projection neurons spike autonomously at just over 10 Hz (12.3±0.3 Hz) in a very regular manner (CV=0.18±0.01) (Fig. 3.1a). In contrast, large basal forebrain cholinergic neurons found along the medioventral border of the GP with the internal capsule were quiescent; these cells were excluded from this study. Although previous work had established the Na^+ channel dependence of autonomous pacemaking in GP neurons, the quantitative features of this relationship have not been examined. To fill this gap, the efficacy of Na^+ channel block tetrodotoxin (TTX) was determined using acutely isolated GP neurons where the Na^+ channel currents could be isolated and voltage–clamped (Narahashi et al., 1960). Similar to findings in other cell types (Goldin, 2001; Maurice et al., 2004), the TTX dose–response relationship was fit with a single site Hill–Langmuir equation having an IC_{50} of near 3 nM (Fig. 3.1b). Next, to determine the effect of Na^+ channel block on pacemaking, increasing doses of TTX were applied and the effect on autonomous discharge of GP neurons in tissue slices was measured. Surprisingly, the effect of TTX on Na^+ channel availability predicted its effect on discharge rate (Fig. 3.1e). Autonomous pacemaking was more sensitive to Na+ channel block than was spiking per se, as blocking roughly 95% of Na^+ channels eliminated pacemaking without preventing generation of a spike in response to a brief current pulse (Fig. 3.1d).

Neurons lacking the Nav1.6 subunit display reduced resurgence and slowed autonomous pacemaking

Channels composed of the Nav1.6 α subunit have been shown to be critical in the physiology of active neurons. First, studies in heterologous systems have demonstrated that Nav1.6 channels yield a larger sub–threshold current than do Nav1.1 or Nav1.2 channels (Smith et al., 1998; Smith and Goldin, 1998). Second, the preferential axonal localization of Nav1.6 channels suggest an important role in action potential initiation (Caldwell et al., 2000; Krzemien et al., 2000; Tzoumaka et al., 2000; Boiko et al., 2001; Boiko et al., 2003; Wittmack et al., 2004). Third,

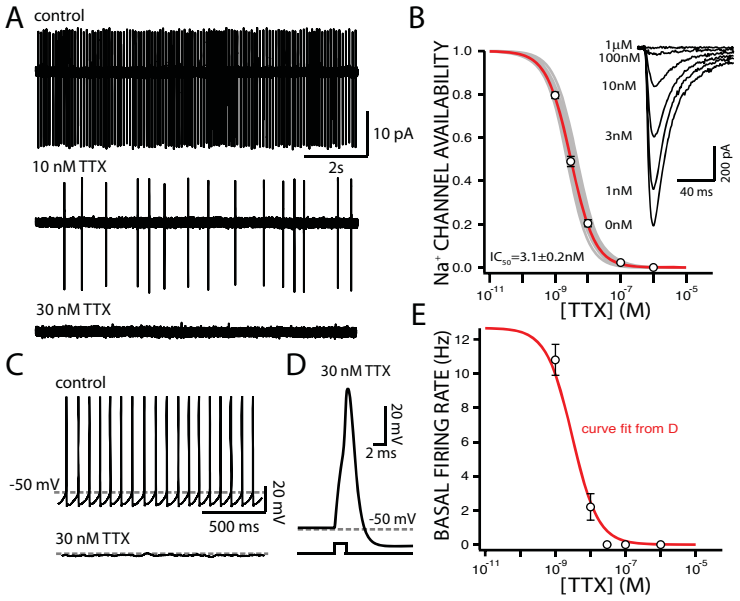

Figure 3.1. Firing rate of GP neurons is sensitive to Na^+ channel availability

a. Unit activity of visually identified GP neuron in standard ACSF (top), 10 nM TTX (middle) and 30 nM TTX (bottom).
b. IC_{50} curve for TTX in the dissociated, voltage–clamped prep. Na^+ current was measured by 5 ms voltage steps to –20 mV from –80 mV (inset). IC_{50}=3.1±0.2 nM.
c. 30nM TTX blocks spontaneous activity and subthreshold oscillatory activity in a GP neuron.
d. A 2 ms, 500 pA depolarizing current injection could still elicit a spike in 30 nM TTX.
e. The basal firing rate in the presence of TTX is accurately predicted by the IC_{50} curve for TTX.

mutations of the Na1.6 gene (SCN8A) that result in loss of function have been connected with motor endplate disease (Burgess et al., 1995; Kohrman et al., 1995; Kohrman et al., 1996). One such mutation, *med*^{JTG}, results in lack of functional Nav1.6 channels in homozygous cells (Nav1.6–/–). In Purkinje neurons from Nav1.6–/– mice, resurgent Na^+ current is lost and there is a significant reduction in spontaneous firing (Khaliq et al., 2003). In STN neurons, loss of Nav1.6 channels leads to a less drastic reduction in resurgence and a modest reduction in spontaneous firing (Do and Bean, 2004). In MS neurons, Nav1.6–/– neurons have a significant reduction in both transient and persistent Na^+ current (Fig. 3.2a,b). In dissociated GP neurons from Nav1.6–/– mice, there was a prominent (~40%) reduction in the amplitude of resurgent current (Fig. 3.3a,b) without a similar reduction in transient and persistent current amplitudes or alterations in voltage dependence or slow inactivation (Fig. 3.4a,b,c,d). Although transient and persistent currents were unchanged in Nav1.6–/– neurons, autonomous pacemaking was dramatically slowed. Wild–type GP neurons spiked autonomously near 12 Hz in the intact slice at room temperature ($frequency_{(median)}$=12.4 Hz, n=101), while Nav1.6–/– neurons spiked at half that rate ($frequency_{(median)}$=5.9 Hz, n=35, $p<0.05$, Mann–Whitney; Fig. 3.3c,e). Action potential threshold was also elevated, shifting from –44±1 mV in wild–type neurons to 37±1 mV in Nav1.6–/– neurons (measured as the voltage at which there was a discontinuity or kink in the dV/dt vs. V phase plot, see Fig. 3.3d; $p<0.05$, Mann–Whitney). These observations of reduced discharge and shifted spike threshold are commonly attributed to reduced Na^+ channel availability.

Nav1.6 channels enhance the response to intracellular current injection

Since resurgent Na^+ current is thought to play an important role in high frequency spiking, maximal spiking rates of Nav1.6–/– neurons were examined using current ramps. Wild–type neurons were frequently able to sustain spiking throughout the ramp, often reaching maximal frequencies over 130 Hz at room temperature (129.6±10 Hz, n=8, 3 of these 8 sustained firing throughout the ramp). In contrast, none of the Nav1.6–/– neurons were able to sustain spiking throughout the ramp and had significantly lower maximal firing frequencies (99.7±7.8 Hz, n=8; $p<0.05$, Mann–Whitney;

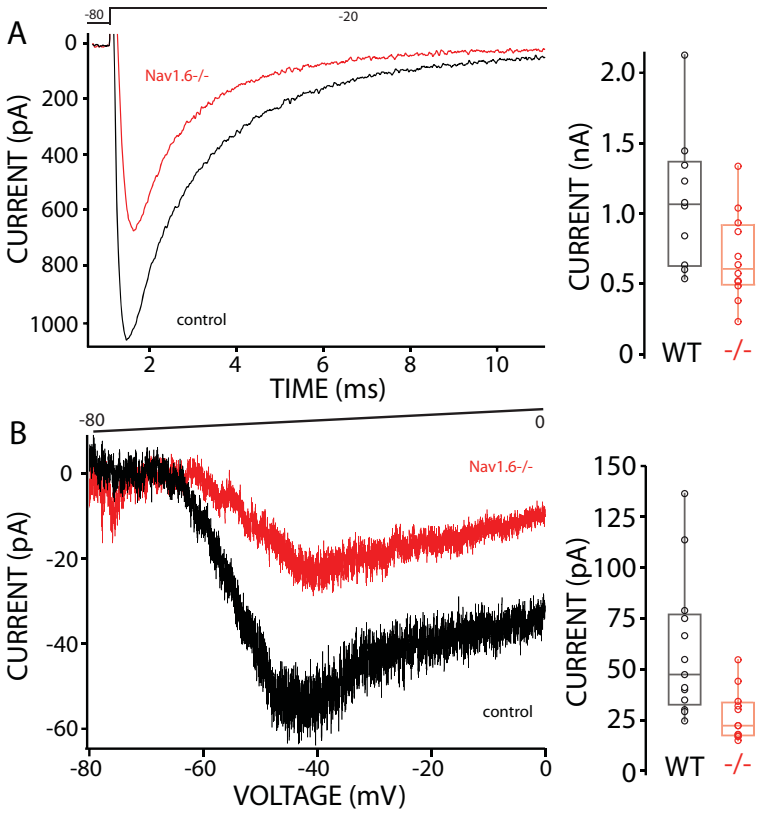

Figure 3.2. Transient and persistent Na^+ currents are reduced in medium spiny Nav1.6–/– neurons.

a. Transient current elicited by a test step from –80 mV to –20 mV is reduced 40% in Nav1.6–/– neurons ($amplitude_{median}$=610 pA for Nav1.6–/– neurons (n=13), $amplitude_{median}$=1070 pA for wild–type neurons (n=10), $p<0.05$ Mann–Whitney Rank Sum Test).

b. The Nav1.6–/– persistent current in the same population of neurons is reduced by 60% ($amplitude_{median}$=22 pA for Nav1.6–/– neurons (n=13), $amplitude_{median}$=55 pA for wild–type neurons (n=5), $p<0.05$ Mann–Whitney Rank Sum Test).

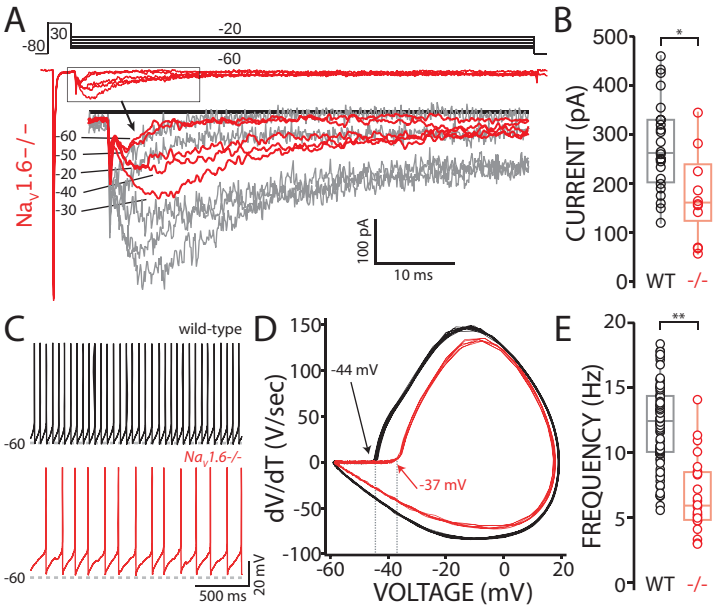

Figure 3.3. Nav1.6–/– GP neurons show a selective decrease in the resurgent Na⁺ current and a reduction in firing frequency.

a. Resurgent current from a typical Nav1.6–/– GP neuron (red traces) overlaying traces from a wild–type neuron (from fig. 5A), measured in physiologic external Na^+ in whole–cell voltage clamp of dissociated neurons.

b. Box plots of resurgent current amplitude in dissociated GP neurons from WT (left) and Nav1.6–/– (right). The median amplitude, measured as peak from baseline at –30 mV, for wild–type is 260 pA (n=37), while the median for Nav1.6–/– GP neurons is reduced 40% to 158 pA (n=11)($p<0.005$, Mann–Whitney Rank Sum Test).

c. Traces of spontaneous activity in wild–type (top trace, 18 Hz) and Nav1.6–/– (bottom trace, 8 Hz) GP neurons recorded in whole–cell mode in an intact slice.

d. The phase plot of the spike wave form, generated by plotting the derivative of the voltage as a function of membrane potential, shows a clear shift in spike threshold between wild–type and Nav1.6–/– neurons, –44±1mV and –37±1mV ($p<0.001$, Mann–Whitney Rank Sum Test, n=11).

e. Population data on spontaneous firing frequency of wild–type (left, median=12.4 Hz, n=101) and Nav1.6–/– (right, median=5.9 Hz, n=35) GP neurons, as measured in the cell attached mode. The basal firing rate is significantly reduced in Nav1.6–/– neurons ($p<0.001$, Mann–Whitney Rank Sum Test).

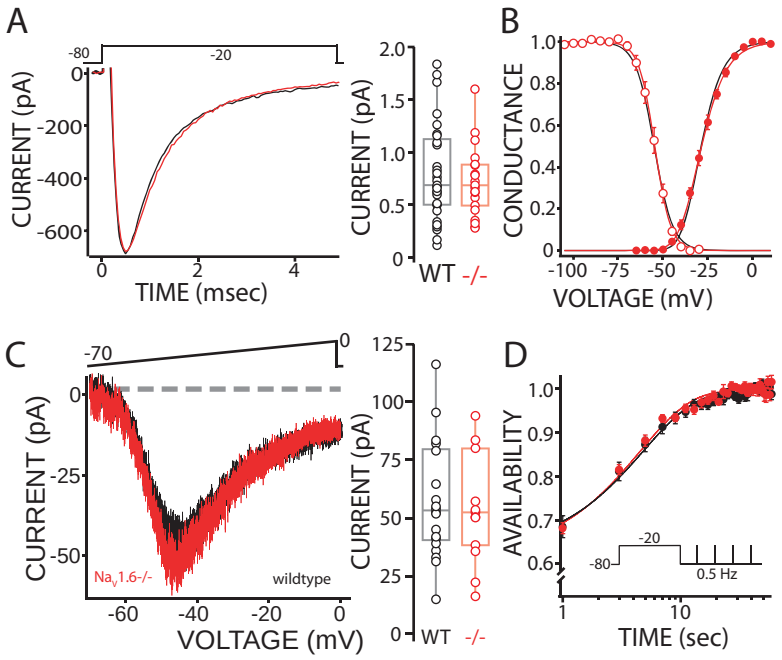

Figure 3.4. Nav1.6–/– neurons show similar transient and persistent current properties.

a. Representative traces of currents elicited by a voltage step to –20 mV for wild–type (black) and Nav1.6–/– GP neurons (amplitude$_{median}$=673.5 pA [n=30] and 667.6 pA [n=20] for wild–type and Nav1.6–/–, respectively, p>0.05 Mann–Whitney).

b. Na^+ channel steady state voltage dependence of activation (closed red circles) and inactivation (open red circles) of Nav1.6–/– neurons are similar to wild–type neurons (black lines). Activation: Vh=–40.2±0.7 mV, Vc=8.4±0.2. Inactivation: Vh=–54.8±1.1, Vc=4.3±0.3.

c. The persistent current trajectory and amplitudes of Nav1.6–/– neurons were similar to wild–type (amplitude$_{median}$=52.1 pA [n=18] and 51.9 pA [n=12] for wild–type and Nav1.6–/–, respectively, p>0.05 Mann–Whitney)

d. Amount of channels slow–inactivated by a 5 second step to –20 mV in Nav1.6–/– neurons and recovery kinetics at –80 mV are similar to wild–type neurons. The time constants for recovery at –80 mV for wild–type and Nav1.6–/– neurons are 3.7±0.5s and 4.4±0.5, respectively.

Fig. 3.5a,c).

Another prominent difference between wild–type and Nav1.6–/– neurons was the magnitude of the hysteresis in their response to current injection. Wild–type neurons displayed relatively little hysteresis in their response to the ramp protocol, spiking at nearly the same rate during the falling phase of the rate as the rising phase. In contrast, Nav1.6–/– neurons frequently were completely silent during the falling phase, typically spiking only briefly at the very end of the pulse. This difference in performance is illustrated in a cumulative frequency plot (Fig. 3.5e).

Were the loss of Nav1.6 important solely for the reduction in resurgent current, it would be predicted that the first spike of the ramp in Nav1.6–/– neurons would have a similar spike threshold to wild–type neurons, since holding the neuron at –70 mV would recover more fast–inactivated channels, normalizing the availability. However, with a ramp speed of 1 nA/sec, the first spike was delayed in Nav1.6–/– neurons and had a more depolarized threshold than wild–type neurons (latency time of 102±10 ms versus 57±8 ms for wild–type, $p<0.05$, threshold of –46±2 mV for Nav1.6–/– and –52±1 mV for wild–type, $p<0.05$; Mann–Whitney; Fig. 3.5b,c). This shift in the threshold of the first spike could result from incomplete localization of Nav1.1 and 1.2 to the initial segment and nodes of the axon, such that the density of Na^+ channels at the spike initiation site is reduced. A second explanation is that Nav1.6, in addition to conducting a larger resurgent current, has other unique gating kinetics that allow for increased conduction of Na^+ current during the ramp towards threshold, allowing it to reach threshold faster before more inactivation has occurred. This explanation would suggest that the gap between spike thresholds of the Nav1.6–/– and the wild–type neurons would be larger at slower ramp speeds, when the neurons are more dependent on subthreshold currents to push the membrane towards threshold. When the ramp speed is slowed to 25 pA/sec, the spike threshold in wild–type neurons is shifted by less than 1 mV, to –51±1 mV, while the spike threshold of Nav1.6–/– is reduced by almost 3 mV, to –43±1 mV (the difference between wild–type and Nav1.6–/– spike threshold at 1 nA/sec is 6 mV, at 25 pA/sec it is 9 mV). While localization of Nav1.6 is likely important for proper activity, this data suggests that the unique

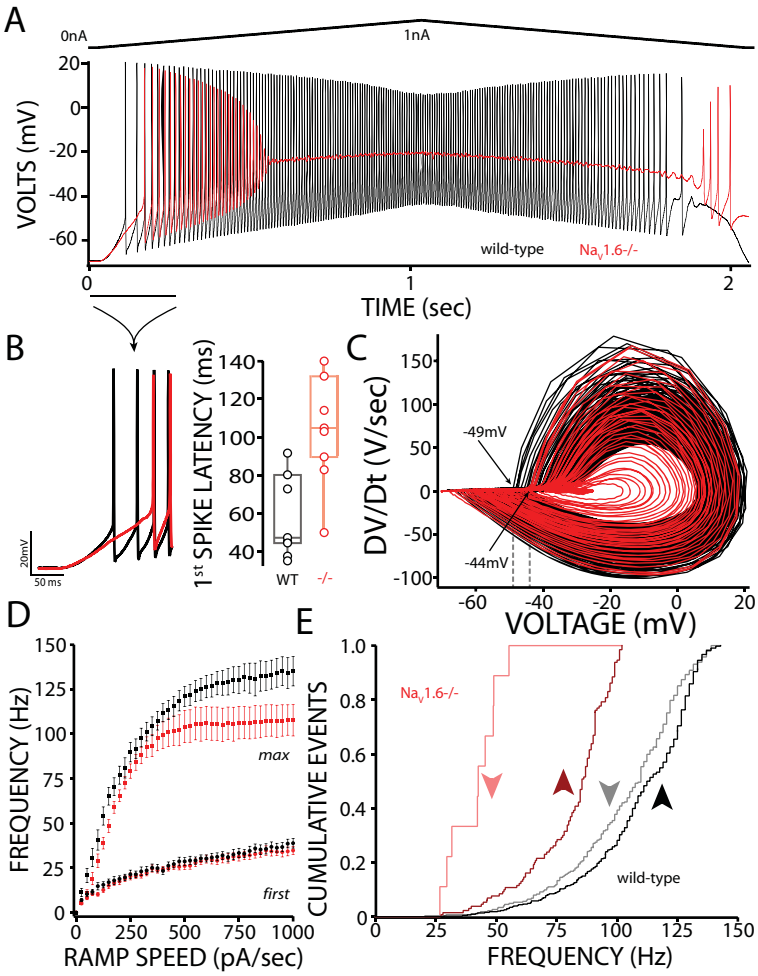
A
0nA
1nA
VOLTS (mV)
wild-type
Nav1.6-/-
TIME (sec)
B
20mV
50 ms
1st SPIKE LATENCY (ms)
WT
-/-
C
DV/Dt (V/sec)
-49mV
-44mV
VOLTAGE (mV)
D
FREQUENCY (Hz)
max
first
RAMP SPEED (pA/sec)
E
Nav1.6-/-
wild-type
CUMULATIVE EVENTS
FREQUENCY (Hz)

Figure 3.5. Nav1.6–/– GP neurons have reduced peak frequencies when driven to fire at high frequencies by a depolarizing ramp current.

a. Voltage traces from a wild–type (black) and Nav1.6–/– neuron (red) during a 1 second ramp to 1 nA current. The ramp protocol was 2 seconds long from a baseline near –70 mV (to stop spontaneous activity): 1 second depolarizing with varying speeds (from 0–1nA/sec) and 1 second relaxing back to 0 pA current.
b. Enlargement of the initial phase of the ramp shows a longer latency for Nav1.6–/– (red, median=103.8 ms) than for wild–type neurons (black,median=46.35 ms)($p<0.005$, Mann–Whitney Rank Sum Test, n=8). Boxplots on the right show population data of wild type (left) and Nav1.6–/– neurons (right).
c. Phase plots of the wave forms from *a* show a shift in the threshold of the first spike from a median of –50 mV for wild type (black) to –42 mV for Nav1.6–/– neurons (red)($p<0.001$, Mann–Whitney Rank Sum Test, n=8).
d. The first and maximum firing frequency as a function of ramp speed reveals a decrease in maximum frequency reached in Nav1.6–/– neurons (mean±SEM=99.7±7.8 Hz) versus wild–type neurons (mean±SEM=129.6±10 Hz)($p<0.05$, Mann–Whitney Rank Sum Test, n=8).
e. Cumulative frequency plot showing a significant shift in the firing frequency of Nav1.6–/– neurons. Also evident is a significant hysteresis in the Nav1.6–/– population generated by the significant period spent in depolarization block where no spiking occurred (n=5).

gating properties of Nav1.6 are also crucial for the availability of channels during the ramp towards threshold and the lower threshold necessary to drive spike initiation in the initial segment.

Nav1.6 channels govern the response to DBS–like stimulation

Despite the proven therapeutic benefit of high frequency deep brain stimulation, the cellular mechanisms by which it alleviates symptoms is unclear. The similarities of outcomes between surgical ablation and DBS suggest it works through inactivation of the targeted nuclei (Bergman et al., 1990; Gill and Heywood, 1997). Direct recordings in the STN during and immediately following DBS support this, proposing that depolarization block (Na^+ channel inactivation) inhibits the pathologically hyperactive STN (Beurrier et al., 2001; Tai et al., 2003). Contradictory to this, nuclei downstream of the STN are activated during DBS of the STN (Jech et al., 2001; Hashimoto et al., 2003; Windels et al., 2003). This suggests that stimulation in the STN might be activating pallidosubthalamic axons running through the STN, leading to simulation of GP neurons (McIntyre et al., 2004a). However, because of the difficulties inherent in interpreting intrinsic activities in the intact network of the basal ganglia, there have been no direct tests as to whether GP neuron can effectively respond to this high frequency stimulation. To test this hypothesis, long trains of brief pulses (2 ms, 500 pA) were applied to GP neurons recorded in the whole cell configuration at 22°C. At 50 Hz, GP neurons were fully capable of following every stimulus (Fig. 3.6a). At 100 Hz, neurons followed the stimuli for a while and then settled into a regular discharge at a lower preferred frequency (Fig. 3.6b). At 250 Hz, again GP neurons followed the stimulus train briefly and then settled into a regular discharge at their preferred frequency near 50 Hz (Fig. 3.6c). Thus, high frequency stimulation did not induce depolarization block and cessation of firing but rather regular spiking at a preferred frequency (Fig. 3.6d). Assuming a Q_{10} of 3 for the gating of channels in the membrane (Hodgkin and Huxley, 1952; Jonas, 1989; Rodriguez et al., 1998), this result suggests that at body temperature (37° C), GP neurons should be capable of sustained spiking at over 150 Hz (50 Hz X 3), within the range of 100–180 Hz used in PD patients (Wu et al., 2001; Vitek et al., 2004).

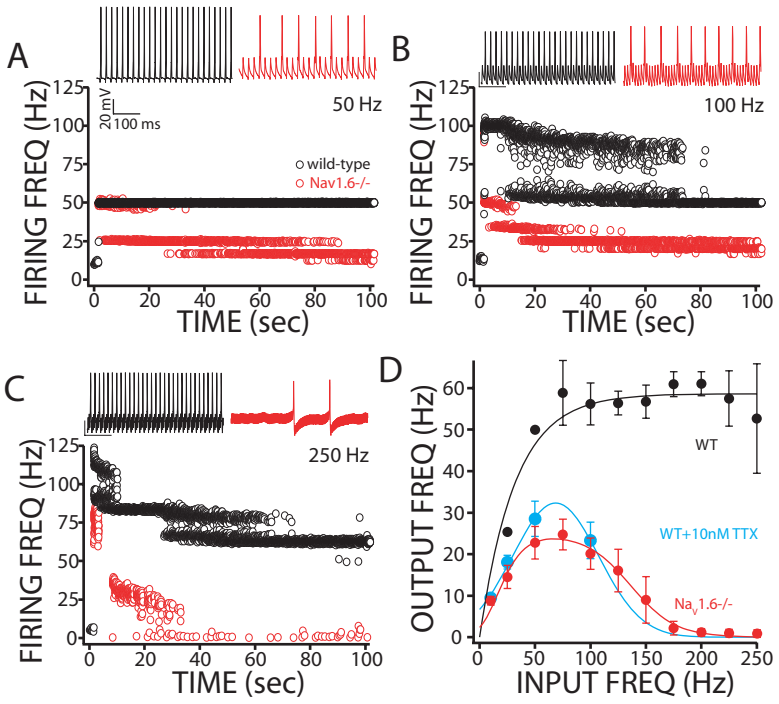

Figure 3.6. High frequency stimulation establishes a set frequency near 50 Hz in wild–type neurons.

a. Raster plot of output frequency as a function of time during 50 Hz high frequency stimulation trains for wild–type (black circles) and Nav1.6–/– (red circles) neurons. Stimulus was a 100 second train of 2 ms, 500 pA pulses.
b. Raster plot of output frequency as a function of time during 100 Hz stimulation.
c. Raster plot of output frequency as a function of time during 250 Hz stimulation.
d. Population data of output frequency as a function of input frequency. Wild–type neurons (black circles) were capable of maintaining firing near 50 Hz, regardless of the stimulus frequency, while Nav1.6–/– neurons (red circles) were incapable of keeping up with the stimulus at frequencies as low as 25 Hz, and became unresponsive to the stimulus at high frequencies. Wild–type neurons bathed in 10 nM TTX (blue circles) showed a similar profile as Nav1.6–/– neurons.

Unlike wild–type neurons, Nav1.6–/– GP neurons were not capable of sustained high frequency discharge. Even at 25 Hz, Nav1.6–/– neurons failed to spike with every pulse. At higher stimulation rates, neurons were essentially unresponsive, firing in a random, intermittent fashion (Fig. 3.6d). Why was there such a dramatic difference between the two cell types when there was no difference in the density of somatodendritic transient and persistent Na^+ current? Spike initiation is widely held to occur in the axon initial segment or first node of Ranvier (Colbert and Johnston, 1996; Fohlmeister and Miller, 1997; Stuart et al., 1997; Colbert and Pan, 2002; Clark et al., 2005; Palmer and Stuart, 2006). These subcellular locations appear to be enriched in Nav1.6 channels (Caldwell et al., 2000; Krzemien et al., 2000; Tzoumaka et al., 2000; Boiko et al., 2001; Boiko et al., 2003; Wittmack et al., 2004). In an attempt to mimic the depletion of Nav1.6 channels at these key sites, TTX was applied to wild–type neurons and the response to high frequency stimulation measured. Only when roughly 80% of all the Na^+ channels were blocked did wild–type neurons perform as poorly as did Nav1.6–/– neurons (Fig. 3.6d). These results suggest that the ability of GP neurons to spike at high frequencies and maintain spiking in response to clinically effective DBS frequencies depends upon their expression of Nav1.6 channels.

Computer simulation confirms the importance of resurgent gating

To better understand the contribution Nav1.6 channels and resurgent gating to the ability of GP neurons to spike at high rates, biophysically accurate channel models were constructed that could be incorporated into a simulation of pacemaking and high frequency spiking. Using the *Neuron* platform (Hines and Carnevale, 1997, 2001), two Na^+ channel models were constructed. Both models had a topology similar to previous models (Kuo and Bean, 1994; Taddese and Bean, 2002; Carr et al., 2003), but added blocked (resurgent) states (Raman and Bean, 2001; Khaliq et al., 2003) and had multiple slow inactivated states to attempt to capture the power law behavior of slow inactivation (Ellerkmann et al., 2001) (Fig. 3.7a). One of these, referred to as the Nav1.1/1.2 model (Na1), accurately reproduced the currents seen in Nav1.6–/– GP neurons. The second model, referred to as Na6, was added to the first to give an accurate reproduction of the wild–type Na^+

currents (Fig. 3.7a; see Fig. 3.9 for a more detailed comparison of the modeled Na^+ currents to those generated in the acutely dissociated preparation).

To generate an estimate of how Na^+ channel availability was affected by pacemaking and DBS, channels were inserted into a spherical soma and the membrane potential driven with a simulated patch electrode. First, pacemaking was studied. Using the voltage trajectory of a GP neuron pacemaking at 12 Hz, Na^+ channel state was monitored by measuring the probability of being in closed or open (not inactivated) states. At steady–state, Na6 availability reached 40% whereas that of Na1 channels never was above 12%. Using the 4.25:1 proportion of Na1:Na6 channels predicted from the change in resurgent current seen following Nav1.6 loss (Fig. 3.7b), the maximum Na^+ channel availability during pacemaking is just under 20% (~17%; Fig. 3.7c,d). The difference in channel availability during pacemaking is largely attributable to the resurgent gating mode. In the first two milliseconds following the repolarization of the spike, the modNa1.6 channel recovers much faster than the Na1 channel, with 16% of these channels becoming available after two milliseconds. Only about 1% of the Na1 channels recover in the same period. When resurgent gating is eliminated (by changing Ob_0 to $1x10^{-9}$ and O_{on} of both channel types to 3), recovery over the first 2 ms was less than 1% and the maximal Na^+ channel availability only 11% (Fig. 3.7c,d).

The same discrepancy in channel occupancy was seen during DBS–like stimulation. Using the voltage of a GP neuron recorded during the experiments described above, channel availability was measured in the simple model. At 50 Hz, Na^+ channel availability stabilized at roughly half that of basal firing (Fig. 3.7e). Na6 channels recovered about 7% in the 2 ms following the stimulus–evoked spike and 17% by the next stimulus. Na1 channels recovered only 2% during the first 2 ms and only 4% by the next stimulus. Combined, total Na^+ channel availability was 7% by the next stimulus, well above the availability threshold determined by the TTX experiments (see Fig. 3.1d). However, without resurgence, channel availability only reached 4% by the time of the next stimulus, below the 5% threshold seen in the TTX experiments.

To extend these simulations to a more realistic setting, a more anatomically correct model

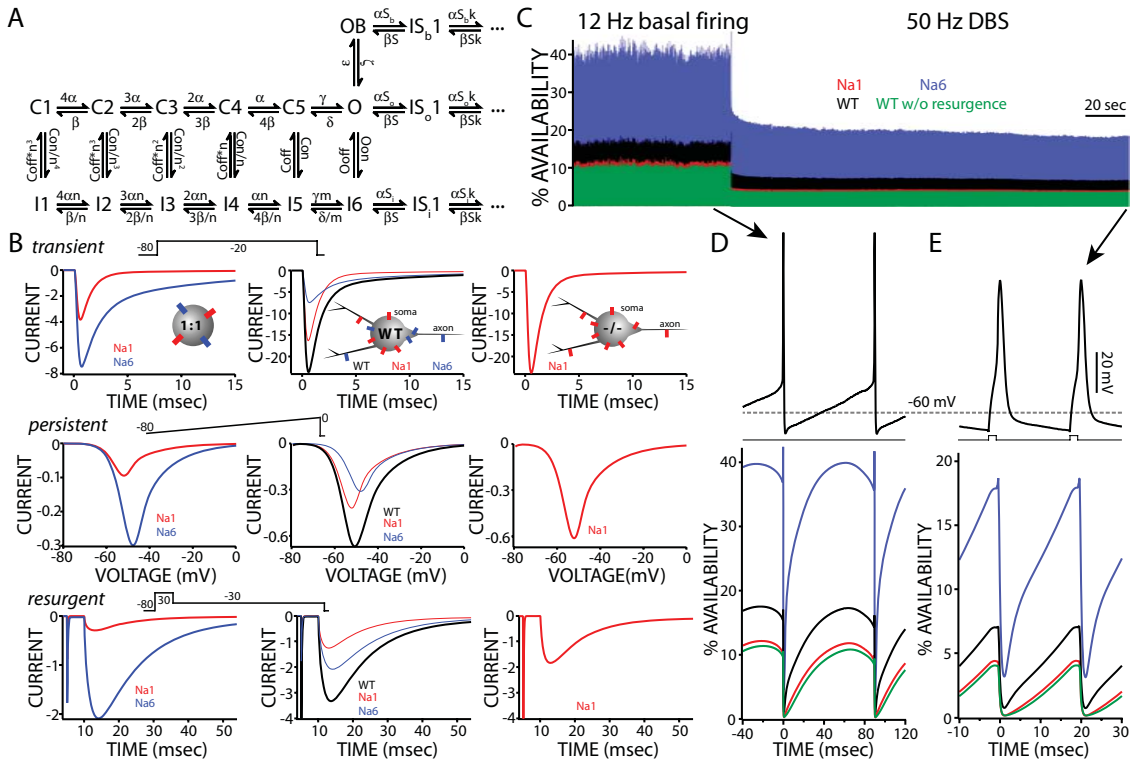

Figure 3.7. Two Na⁺ channel model of wild type and Nav1.6–/– neurons.

a. Markov model based on previous work (Kuo and Bean, 1994; Raman and Bean, 2001; Carr et al., 2003) modified by adding additional slow inactivated states to better mimic the time–dependence of this process (see Fig. 3.9e,f for a more complete analysis) as well as adjusting some rate constants to better predict the kinetic properties measured in this paper (see methods & materials for a more complete description of model parameters).

b. Transient (top), persistent (middle) and resurgent (bottom) current traces generated by a 1 Na1:1 Na6 ratio of insertion (left), 4.25 Na1:1 Na6 ratio (middle) and 5 Na1:0 Na6 ratio (right) of the Na1 (red) and Na6 (blue) channels. Na6 is a modified version of Na1 with ζ increased and Oon decreased to enlarge the relative amplitude of the resurgent current. In the middle column, the WT Na⁺ current is shown as a sum of the Na1 and Na6 traces.

c. Availability of Na⁺ channels, measured as the sum of channels in the O and $C_{1–5}$ states during a voltage command created by basal firing at 12 Hz, followed by the voltage response of a representative neuron to 50 Hz high frequency stimulation for 100 seconds. Plotted are Na1 (red), Na6 (blue), the wild–type population estimate calculated by (4.25*Na1+Na6)/5.25 (black) and the wild–type estimate with no resurgence (green).

d. An enlarged view of the availability of Na⁺ channels in the model neuron during basal firing.

e. An enlarged view of the availability of Na⁺ channels in the model neuron during the 50 Hz DBS protocol.

was created that had an axon, initial segment, soma and four primary dendrites (see Materials and Methods). The axon and initial segment were populated with Na6 channels whereas the dendrites and soma were largely populated with Na1 channels (densities [in S/cm^2]: axonal nodes/initial segment= 0 Na1, 0.9 Na6; soma/axon hillock=0.04 Na1, 0.01 Na6; dendrites=0.02 Na1, 0 Na6). In addition, K^+, Ca^{2+} and cationic (HCN) channels were inserted at densities similar to those used in previous models (Chan et al., 2004); see Materials and Methods). The model displayed autonomous pacemaking, spiking in a regular way at around 12 Hz (Fig. 3.8a). Replacing Na6 channels with Na1 channels (mimicking the Nav1.6–/– situation) reduced the autonomous rate to 7 Hz. In parallel, there was a positive shift in spike threshold (Fig. 3.8b). In response to a current ramp similar to that shown in Figure 3.5, the model responded in a similar manner, increasing its spike rate through the rising phase of the ramp and then decelerating in the falling phase with relatively little hysteresis. In contrast, replacing the Na6 channels created a model incapable of smooth acceleration in spiking as the injected current increased; spiking failed entirely relatively early in the rising phase of the ramp and showed significant hysteresis during the falling phase, much like Nav1.6–/– GP neurons (Fig. 3.9c). These results demonstrate that the loss of Nav1.6 alone is sufficient to explain the diminished spiking capacity of Nav1.6–/– GP neurons.

Discussion

Resurgence distinguishes Na^+ channels in pacemakers

Despite previous reports suggesting alterations in Na^+ channel properties in autonomous pacemakers, a direct comparison of Na^+ channels in quiescent and pacemaking neurons in the basal ganglia reveals that the ability to conduct a resurgent current is the only distinguishing characteristic. All three pacemaking neurons analyzed here — GP neurons, striatal cholinergic interneurons and dopaminergic neurons — exhibit resurgence in their Na^+ channels. Is this enough to drive spontaneous activity? Looking at the other types of neurons that possess this Na^+ channel quality suggest a correlation. After being initially discovered in fast–spiking Purkinje neurons of the cerebellum (Raman and Bean, 1997), the resurgent current has only been reported in other neurons

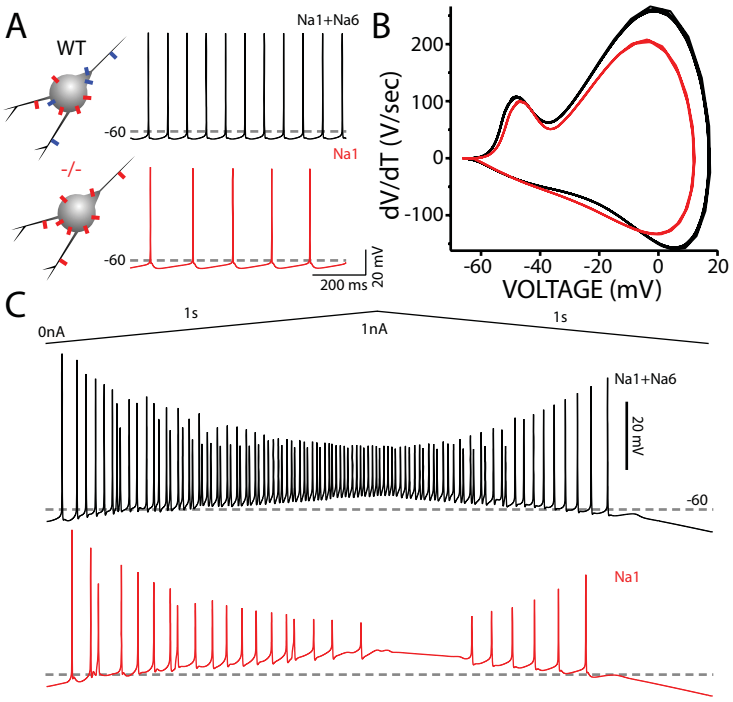

Figure 3.8. Model neuron stresses importance of axonal localization of a channel with large amounts of resurgent current.

a. Spontaneous activity in the model neurons, as measured in the soma. Top trace – firing of the model neuron at 12.2 Hz when the complete complement of Na^+ channels is present on the membrane, with Na6 localized to the axon and Na1 in the soma (mimicking wild–type neurons). Bottom trace – firing of the model neuron at 7.2 Hz when only Na1 is inserted on the membrane (mimicking Nav1.6–/– neurons).

b. Phase plot of the firing activity from *a* showing a significant positive shift in threshold in the model neuron containing only Na1 (red).

c. Model neuron response to a ramp stimulus. The maximum frequency obtained by Na1+Na6 (black) was 125 Hz, while the Na1–only model failed after reaching only 50 Hz.

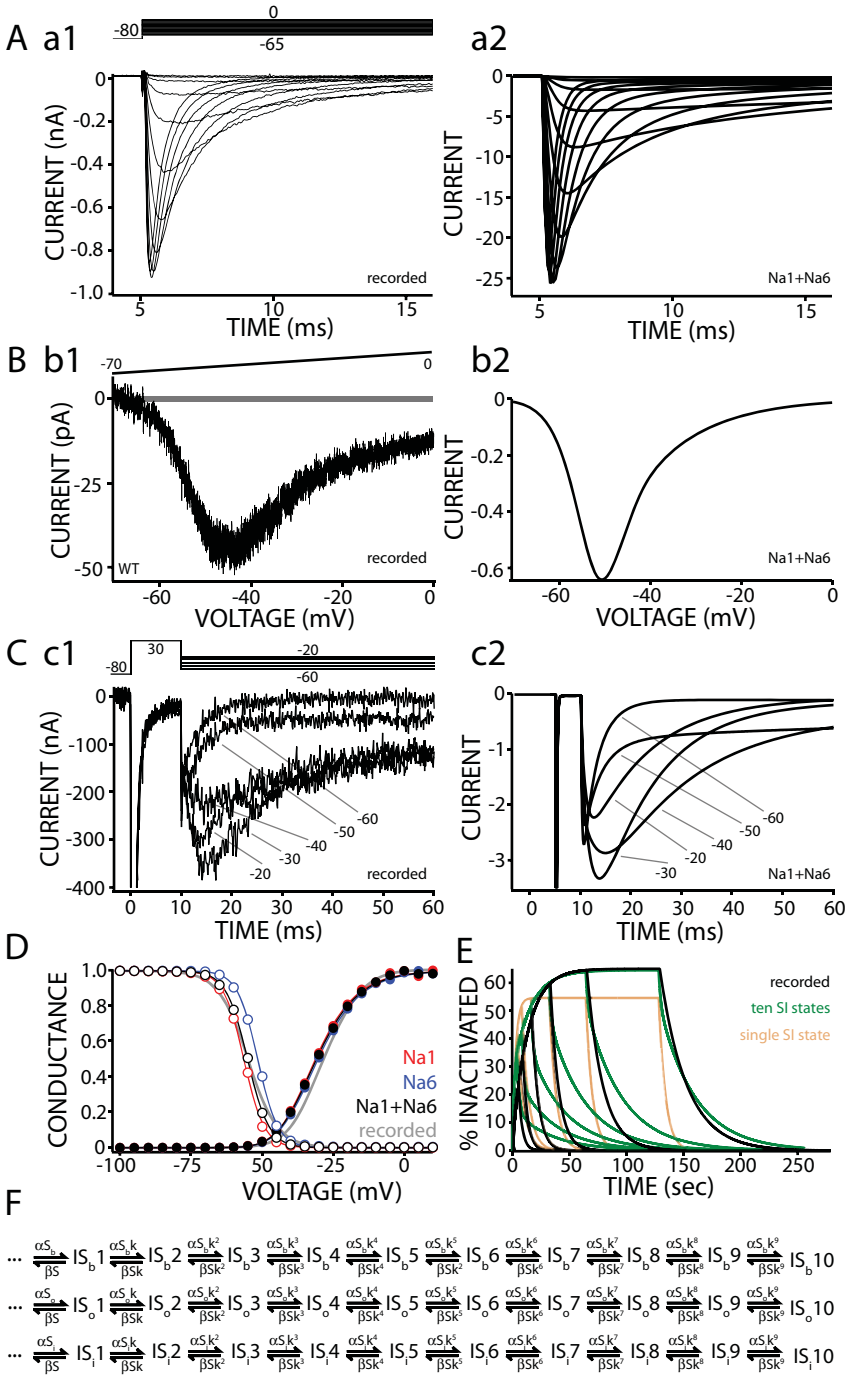
A a1
-80
0
-65
CURRENT (nA)
recorded
TIME (ms)
a2
CURRENT
Na1+Na6
TIME (ms)
B b1
-70
0
CURRENT (pA)
WT
recorded
VOLTAGE (mV)
b2
CURRENT
Na1+Na6
VOLTAGE (mV)
C c1
30
-80
-20
-60
CURRENT (nA)
-60
-50
-40
-30
-20
recorded
TIME (ms)
c2
CURRENT
Na1+Na6
TIME (ms)
D
CONDUCTANCE
Na1
Na6
Na1+Na6
recorded
VOLTAGE (mV)
E
% INACTIVATED
recorded
ten SI states
single SI state
TIME (sec)
F

Fig. 3.9. The kinetics of the model neuron accurately mimic the characteristics of currents measured in acute preparation.

a. Transient current traces from acute prep (a1) and the model neuron (a2).
b. Persistent current traces from acute prep (b1) and the model neuron (b2).
c. Resurgent current traces from acute prep (c1) and the model neuron (c2).
d. Steady state voltage dependence of Na1, Na6 and WT (4.25:1 Na1:Na6 ratio) channels from the neuron are consistent with those recorded in the acute prep.
e. Development kinetics of slow inactivation measured in the acute prep (black traces) were significantly better predicted by the ten–state model (green) than the one–state model (brown), while recovery kinetics of the ten–state model were only accurate at the longer prepulse lengths and kinetics of the one–state model were only accurate at the shorter prepulse lengths. The dependence on time was partially achieved, with the time constants of recovery for the ten–state model slowed with longer prepulse lengths, but not as significantly as measured in the acute preparation. Slow inactivation kinetics were not different between Na1 and Na6 channels.
f. Complete kinetic model of the ten slow inactivation states.

with elevated levels of excitability, either in high frequency pacemakers like STN and cerebellar nuclear neurons (Raman et al., 2000; Do and Bean, 2003), neurons that fire at high frequency upon stimulation, as in the cerebellar granule cells (Afshari et al., 2004; Magistretti et al., 2006), and in bursting cells found in the trigeminal mesencephalic nucleus, sensory dorsal root ganglion and cerebellum (Afshari et al., 2004; Cummins et al., 2005; Enomoto et al., 2006).

In order to conduct a resurgent current, these neuron types must contain a unique molecular product that functions as a blocking particle. The first place to look would be at the Na^+ channel subunits. Na^+ channels in the brain are composed of one of three different α–subunits, Nav1.1, 1.2 and 1.6, and a heterogeneous collection of one or more accessory β subunits, Navβ1, 2, 3 or 4. Of these, Nav1.6 and the β4 subunit have been proposed to play an active role in the development of resurgence. In *med*^{TG} Purkinje neurons lacking functional Nav1.6 channels on the membrane, the resurgent current is almost completely eliminated (Raman et al., 1997; Khaliq et al., 2003). In Purkinje neurons where the blocking particle has been eliminated by Trypsin treatment, the resurgent current is rescued by addition of a peptide composed of the cytoplasmic tail of the Navβ4 subunit (Grieco et al., 2005). However, in *med*^{TG} GP and STN neurons, elimination of Nav1.6 does not completely eliminate resurgence, though it does selectively reduce resurgence more than the other currents (Do and Bean, 2004). Furthermore, expression levels of Navβ4 in the basal ganglia do not correlate with neurons displaying resurgence. In resurgent–lacking striatal medium spiny neurons, Nav1.6 and Navβ4 are abundantly expressed, while dopaminergic neurons exhibit resurgence despite the absence of Navβ4. Regardless, the Nav1.6 subunit and its ability to conduct a sizable resurgent current is important in the discharge patterns of GP neurons.

Nav1.6 and the blocked state accommodate pacemaking by accelerating recovery following an action potential

Application of the Na^+ channel blocker TTX to spontaneously active GP neurons demonstrates that the firing rate of these neurons is correlated with the availability of Na^+ channels. In order to maintain spontaneous activity, GP neurons require their Na^+ channels to rapidly recover

from the previous spike to conduct enough current during the interspike interval (ISI) to drive the subsequent action potential. With the unique recovery kinetics from the blocked state AHP, Na^+ channels that are blocked instead of inactivated have two potential ways at which they contribute to high frequency discharge. First, since reentry into the open state leads to conduction of a depolarizing current during the AHP, the resurgent current can lessen hyperpolarization and jump–start the voltage trajectory back towards threshold. Second, channels that are blocked are more easily recovered and returned to the available pool than channels that are inactivated. During repolarization from a spike, recovery from the blocked state begins at –10 mV (evident by the presence of a current upon repolarization to that voltage), whereas recovery from the fast–inactivated state does not begin until near –40 mV. In addition to recovering at more depolarized potentials, blocked channels also recover faster. The time constant of recovery from the blocked state is in 0.6–1.0 ms (τ_{act} for the resurgent current, Fig. 1.8c), whereas recovery from the fast–inactivated state is ten times slower (τ_{fast}, Fig. 1.3f) in the same voltage range. As a result, channels that were blocked are quickly made available following a spike, but channels that were fast–inactivated require more time to be made available for the subsequent spike.

A reduction in the number of Na^+ channels that undergo block during the action potential would result in more channels being inactivated and a reduction in the availability of channels during the following ISI. With fewer Na^+ channels conducting depolarizing current during the ISI, the ramp towards threshold would be slowed and autonomous pacemaking would be reduced. This is seen in the *med*^{TG} GP neurons, where a 40% reduction in resurgent current decreases the spontaneous discharge rate 50%.

The model predicts the decrease in activity with elimination of Nav1.6

This behavior can be accurately described using the two–channel model we generated. Channel one, Na1, has biophysical properties similar to those recorded in the *med*^{TG} neurons in the dissociated, Na^+ channel isolated preparation. With the addition of the second channel, Na6, at a ratio of 4.25 Na1 to 1 Na6, we can reconstruct the Na^+ channel biophysical characteristics recorded

in the wild–type GP neuron. By using the traces of basal firing rate at high–frequency stimulation as voltage commands, we can track the availability of Na^+ neurons during spontaneous and driven firing. Under both conditions, Na6 availability was four times greater than Na1, significantly contributing to the total availability of Na^+ channels immediately following a spike. This increase in availability is especially apparent in the first few milliseconds following a spike, when channels that were blocked return to the open state before channels can recover from fast–inactivation. This stresses the importance of 'rescue' from inactivation over actual conductance of current, since subthreshold currents do not play a major role in firing during high frequency stimulation because the depolarizing pulse supplies the necessary current to reach threshold if there are enough Na^+ channels available.

When combined at the 4.25:1 ratio, the estimate of Na^+ channel availability is roughly 7% at the beginning of the subsequent stimulus, which is greater than the threshold predicted to be necessary by the TTX–titration experiment. But even 7% is a conservative estimate, because it assumes homogenous distribution of Na^+ channels throughout the membrane, while localization studies demonstrate that Nav1.6 is localized to the axon and initial segment. This means that in this particular region, Na^+ channel availability would be closer to that predicted by the Na6 curve, making it significantly more excitable than the predominantly Na1 containing soma. Also suggestive of a localized role of Nav1.6 subunits in the intact neuron is the shift in spike threshold of the first spike during the ramp protocol. By holding the neuron at –70 mV prior to injecting the depolarizing ramp, Na^+ channels should be able to recover from fast–inactivation and channel availability between wild–type and Nav1.6–/– neurons should be comparable. Nevertheless, Nav1.6–/– neurons have significantly positive–shifted thresholds and require more current injection to initiate a spike. This is suggestive that local channel density at the spike initiation site is reduced, possibly because Nav1.1 and 1.2 insufficiently compensate for Nav1.6 in the initial segment and axon, where spike initiation is believed to occur (Palmer et al., 2006; Stuart et al., 1997ab; Clark et al., 2005; Colbert and Johnston, 1996; Van Wart and Matthews, 2006).

With this in mind, we inserted Na1 and Na6 into a more complete cell model that, when the axon contained only Na6 and the soma predominantly Na1, as would be predicted by localization studies, the model neuron is capable of firing spontaneously at a frequency of 12 Hz. When Na6 is removed and Na1 is put in the axon in its place, the model neuron only fires at 7 Hz. This demonstrates that both the unique biophysical properties and localization of Nav1.6 subunits are crucial for the proper firing properties in GP neurons. The elevated presence of the blocked state in Nav1.6 neurons enables this subtype to be more readily available to initiate spiking activity in the initial segment and drive spontaneous activity in GP neurons.

Nav1.6 and the blocked state sustain high frequency firing

The ability to fire at elevated frequencies is also correlated with Na^+ channel availability. During driven firing by a ramp stimulus, Nav1.6–/– neurons are much less capable of sustaining activity at higher frequencies, failing at around 100 Hz, and remain in depolarization block until the depolarizing current injection is sufficiently reduced to allow enough recovery of Na^+ channels to reinitiate spiking. Meanwhile, GP neurons with a full complement of Na^+ channels and currents are less susceptible to depolarization block and are capable of sustaining activity throughout the depolarizing ramp and showing very little hysteresis during the falling phase of the ramp. This is made possible through the increased ability to recover blocked channels quickly at depolarized potentials.

During a DBS–like high frequency stimulation, when wild–type GP neurons stabilize at 50 Hz firing frequency in response to higher stimulating frequencies, Nav1.6–/– neurons are barely capable of responding to 10 Hz stimulation, fire half the time during 25 and 50 Hz stimulations and become less and less responsive to stimulation with higher frequencies, failing completely by 200 Hz.

Implications of high–frequency firing

This ability of wild–type GP neurons to re–establish rhythmic discharge at an elevated frequency during high frequency stimulation has significant implications for the treatment of

Parkinson's Disease. PD is precipitated by a loss of dopaminergic neurons in the midbrain that results in loss of a modulatory signal and changes in excitability and activity patterns in neurons of multiple sites within the basal ganglia that lead to serious motor symptoms (Miller and DeLong, 1988). In the GP, neurons switch from uncorrelated, rhythmic, autonomous pacemakers to bursting neurons that are more correlated with their neighbors as well as establishing oscillatory network activity with neurons from other nuclei, such as cholinergic interneurons of the striatum and neurons of the STN (Miller and DeLong, 1987; Plenz and Kitai, 1999; Magill et al., 2000; Raz et al., 2001). Impalement of an electrode in one of the involved nuclei and stimulating at high frequencies (>90Hz) can disrupt this oscillatory behavior. This method, known as deep brain stimulation (DBS), is believed to either result in depolarization block, thus inhibiting output from the stimulated nuclei (Beurrier et al., 2001; Tai et al., 2003), or by overriding the cellular machinery and resetting firing properties to a new rhythm dictated by the stimulus (Bar-Gad et al., 2004; McIntyre et al., 2004a). The ideal downstream effect of DBS in the STN is an increase in and re–patterning of GP activity that would be more effective at inhibiting the GPi and SNr and reducing the inhibitory output of the basal ganglia.

This work demonstrates that GP neurons re–pattern their discharge properties in response to direct high frequency stimulation and can sustain high frequency firing for extended periods of time without undergoing depolarization block. This stabilization of activity supports evidence that DBS of the STN can increase output from GP neurons (Jech et al., 2001; Hashimoto et al., 2003; Windels et al., 2005). Much like normal activity patterns, stimulated GP neurons are phase locked to the stimulation in a very rhythmic fashion, firing every 20 milliseconds regardless of how many stimuli occur between spikes. This return to rhythmic firing from the pathological oscillatory bursting observed in PD could potentially trigger the therapeutic benefit of DBS for those afflicted with PD.

Conclusions

The unique properties and localization of Nav1.6 channels enables GP neurons to spontaneously fire and to sustain high–frequency firing. With this intact machinery, GP neurons are capable of attaining enough availability to prevent depolarization block during DBS, instead establishing a new, high frequency rhythm. This supports the theory that the mechanism behind DBS stimulation is not cessation of firing but disruption of pathological firing and reestablishing a new rhythm that allows for a more physiological output from the basal ganglia.

Section 3.4: Intrinsic silencing of globus pallidus neurons in a Parkinson's Disease model is mediated by diminished HCN channel activity

Introduction

Parkinson's Disease (PD) is a common neurodegenerative disorder whose motor symptoms include bradykinesia, rigidity and resting tremor. These symptoms are a result of pathological changes that take place within the basal ganglia following the loss of midbrain dopamine (DA) neurons. Within this network, neurons in the striatum are the primary recipients of this dopaminergic innervation, as striatal levels of DA, synthesizing enzymes and DA receptors are among the highest of any brain region (Hornykiewicz, 1982; Gerfen et al., 1990; Graybiel et al., 1990). Despite this, only subtle changes in membrane properties and activity patterns of striatal medium spiny neurons have been described following depletion of DA (Nisenbaum et al., 1996; Tseng et al., 2001; Mallet et al., 2006). In contrast, extracellular unit recordings from DA depleted animal models and human patients with PD have found that neurons in the external globus pallidus (GP), which have far less dopaminergic input, change their spiking pattern in parallel with the severity of symptoms (Miller and DeLong, 1987; Pan and Walters, 1988; Filion and Tremblay, 1991; Nini et al., 1995; Hassani et al., 1996; Magnin et al., 2000; Raz et al., 2000; Raz et al., 2001; Wichmann and Soares, 2006). Upon DA depletion, activity within GP transitions from rhythmic pacemaking activity to a "burst–pause" pattern of firing, while elevated levels of intra–nuclear correlated activity.

However, these discoveries of altered firing patterns have relied on *in vivo* recording techniques that bias toward sampling from active neurons and, because of restricted pharmacological manipulations, are not capable of distinguishing between autonomous and synaptically driven activity. Despite the immediate correlations between altered pallidal activity and the motor symptoms of PD, relatively little is known about the cellular mechanisms behind this aberrant

activity. The synchrony among neurons in the DA depleted state is suggestive of an extrinsic component, such as a converging synaptic input, that is shared among GP neurons. Computer simulations based on observations that there are changes to GABAergic signaling mechanisms within the GP support this theory by suggesting that an elevation of striatopallidal GABAergic inhibition disrupts the normal autonomous pacemaking of GP neurons (Terman et al., 2002). In addition to potentially increased striatal input, neurons of the GP and reciprocally connected glutamatergic neurons of the subthalamic nucleus (STN) establish an oscillatory network which could be the underlying cause of aberrant pallidal activity (Plenz and Kitai, 1999). While both of these models favor a synaptic origin of aberrant activity in the GP, the possibility that alterations in the intrinsic membrane properties of these neurons contribute to the pathologic firing patterns observed in PD has not been explored. In particular, the cellular mechanisms that could underly the generation of the "burst–pause" firing pattern has not been experimentally determined.

To pursue this, GP neurons from DA depleted mice were studied using patch–clamp recording in tissue slices under direct visual guidance. To our surprise, we found that a consequence of DA depletion is the silencing of GP neurons. This is not due to an enhanced GABAergic transmission predicted by the classical "parallel processing" model, as this silencing is not rescued by the addition of $GABA_A$ blockers. In contrast, this reduction in spontaneous activity is attributable to diminished HCN channel activity following DA depletion. This 'intrinsic' silencing, rather than synaptically mediated silencing, might be a critical trigger in initiating rhythmic bursting in PD.

Results

GP neurons resting activity after dopamine depletion

GP neurons receive DA from collaterals of the nigrostriatal axons that form en passant boutons within GP along the projection to the striatum. We thus performed DA depletion by an intrastriatal 6–OHDA injection, which led to a widespread lesion of tyrosine hyrdoxylase (TH) positive axons (Ding et al., 2006), including those projecting through the GP (Fig. 4.1a). Visually–identified GP neurons were recorded from tissue slices taken from animals 4–6 days post–injection

(Fig. 4.1b). Using the cell–attached recording method, roughly 60% of GP neurons exhibited no autonomous activity and another 15% had significantly reduced basal discharge rate (Fig. 4.1c,d, n=22). Similar results were found with partial DA depletion by antagonizing TH with a 4 day course of α–methyl–tyrosine and broad spectrum monoamine depletion with a 5 day treatment of reserpine (Fig. 4.1d, n=19 and 55, respectively). One potential complication of reserpine treatment is the collateral depletion of pallidal serotonin, but selective depletion of serotonin by a 3–5 day treatments of DL–*p*–chlorophenylalanine methyl ester hydrochloride (*p*CPA) did not significantly affect the autonomous activity of GP neurons (n=13, data not shown).

Silencing is not dependent upon enhanced GABAergic input

The classical circuitry model of the basal ganglia would predict that the doparminergic denervation that results in PD would lead to an increase in striatopallidal outflow (Albin et al., 1989). This is supported by experimental observations that there are increases in GABAergic signaling molecules in PD (Bianchi et al., 2003) and computer simulations that suggest a disruption of autonomous pacemaking activity in GP neurons could arise from elevations in GABAergic inhibition from striatalpallidal fibers (Terman et al., 2002). If increased GABAergic tone is underlying the significant reduction in excitability and autonomous activity in GP neurons, we would predict that addition of blockers of $GABA_A$ transmission in our recording solution would rescue spontaneous activity in silent neurons and increase activity in slow neurons following DA depletion by reserpine. However, SR95531 (gabazine), a competitive, selective $GABA_A$ receptor antagonist, had no effect on rate and regularity of spiking in control or DA depleted active neurons. The relationship between resting firing rate in the presence and absence of SR95531 was close to unity (with slope equal to 1; Fig. 4.2a). Similarly, application of SR95531 did not resume spontaneous firing in silent neurons (n=8). On the other hand, the coefficient of variation of interspike intervals was not different between control and reserpine–treated animals in both the presence and absence of SR95531 (Fig. 4.2b,c). This suggests that the silencing or reduced activity of GP neurons after DA depletion is not dependent upon an enhanced GABAergic input onto GP

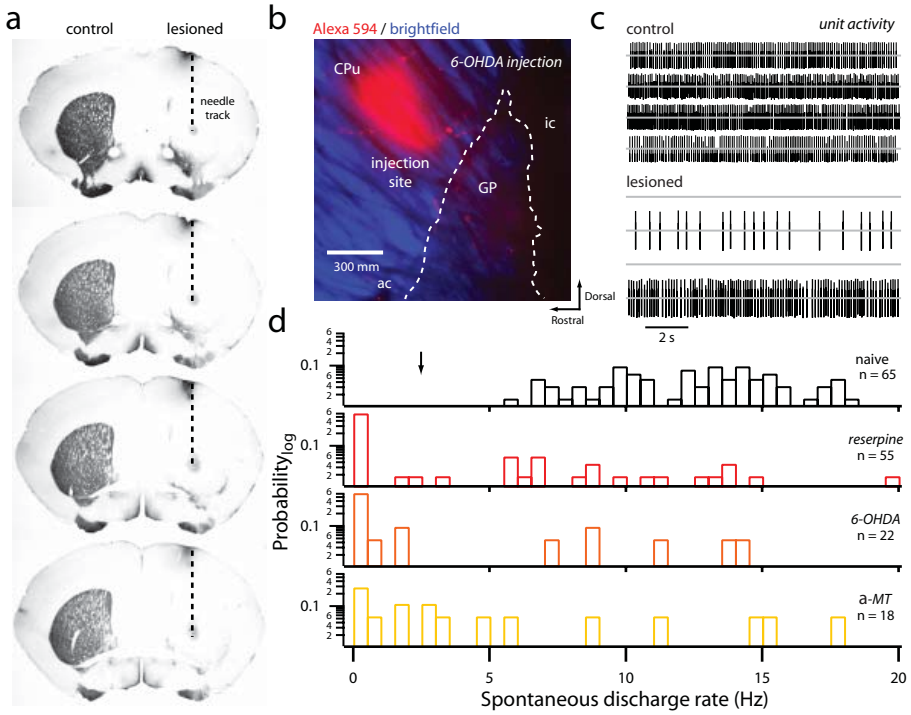

Figure 4.1. Dopamine depletion reduces spontaneous activity of GP neurons.

a. Unilateral intrastriatal 6–OHDA injection leads to massive dopamine dennervation assessed by tyrosine hydroxylase immunoreactivity.

b. Light micrograph of a parasagittal mouse slice showing the site of 6–OHDA injection and its relationship with GP (caudal to anterior commissure (ac), rostral to internal capsule (ic)). Alexa 594 dextran (MW10,000) was included routinely for visual identification of the injection site (red).

c. Unit activities of visually identified GP neurons from control and 6–OHDA lesioned animals.

d. Complete dopamine depletion with intrastriatal 6–OHDA injection and systemic reserpine–treatment induces the emergence of silencing and a reduction in autonomous pacemaking rate of GP neurons. Similar observations were found following partial lesioning with α–methyl–tyrosine.

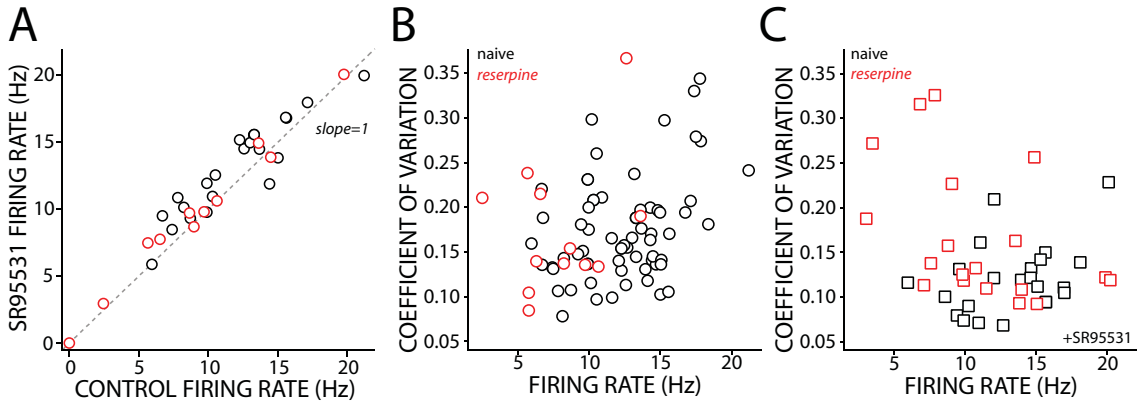

Figure 4.2. Silencing and reduction in spontaneous pallidal activity is not attributable to an increase in GABAergic tone.

a. The correlation of firing rate of neurons before and after SR95531 application is close to unity in both naive and reserpine–treatment group.
b. Relationship between ISI coefficient of variation and discharge frequency under control conditions in both naive and reserpine–treated animals.
c. Relationship between ISI coefficient of variation and discharge frequency in the presence of SR95531/gabazine in both naive and reserpine–treated animals. The correlation of firing rate of neurons before and after SR95531 application is close to unity in both naive and reserpine–treatment group.

neurons.

Silent neurons exhibit reduced excitability in response to depolarizing current

If the reduction in basal firing rate is a result of reduced intrinsic excitability, we would expect to see a recovery of firing upon injection of depolarizing current. With a +40 pA current injection, silent neurons can sustain firing at 11 Hz (Fig. 4.3a), which approaches the 12 Hz basal firing rate of naïve GP neurons (Chan et al., 2004). With increasing amplitudes of current injection, silent GP neurons can continue to respond by increasing their firing rate respectively (Fig. 4.3a,b). However, as a population, silent neurons cannot match the response frequencies of active neurons from reserpine–treated animals or naïve animals, maintaining lower activity patterns throughout the current–frequency (F–I) curve. Active neurons have similar responses to current injection as that of naïve neurons. Similar to that demonstrated using immunocytochemistry (Ruskin and Marshall, 1997; Marshall et al., 2001), some subpopulations of GP neurons do not respond to D_2 receptor antagonism, this population of neurons does not appear to be adversely affected by DA depletion.

Studies on *med*^{TG} GP neurons, which lack functional Nav1.6 subunits, demonstrate that neurons with decreased intrinsic excitability are less capable of reaching and sustaining high frequency firing with injected ramp stimuli (section 3.3). While active neurons show a modest reduction from the control group with regards to maximum frequency, silent neurons from reserpine–treated animals reach significantly smaller max frequencies, in agreement with a global decrease in intrinsic membrane excitability (Fig. 4.3c).

Na^+ channel expression and gating are not altered following DA depletion

The F–I curves suggest that DA depletion does not compromise the ability of GP neurons to spike repetitively, but induces a reduction in excitability of GP neurons but by shifting the balance between depolarizing and hyperpolarizing currents to a level that no longer favor spontaneous activity. Autonomous activity in GP neurons is normally sustained by expression of specific sets of voltage–gated channels that provide depolarizing currents, namely Na^+ and HCN channels (Chan

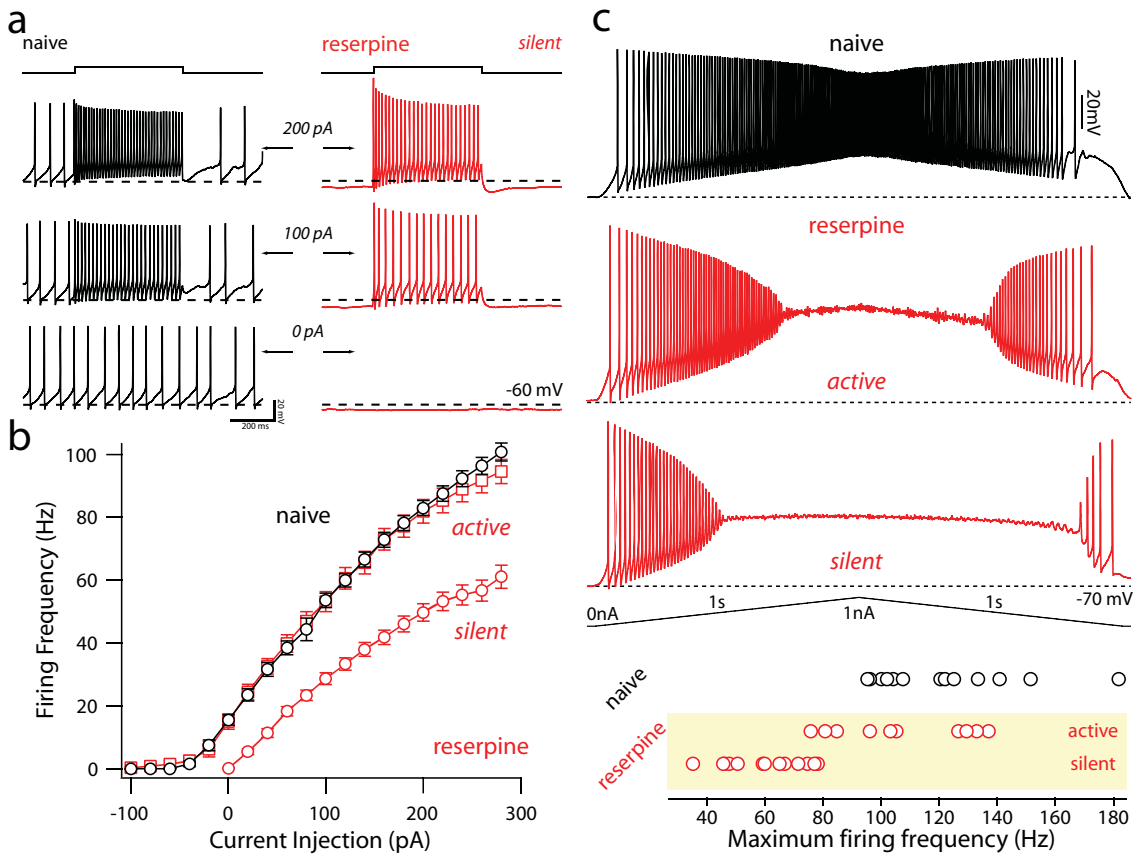

Figure 4.3. Driven activity of GP neurons in naive and reserpine–treated animals.

a. Somatic whole–cell recording of action potential firing elicited by step currents (0, 100 and 200pA) in GP neurons from naive and reserpine–treated animals.

b. Summary of frequency–current relationship of GP neurons from naive and reserpine–treated animals. Note the similarity between naive and active neurons from reserpine–treated group.

c. Top, somatic whole–cell recording of action potential firing elicited by ramp currents (1nA/s) in GP neurons from naive and reserpine–treated animals. Retardation in somatic excitability is apparent from neurons from both active and silent group after reserpine–treatment. Bottom, this data is summarized in a scatter plot. similar maximum firing frequencies were attained with step and ramp protocol.

et al., 2004; Chan et al., 2005; Surmeier et al., 2005). In *med*^{TG} neurons, there is a direct correlation between Na^+ channel expression levels (elimination of Nav1.6) and a reduction in membrane excitability (reduced basal firing rate and reduced ability to maintain high frequency discharge, see section 3.3). To further understand whether the compromised spontaneous activity in GP neurons after DA depletion is similarly attributable to reductions in functional expression of Na^+ channels, semi–quantitative, single–cell reverse transcriptase polymerase chain reaction (scRT–PCR) experiments measuring Nav1.1 and 1.6 α–subunit mRNA levels and whole–cell voltage clamp experiments on acutely dissociated neurons measuring Na^+ current amplitudes were performed. Expression of mRNA was measured as the detection threshold of PCR product during serial dilution of the cDNA acquired from reverse transcription of the mRNA collected from individually aspirated GP neurons (Fig. 4.4a). Current amplitudes were measured as peak deflections from baseline during standard protocols used to measure transient, persistent and resurgent Na^+ current (Fig. 4.4b). Both physiological and molecular profiling data suggest that there is no change in the functional expression levels of Na^+ channel α–subunits following DA depletion. This data suggest that silencing of GP neurons following reserpine treatment is not a result of down–regulation of voltage–gated Na^+ channels.

Reduction in HCN channel activity after DA depletion

HCN channels in GP neurons are critical in shaping the autonomous activity and responses to striatal input. We have previously found that HCN channels in GP begin to activate at around –55 mV and conduct an inward, depolarizing current that ensures the membrane potential does not stabilize below Na^+ channels voltage of activation (Chan et al., 2004). In addition, HCN channel activity and expression levels have been found to be closely linked with perturbed or diseased states (Chen et al., 2002; Santoro and Baram, 2003). Initial observations of the resting membrane potential upon breaking into the neuron reveals that the silent neurons sat at –62 mV, a membrane potential close to the threshold (~–65 mV) for activation of Na^+ channels and roughly 10 mV lower than the resting membrane potential of TTX–treated naïve neurons (section 3.3).

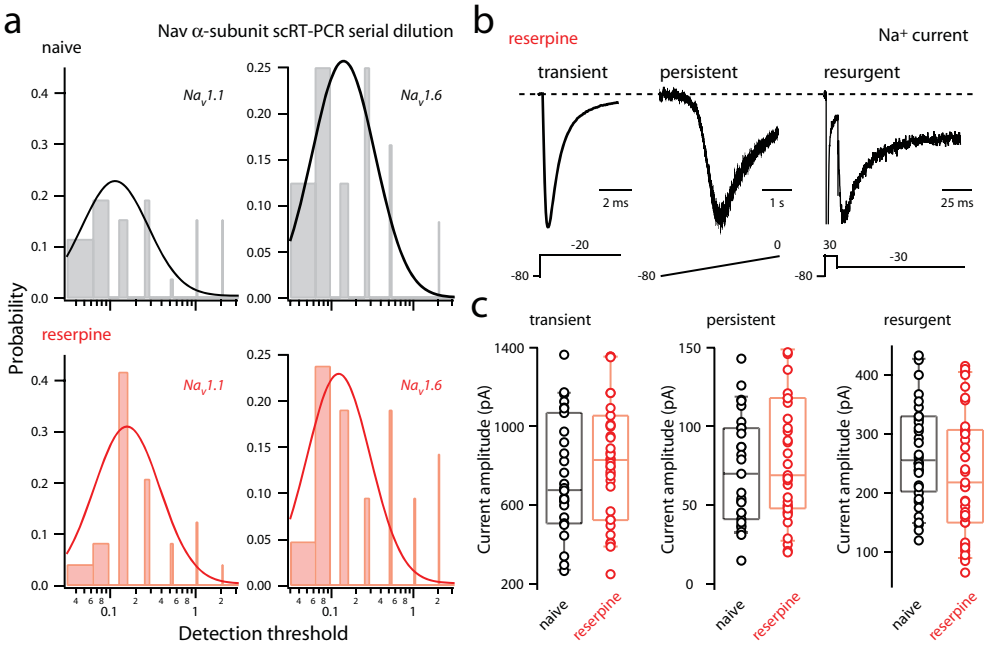

Figure 4.4. Na^+ channel α–subunit mRNA abundance and current amplitudes are not altered following dopamine depletion.

a. Single–cell RT–PCR serial dilution revealed no detectable changes in Na^+ α–subunit mRNA abundance in GP neurons following reserpine–treatment. No significant difference was found in the threshold of detection for both Nav1.1 and Nav1.6 α–subunits following reserpine–treatment (P values > 0.5, Kolmogorov–Smirnov test). Smooth lines represent best fits of the threshold distribution with a log–normal function, yielding the modal thresholds as follows: $Nav1.1_{(control)}$=0.11 (n=26), $Nav1.1_{(reserpine)}$=0.16 (n=24), $Nav1.6_{(control)}$=0.14 (n=24), $Nav1.6_{(reserpine)}$=0.12 (n=21).

b. Voltage protocols (bottom) and representative traces (top) of transient, persistent and resurgent Na^+ currents recorded from typical reserpine–treated GP neurons.

c. Population data on Na^+ current amplitudes from control and reserpine–treated animal groups. These paraemeters are not significantly different from their corresponding controls (P values > 0.05, Mann–Whitney Rank Sum Test). $Transient_{(median)}$: control=677pA (n=31), reserpine=830pA (n=39). $Persistent_{(median)}$: control=70pA (n=27), reserpine=69pA (n=35). $Resurgent_{(median)}$: control=255pA (n=36), reserpine=218pA (n=39)

Furthermore, voltage trajectories during –100 pA hyperpolarizing current injections of neurons from reserpine–treated animals showed a significantly larger deflection in silent neurons than active neurons. The median voltage deflection by a –100 pA current for silent neurons was –148 mV, while the membrane potential for active neurons reached a minimum of –110 mV (Fig. 4.5a, n=27 and 18, respectively). This maximum voltage deflection was directly correlated with the spontaneous discharge rate of the neuron (Fig. 4.5c). A non–linearity can be observed in the V–I plot of silent neurons at –60 mV, which is suggestive of an increase in input resistance to hyperpolarizing current injection (Fig. 4.5b). To determine whether these changes in membrane properties were attributable to alterations in HCN channels, currents were directly measured under voltage–clamp configuration with a standard 2–step protocol (Chan et al., 2004). Measurement of the maximum HCN current amplitude elicited by stepping voltage–clamped cells from –50 to –130 mV revealed that silent neurons have smaller HCN current than active neurons (Fig. 4.5d,e,f). Plotting the peak amplitude of the HCN current as a function of the maximum voltage deflection in response to hyperpolarizing current injection suggests a tight correlation between the two observations (Fig. 4.5h). This is consistent with the idea that HCN channels are sole carriers for an active conductance that controls the input resistance and membrane response during modal membrane potential and "inhibitory input". No systemic difference in the voltage–dependence is found between control and reserpine–treated animal groups (data not shown); however, the small HCN current amplitude observed after reserpine treatment together with limitations on space clamp and whole–cell dialysis, do not permit us to conclude that the voltage–dependence of the HCN currents remained constant under DA depletion. Plots of the HCN current amplitude as functions of maximum voltage deflection with –100 pA current injection (Fig. 4.5h) and spontaneous firing rate (Fig. 4.5i) shows close correlations between the parameters, demonstrating that reduced levels of HCN current in the reserpine–treated neurons were responsible for increases in the input resistance and potentially responsible for the reduction in firing rate seen in these neurons.

The HCN2 subunit is the predominant isoform of HCN channels being expressed in GP

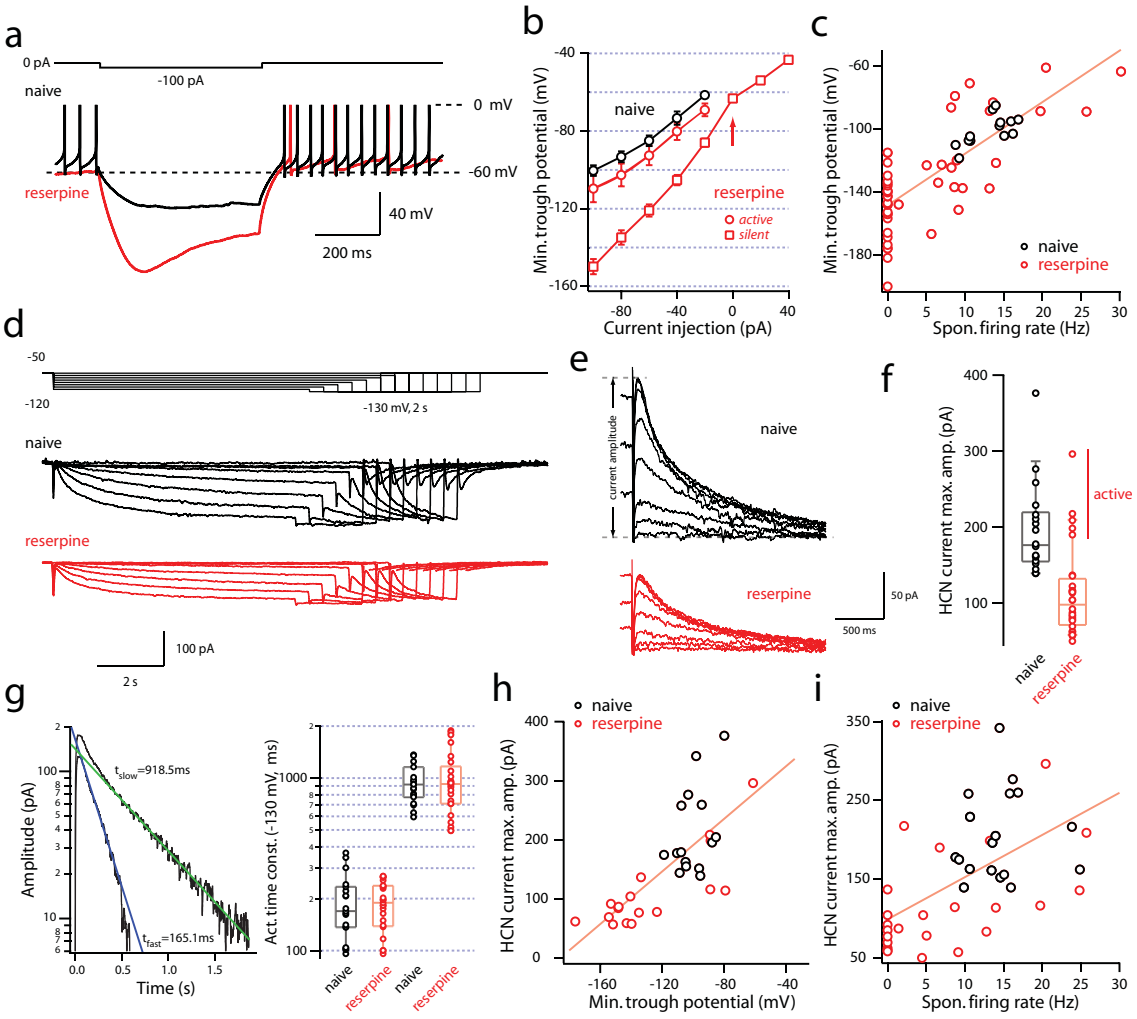
a
0 pA
-100 pA
naive
0 mV
-60 mV
reserpine
40 mV
200 ms
b
Min. trough potential (mV)
naive
reserpine
active
silent
Current injection (pA)
c
Min. trough potential (mV)
naive
reserpine
Spon. firing rate (Hz)
d
-50
-120
-130 mV, 2 s
naive
reserpine
100 pA
2 s
e
current amplitude
naive
reserpine
50 pA
500 ms
f
HCN current max. amp. (pA)
active
naive
reserpine
g
Amplitude (pA)
t_slow=918.5ms
t_fast=165.1ms
Time (s)
Act. time const. (-130 mV, ms)
naive
reserpine
naive
reserpine
h
naive
reserpine
HCN current max. amp. (pA)
Min. trough potential (mV)
i
naive
reserpine
HCN current max. amp. (pA)
Spon. firing rate (Hz)

Figure 4.5. Diminished HCN channel activity in GP neurons following reserpine treatment.

a. Membrane response of GP neurons from naïve (black) and reserpine–treated (red) animals to hyperpolarization current injection. The increased responsiveness following DA depletion is indicative of an increase in input resistance. For clarity purposes, action potentials are truncated.
b. Summary of the membrane response of GP neurons to series of current injections. Note the discontinuity (arrow) of the membrane response from –60 mV and below in silent neurons from reserpine–treated group. A steep increase in trough amplitude in response to hyperpolarizing current injection is observed.
c. Plotting minimal trough potential (measured during a –100 pA current injection) against basal discharge rate of GP neurons suggests a positive correlation (correlation coefficient=0.575 $p<0.05$, Spearman rank correlation).
d. HCN current evoked by a 2-step voltage-clamp protocol (top; prepulse=-50 to -120 mV, test pulse = -130 mV). The amplitude of the HCN current is reduced following DA depletion (red traces, $p<0.05$, Mann-Whitney).
e. Current traces from *d* are aligned at the onset of the test pulses (-130 mV) to accurately measure the tail current. Fitting the current-voltage relationship of the HCN channel with a Boltzmann function reveals no difference ($p>0.05$, Mann-Whitney) in the voltage dependence of activation (naivemedian=-90.1 mV, n=5; reserpinemedian=-87.3 mV, n=12; data not shown).
f. Box plot summarizing the HCN current amplitude from naive and reserpine treated animals. The five reserpine-treated neurons with HCN current amplitudes greater than 180 pA (denoted by *) were spontaneously active.
g. Left, two (fast and slow) time constants (t) were extracted from HCN channel activation at -130 mV. The upper trace is the current record plotted on a log scale and fit with a single expotential function (red line), yielded a time constant of 918.5 msec. Deviation from this fit was subtracted from the single exponential function and plotted on the same coordinates. Fitting this with a single expotential function (blue line), yielded a time constant of 165.1 msec. Right, data is summarized in non-parametric format.
h. A tight correlation (correlation coefficient=0.756, $p<0.0001$, Spearman rank correlation) between maximum HCN current amplitude (Vtest=-130 mV) and minimal through potential (with -100 pA at the soma).
i. A positive correlation was seen between maximum HCN current amplitude and basal discharge rate of GP neurons (correlation coefficient=0.638, $p<0.0001$, Spearman rank correlation).

neurons (Chan et al., 2004). This subunit is exquisitely sensitive to intracellular cAMP modulation (Chen et al., 2001; Wainger et al., 2001; Chen et al., 2005). To exclude the possibility that a decrease in intracellular cAMP level is attributable to the silencing and reduced pallidal activity, a saturating concentration of a cAMP analog (cBIMPS, 50 μM) on resting firing rate of reserpine–treated animals was tested. In spontaneously active GP neurons, cBIMPs does not have a consistent effect on pacemaking (decrease, n=3; increase, n=4). Application of cBIMPS to silent neurons did not rescue spontaneous pacemaking (n=6). This data suggests that silencing is not due to a lowering of intracellular cAMP level but to a reduction in channel conductance due to a down regulation of channel expression or membrane insertion following DA depletion.

Discussion

The importance of DA in GP function

In this study, we found that an important consequence of DA depletion is the silencing of GP neurons. The classical basal ganglia circuitry model (Albin et al., 1989; Alexander and Crutcher, 1990) suggests that DA released from terminals of the nigrostriatal projection is thought to modulate basal ganglia output by inhibiting activity along the indirect pathway and enhancing the direct pathway. Given the polarity of connections along the direct and indirect pathway, striatal release of DA would result in an overall increase in basal ganglia output from the entopeduncular nucleus (EP) and substantia nigra pars reticulata (SNr). Within the indirect pathway, loss of striatal dopamine is believed to result in increased striatal inhibition of GP, leading to disinhbition of STN neurons and subsequent increased basal ganglia output from CPu and SNr (Wichmann and DeLong, 2003). In conjunction with these synaptic alterations and network activity in the basal ganglia, findings in this study demonstrate that loss of DA has a direct effect on GP neurons through a reduction in their intrinsic membrane excitability that results from a reduction in HCN current density and leads to a silencing of these neurons. This ‘intrinsic’ silencing, rather than a synaptically mediated silencing, might be a critical trigger for the emergence of rhythmic bursting and the resultant motor symptoms in PD.

The importance of a dopaminergic modulation of GP neurons is supported by numerous observations. DAergic fibers traverse GP (Ferre et al., 1996; Gaykema and Zaborszky, 1996) and small varicose processes immunoreactive for TH form symmetrical synapses with pallidal neurons (Smith et al., 1989). Both D_1– and D_2–class receptor binding are evident in the rat GP (Mengod et al., 1992), and in situ hybridization and scRT–PCR studies have argued that at least some of the D_2 receptors are postsynaptic, as D_2 receptor mRNA is present in GP neurons. Given the absence of D_1a mRNA in GP neurons, the D_1–class binding is either at presynaptic receptors or postsynaptic D_1b receptors (which are expressed in GP neurons). In MPTP treated monkeys, the loss of DA leads to significant alterations in pallidal activity that correlate to diminished motor control (Pan and Walters, 1988; Raz et al., 2000; Raz et al., 2001). Furthermore, bilateral infusions of D_1 or D_2 receptor antagonists into the GP that induce akinesia and catalepsy (Costall et al., 1972; Hauber and Lutz, 1999) and amelioration of the motor symptoms of hemiparkinsonian rats by the infusion of DA into the GP (Galvan et al., 2001) suggest direct actions of DA in the GP. Paradoxically, D_2 selective agonists (quinpirole and RU24926) induce only modest rate effects on pallidal activity in awake, locally anesthetized and gallamine–immobilized rats (Carlson et al., 1987; Walters et al., 1987). The reduction in intrinsic excitability and autonomous pacemaking of GP neurons following DA depletion further suggest a potential direct role of DA on the normal activity of pallidal neurons.

Plasticity of HCN channels

HCN channels have a widespread expression pattern and play a critical role in the intrinsic excitability of neurons throughout the central nervous system (Santoro et al., 2000; Robinson and Siegelbaum, 2003) This ranges from setting the resting potential/conductance, generation of rhythm and pacemaking, synaptic integration, rebound excitation and synaptic resetting of discharge. This depends on their heterogeneous molecular composition (with varying affinities to intracellular cAMP, kinetic features and targeting of the channels), and their partnerships with other ionic conductances at specific subcellular structures (Chan et al., 2004; Day et al., 2005; Wilson, 2005).

In addition, HCN channels are also involved in the cellular adaptation and intrinsic

plasticity observed in a broad variety of neurons associated with development (Bender et al., 2001; Vasilyev and Barish, 2002; Lujan et al., 2005; Brewster et al., 2006), epilepsy (Brewster et al., 2002; Bender et al., 2003; Ludwig et al., 2003; Shah et al., 2004; Strauss et al., 2004; Budde et al., 2005), denervation (Abdulla and Smith, 2001b, a; Brauer et al., 2001) and other perturbed states and insults (Mayer et al., 1986; Ingram and Williams, 1996; Dalle and Eisenach, 2005).

It has been observed that increased excitatory synaptic drive over a short period of time in quiescent pyramidal neurons upregulates HCN currents and alters excitability (van Welie et al., 2004; Fan et al., 2005). It is thus possible that reductions in HCN channel activity in GP neurons following DA depletion could be triggered by in increase in inhibitory input from the striatum and lead to a reduction in depolarizing current. If the loss of depolarizing HCN currents is great enough that the membrane potential is driven below –60 mV by K^+ channels, there would be insufficient Na^+ current to push the cell towards threshold, leading to a decrease in autonomous activity. Other forms of activity–dependent regulation of the HCN channel activity have also been noted. In lobster stomatogastric ganglion neurons, overexpression of K^+ channels leads to a compensatory increase in HCN activity that maintains the appropriate firing properties (MacLean et al., 2005). In mibrain DA neurons, a positive shift in the voltage dependence of HCN channels following elimination of Cav1.3 channels (by pharmacologic manipulation or genetic deletion) results from decreased Ca^{2+}–dependent inhibition of adenylyl cyclases (AC5 and AC9) and an increase in intracellular cAMP level. The resultant upregulation of HCN channel activity at near threshold potentials leads to a resumption of autonomous activity in these neurons (unpublished observations). While very little is known regarding the AC expression profile in GP neurons, the lack of a consistent effect by extracellular application of a cAMP analog on spiking together with the absence of an apparent shift in the voltage–dependence in the aggregated current argue against such a scenario in GP neurons following DA depletion. The exact cellular mechanisms that trigger the reduced HCN function in GP neurons following DA depletion await further experiments.

Role of GP within the basal ganglia macrocircuit, functional and network consequence of silencing

The centrality of GP neurons to motor activity is highlighted by movement–correlated pauses in activity (DeLong, 1971; Heimer et al., 2006) and aberrant activity patterns that are precipitated by the loss of dopamine in PD (Filion, 1979; Filion and Tremblay, 1991; Raz et al., 2000; Raz et al., 2001). While the GP has traditionally been viewed as a mere 'relay' in the 'indirect pathway' (Albin et al., 1989), recent anatomical and electrophysiological studies have shown that the GP is richly interconnected with all other major elements in the basal ganglia macrocircuit (Kita and Kitai, 1994; Bevan et al., 1998; Kita et al., 1999; Parent et al., 2000).

Because of the rich interconnections throughout the basal ganglia, alteration of the firing pattern of GP neurons can result in aberrant activity from numerous mechanisms and disrupt several network processing tasks. First, silencing of GP neurons leads to a disinhibiton of neurons that typically receive input from pallidal neurons. In the STN, loss of GP activity through lesioning of the nucleus leads to a significant increase in firing rate and a transition to burst firing (Ryan and Clark, 1992; Ryan et al., 1992). This bursting activity is also seen in PD and not altered by subsequent lesioning of the GP (Hassani et al., 1996), suggesting an important role for tonic pallidal activity in maintaining physiologic firing in the STN. Second, tonic firing endows GP neurons with greater sensitivity to excitatory inputs, as small inputs are not required to summate with each other in order to exceed spike threshold. Silencing increases the threshold necessary for excitation and filters weak from strong inputs. By starting in the paused state, convergent bursting activity from the STN can drive silent GP neurons to exhibit synchronous bursting activity. Third, since background rates can be modulated bidirectionally, spontaneously firing GP neurons can respond to changes in levels of inhibition and excitation. Silencing makes GP neurons essentially unresponsive to local collateral and striatal GABAergic input.

Chapter Four

Discussion

Prevalence and motor symptoms of Parkinson's Disease

Parkinson's disease (PD) is the most common form of basal ganglia disorders, afflicting roughly 1 in 1000 adults, rising exponentially in incidence after the age of fifty (Bradford, 1986). The motor symptoms include bradykinesia, resting tremor and rigidity. Human and animal studies have shown that Parkinsonism results from the degeneration of the nigrostriatal dopaminergic neurons (Hornykiewicz, 1966; Albin et al., 1989; Wooten, 1990). The therapeutic strategies for treating PD are limited. The most widely used treatment for PD, l–DOPA therapy, attempts to restore dopamine levels by enhancing the release of dopamine from the remaining dopaminergic terminals (Lloyd and Hornykiewicz, 1970). Although initially effective in a subpopulation of PD patients, the benefits of this therapy are relatively short–lived (Obeso et al., 2000). DBS has been found to be extremely effective in alleviating symptoms in PD and improving the effectiveness of pharmacological treatments, though its mechanism of action is not explicitly understood.

Disruption in GP neuron activity underlies motor symptoms in PD.

Advances have been made in the past decades in understanding the involvement of different basal ganglia nuclei in mediating the motor symptoms seen in PD. One of the most striking findings is the alterations in activity patterns of GP neurons from rhythmic spiking to correlated burst discharge (Filion, 1979; Filion and Tremblay, 1991; Nini et al., 1995; Lozano et al., 1996; Taha et al., 1996; Hutchison et al., 1997; Bergman et al., 1998; Magnin et al., 2000; Raz et al., 2000; Raz et al., 2001; Soares et al., 2004). This abnormal activity pattern is thought to be closely linked to

rigidity and tremor (El-Deredy et al., 2000), as well as dyskinesias (Bergman et al., 1998; Magnin et al., 2000; Raz et al., 2000). Disruption of this aberrant activity pattern with DBS alleviates PD symptoms, strengthening the causal linkage in PD (Vitek et al., 2004). In this dissertation, focus was made on the membrane properties of GP neurons and other pacemakers because of their critical role in basal ganglia function and dysfunction. Using a systematic approach, we have analyzed ionic condutances of pacemakers in the basal ganglia, paying particular attention to fast spiking neurons in the GP to understand what properties are important for the activity patterns observed in these neurons and how manipulation of these attributes through the use of pharmacological manipulations, transgenic animals and animal models of PD can alter pacemaking. This research has shed new light on the ionic conductances that govern autonomous activity, the abilities of GP neurons to fire at high frequencies and the impact DA depletion has on intrinsic excitability.

Major Findings

Availability of Na^+ channels is important for pacemaking and high frequency firing

The ability for pacemakers to be spontaneously active relies on the presence of depolarizing currents that drive the membrane towards spike threshold. In autonomous pacemakers of the basal ganglia, the primary channels responsible for this are voltage gated Na^+ channels and HCN channels. While many of the biophysical properties of Na^+ channels in pacemakers are similar to those in quiescent medium spiny neurons, the presence of the blocking particle and resultant resurgent current is unique to these neurons. The blocking particle is capable of releasing from the intracellular pore at membrane voltages in the suprathreshold region (–20 mV to –40 mV) at rates significantly faster than recovery from inactivation at more hyperpolarized potentials. As a result, channels that are blocked during the action potential are made available sooner in the interspike interval than those that were inactivated. This increase in the total number of available Na^+ channels leads to an increase in the subthreshold persistent current amplitude and a faster ramp towards threshold. This accelerated rate of Na^+ channel recovery following a spike is increasingly more important the faster the neuron fires, as there is less time for Na^+ channels to recover.

The firing rate of GP neurons is likely partially dictated by the ratio of entry into the blocked state and inactivated states. In computer simulations, increasing the ratio favoring the blocked state leads to increased excitability and firing rate, while shifting it towards the inactivated state reduces the firing rate accordingly. Likewise, during DBS a new ratio of inactivated to blocked entry is established that determines the frequency at which neurons can sustain high frequency firing. For GP neurons at 22°C, the new maximum set frequency for sustained firing is 50 Hz.

Availability of Na^+ channels is compromised in the presence of neuromodulators or genetic mutations that alter the interactions between the Na^+ channel and the blocking particle. In cholinergic interneurons, reducing the availability of Na^+ channels by only 10% leads to a 20% reduction in firing rate. In Nav1.6–/– channels, where availability is significantly reduced because of the reduced ratio between blocked to inactivated channels during a spike, firing properties are even more severely affected. These studies demonstrate the delicate balance placed on neurons in the basal ganglia to accurately modify their Na^+ channel availability in order to get the proper output.

It is also possible that the increased availability of Na^+ channels in the initial segment and nodes of the axon is dictated by the density of channels inserted into the membrane, which is determined by the unique localization of Nav1.6 to this region. With the loss of functional Nav1.6, med^{TG} neurons attempt unsuccessfully to compensate by inserting Nav1.1 and 1.2 into this important region, but are unable to match the normal density. Until we are capable of selectively eliminating the resurgent current without eliminating a particular channel or global protein degradation, we must rely on our modeling techniques to suggest an important role for the unique biophysical properties of Nav1.6 at the initial segment and node of the axon to provide enough available Na^+ channels to drive spontaneous firing and effectively respond to stimulation.

DA depletion leads to a decrease in excitability

Animal studies demonstrate that the activity of GP neurons transitions from high frequency, rhythmic activity to slightly lower frequency, burst activity with increased intranuclear correlation following DA depletion (Filion, 1979; Miller and DeLong, 1987; Pan and Walters, 1988; Filion

and Tremblay, 1991; Boraud et al., 1998; Raz et al., 2000; Raz et al., 2001). How this pattern is established remains a mystery, as the elaborate interconnections within the basal ganglia make specific identifications of effectors difficult, especially under *in vivo* conditions. Furthermore, because the majority of this early work was done using the extracellular recording technique, which presents a potential sampling bias towards active versus silent neurons, the origin of disrupted activity was never resolved. In our preparation, visualized recording from tissue slices revealed that DA depletion resulted in a reduction of GP activity that is independent of synaptic changes, suggesting intrinsic mechanisms are at least partially responsible for the altered firing properties observed. While this reduction in firing is not correlated with any alterations in Na^+ channel properties, there is a significant reduction in HCN current amplitude. This results in a reduction of depolarizing current during the interspike interval, leading to a reduction in the modal membrane potential below the gating threshold of the persistent Na^+ current.

GP neurons are capable of sustained high frequency firing during DBS

Since the use of DBS as a viable treatment for PD was introduced, the mechanism of action behind its effects has been under debate. Initial studies comparing DBS–induced phenotypes to those following resection suggested that DBS mimicked the action of lesion by inhibiting activity from the stimulated nuclei. This was supported by evidence showing a reduction in activity following termination of the high frequency stimulus (Beurrier et al., 2001; Tai et al., 2003). Contrary to this, recent work suggests that there is an increase in activity during stimulation (Benabid et al., 2002; Lee et al., 2004; Vitek et al., 2004) and a phase–locking of activity in the GP to the stimulus (Bar-Gad et al., 2004). This is also supported by indirect evidence that shows an increase in GABA from the GP and glutamate from the STN in the SNr during DBS (Windels et al., 2000; Windels et al., 2005).

In our slice preparation, GP neurons were capable of sustaining activity for long periods of time during high frequency stimulation. While incapable of matching the frequency set by the stimulus, they were able to adapt their membrane properties to establish a new, high frequency rhythm. This is important for the ability of DBS to successfully alter the pathological firing

patterns that are inherent in PD. By re–establishing a pattern more representative of their original autonomous activity, DBS could enable the GP to once again properly modulate the information it receives from the striatum and integrate it into its own output to the EP and SNr. While naïve neurons are capable of resetting their firing frequency to near 50 Hz during high frequency stimulation, it remains to be seen whether neurons with reduced levels of excitability, as is seen in the DA depleted state, are capable of sustained high frequency firing. The silencing of neurons appears to be independent of any alterations in Na^+ channels, suggesting that Na^+ channel availability is still high, but not capable of overcoming the loss of HCN channels without injected depolarizing current. As such, silent neurons should still be capable of sustained high frequency firing during DBS.

Implications

Silencing of the GP in PD could be a trigger for global aberrant activity

Because of its interconnections with multiple nuclei within the basal ganglia, alterations in GP firing patterns can impact the properties of multiple neuron groups. In physiological conditions, tonic GABAergic transmission from GP neurons back to the striatum and to the STN regulates the amount of information that is received. This, combined with high levels of spontaneous activity, the GP can properly function as a filter that ensures only coordinated inputs provide a sufficient enough stimulus to pause GP firing and transmit information through. Following DA depletion, this high level of discharge is severely reduced, which shifts the balance from autonomous activity towards increased synaptic input. Following silencing of the GP either through direct lesion or DA depletion, firing in the STN shifts to a bursting firing pattern that in turn is transmitted to the GP and induces burst firing in the GP (Ryan and Clark, 1992; Ryan et al., 1992). This establishes an oscillatory network that leads to motor symptoms in PD. A similar network is established between GP and cholinergic interneurons (Raz et al., 2001). GABAergic transmission has shown to be critical in generation of rhythm and network synchronization. It is tempting to speculate that intranuclear collaterals of GP neurons help to maintain a low level of synchrony within the nucleus. Since

DA–depleted GP neurons transmit less GABAergic information through collaterals to neighboring neurons that are receiving the same input from the STN, there is an increase in correlated activity within the GP. Again, through their broad connections within the basal ganglia circuit, their perisomatic GABAergic input can have far reaching consequence in entraining global synchrony and aberrant firing within the network. This is supported by modeling work showing that recurrent collateral GABAergic connections are important to the emergence of rhythmic bursting (Terman et al., 2002).

References

Abdulla FA, Smith PA (2001a) Axotomy- and autotomy-induced changes in the excitability of rat dorsal root ganglion neurons. J Neurophysiol 85:630-643.

Abdulla FA, Smith PA (2001b) Axotomy- and autotomy-induced changes in Ca2+ and K+ channel currents of rat dorsal root ganglion neurons. J Neurophysiol 85:644-658.

Afshari FS, Ptak K, Khaliq ZM, Grieco TM, Slater NT, McCrimmon DR, Raman IM (2004) Resurgent Na currents in four classes of neurons of the cerebellum. J Neurophysiol 92:2831-2843.

Agrawal N, Hamam BN, Magistretti J, Alonso A, Ragsdale DS (2001) Persistent sodium channel activity mediates subthreshold membrane potential oscillations and low-threshold spikes in rat entorhinal cortex layer V neurons. Neuroscience 102:53-64.

Akemann W, Knopfel T (2006) Interaction of Kv3 potassium channels and resurgent sodium current influences the rate of spontaneous firing of Purkinje neurons. J Neurosci 26:4602-4612.

Albin RL, Young AB, Penney JB (1989) The functional anatomy of basal ganglia disorders. Trends Neurosci 12:366-375.

Alexander GE, Crutcher MD (1990) Functional architecture of basal ganglia circuits: neural substrates of parallel processing. Trends Neurosci 13:266-271.

Amini B, Clark JW, Jr., Canavier CC (1999) Calcium dynamics underlying pacemaker-like and burst firing oscillations in midbrain dopaminergic neurons: a computational study. J Neurophysiol 82:2249-2261.

Aosaki T, Graybiel AM, Kimura M (1994) Effect of the nigrostriatal dopamine system on acquired neural responses in the striatum of behaving monkeys. Science 265:412-415.

Bar-Gad I, Elias S, Vaadia E, Bergman H (2004) Complex locking rather than complete cessation of neuronal activity in the globus pallidus of a 1-methyl-4-phenyl-1,2,3,6-tetrahydropyridine-treated primate in response to pallidal microstimulation. J Neurosci 24:9410-9419.

Baranauskas G, Tkatch T, Surmeier DJ (1999) Delayed rectifier currents in rat globus pallidus neurons are attributable to Kv2.1 and Kv3.1/3.2 K(+) channels. J Neurosci 19:6394-6404.

Baranauskas G, Tkatch T, Nagata K, Yeh JZ, Surmeier DJ (2003) Kv3.4 subunits enhance the repolarizing efficiency of Kv3.1 channels in fast-spiking neurons. Nat Neurosci 6:258-266.

Baufreton J, Atherton JF, Surmeier DJ, Bevan MD (2005) Enhancement of excitatory synaptic integration by GABAergic inhibition in the subthalamic nucleus. J Neurosci 25:8505-8517.

Benabid AL, Benazzous A, Pollak P (2002) Mechanisms of deep brain stimulation. Mov Disord 17 Suppl 3:S73-74.

Benabid AL, Benazzouz A, Hoffmann D, Limousin P, Krack P, Pollak P (1998) Long-term electrical inhibition of deep brain targets in movement disorders. Mov Disord 13 Suppl 3:119-125.

Benazzouz A, Gross C, Feger J, Boraud T, Bioulac B (1993) Reversal of rigidity and improvement in motor performance by subthalamic high-frequency stimulation in MPTP-treated monkeys. Eur J Neurosci 5:382-389.

Bender RA, Brewster A, Santoro B, Ludwig A, Hofmann F, Biel M, Baram TZ (2001) Differential and age-dependent expression of hyperpolarization-activated, cyclic nucleotide-gated cation channel isoforms 1-4 suggests evolving roles in the developing rat hippocampus. Neuroscience 106:689-698.

Bender RA, Soleymani SV, Brewster AL, Nguyen ST, Beck H, Mathern GW, Baram TZ (2003) Enhanced expression of a specific hyperpolarization-activated cyclic nucleotide-gated cation channel (HCN) in surviving dentate gyrus granule cells of human and experimental epileptic hippocampus. J Neurosci 23:6826-6836.

Bennett BD, Wilson CJ (1998) Synaptic regulation of action potential timing in neostriatal cholinergic interneurons. J Neurosci 18:8539-8549.

Bennett BD, Wilson CJ (1999) Spontaneous activity of neostriatal cholinergic interneurons in vitro. J Neurosci 19:5586-5596.

Bennett BD, Callaway JC, Wilson CJ (2000) Intrinsic membrane properties underlying spontaneous tonic firing in neostriatal cholinergic interneurons. J Neurosci 20:8493-8503.

Bergman H, Deuschl G (2002) Pathophysiology of Parkinson's disease: from clinical neurology to basic neuroscience and back. Mov Disord 17 Suppl 3:S28-40.

Bergman H, Wichmann T, DeLong MR (1990) Reversal of experimental parkinsonism by lesions of the subthalamic nucleus. Science 249:1436-1438.

Bergman H, Feingold A, Nini A, Raz A, Slovin H, Abeles M, Vaadia E (1998) Physiological aspects of information processing in the basal ganglia of normal and parkinsonian primates. Trends Neurosci 21:32-38.

Bergson C, Mrzljak L, Smiley JF, Pappy M, Levenson R, Goldman-Rakic PS (1995) Regional, cellular, and subcellular variations in the distribution of D1 and D5 dopamine receptors in primate brain. J Neurosci 15:7821-7836.

Bergstrom DA, Walters JR (1981) Neuronal responses of the globus pallidus to systemic administration of d-amphetamine: investigation of the involvement of dopamine, norepinephrine, and serotonin. J Neurosci 1:292-299.

Bertorelli R, Zambelli M, Di Chiara G, Consolo S (1992) Dopamine depletion preferentially impairs D1- over D2-receptor regulation of striatal in vivo acetylcholine release. J Neurochem 59:353-357.

Beurrier C, Bioulac B, Hammond C (2000) Slowly inactivating sodium current (I(NaP)) underlies single-spike activity in rat subthalamic neurons. J Neurophysiol 83:1951-1957.

Beurrier C, Bioulac B, Audin J, Hammond C (2001) High-frequency stimulation produces a transient blockade of voltage-gated currents in subthalamic neurons. J Neurophysiol 85:1351-1356.

Bevan MD, Wilson CJ (1999) Mechanisms underlying spontaneous oscillation and rhythmic firing in rat subthalamic neurons. J Neurosci 19:7617-7628.

Bevan MD, Booth PA, Eaton SA, Bolam JP (1998) Selective innervation of neostriatal interneurons by a subclass of neuron in the globus pallidus of the rat. J Neurosci 18:9438-9452.

Bevan MD, Magill PJ, Hallworth NE, Bolam JP, Wilson CJ (2002a) Regulation of the timing and pattern of action potential generation in rat subthalamic neurons in vitro by GABA-A IPSPs. J Neurophysiol 87:1348-1362.

Bevan MD, Magill PJ, Terman D, Bolam JP, Wilson CJ (2002b) Move to the rhythm: oscillations in the subthalamic nucleus-external globus pallidus network. Trends Neurosci 25:525-531.

Bianchi L, Galeffi F, Bolam JP, Della Corte L (2003) The effect of 6-hydroxydopamine lesions on the release of amino acids in the direct and indirect pathways of the basal ganglia: a dual microdialysis probe analysis. Eur J Neurosci 18:856-868.

Boiko T, Van Wart A, Caldwell JH, Levinson SR, Trimmer JS, Matthews G (2003) Functional specialization of the axon initial segment by isoform-specific sodium channel targeting. J Neurosci 23:2306-2313.

Boiko T, Rasband MN, Levinson SR, Caldwell JH, Mandel G, Trimmer JS, Matthews G (2001) Compact myelin dictates the differential targeting of two sodium channel isoforms in the same axon. Neuron 30:91-104.

Bolam JP, Hanley JJ, Booth PA, Bevan MD (2000) Synaptic organisation of the basal ganglia. J Anat 196 (Pt 4):527-542.

Boraud T, Bezard E, Bioulac B, Gross C (1996) High frequency stimulation of the internal Globus Pallidus (GPi) simultaneously improves parkinsonian symptoms and reduces the firing frequency of GPi neurons in the MPTP-treated monkey. Neurosci Lett 215:17-20.

Boraud T, Bezard E, Guehl D, Bioulac B, Gross C (1998) Effects of L-DOPA on neuronal activity of the globus pallidus externalis (GPe) and globus pallidus internalis (GPi) in the MPTP-treated monkey. Brain Res 787:157-160.

Bracci E, Centonze D, Bernardi G, Calabresi P (2002) Dopamine excites fast-spiking interneurons in the striatum. J Neurophysiol 87:2190-2194.

Bradford HF (1986) Chemical neurobiology : an introduction to neurochemistry. New York: W.H. Freeman.

Brauer AU, Savaskan NE, Kole MH, Plaschke M, Monteggia LM, Nestler EJ, Simburger E, Deisz RA, Ninnemann O, Nitsch R (2001) Molecular and functional analysis of hyperpolarization-activated pacemaker channels in the hippocampus after entorhinal cortex lesion. Faseb J 15:2689-2701.

Brewster A, Bender RA, Chen Y, Dube C, Eghbal-Ahmadi M, Baram TZ (2002) Developmental febrile seizures modulate hippocampal gene expression of hyperpolarization-activated channels in an isoform- and cell-specific manner. J Neurosci 22:4591-4599.

Brewster AL, Chen Y, Bender RA, Yeh A, Shigemoto R, Baram TZ (2006) Quantitative Analysis and Subcellular Distribution of mRNA and Protein Expression of the Hyperpolarization-Activated Cyclic Nucleotide-Gated Channels throughout Development in Rat Hippocampus. Cereb Cortex.

Budde T, Caputi L, Kanyshkova T, Staak R, Abrahamczik C, Munsch T, Pape HC (2005) Impaired regulation of thalamic pacemaker channels through an imbalance of subunit expression in absence epilepsy. J Neurosci 25:9871-9882.

Burgess DL, Kohrman DC, Galt J, Plummer NW, Jones JM, Spear B, Meisler MH (1995) Mutation of a new sodium channel gene, Scn8a, in the mouse mutant 'motor endplate disease'. Nat Genet 10:461-465.

Caldwell JH, Schaller KL, Lasher RS, Peles E, Levinson SR (2000) Sodium channel Na(v)1.6 is localized at nodes of ranvier, dendrites, and synapses. Proc Natl Acad Sci U S A 97:5616-5620.

Cantrell AR, Catterall WA (2001) Neuromodulation of Na+ channels: an unexpected form of cellular plasticity. Nat Rev Neurosci 2:397-407.

Carlson JH, Bergstrom DA, Walters JR (1987) Stimulation of both D1 and D2 dopamine receptors appears necessary for full expression of postsynaptic effects of dopamine agonists: a neurophysiological study. Brain Res 400:205-218.

Carr DB, Day M, Cantrell AR, Held J, Scheuer T, Catterall WA, Surmeier DJ (2003) Transmitter modulation of slow, activity-dependent alterations in sodium channel availability endows neurons with a novel form of cellular plasticity. Neuron 39:793-806.

Chan CS, Surmeier DJ, Yung WH (2005) Striatal information signaling and integration in globus pallidus: timing matters. Neurosignals 14:281-289.

Chan CS, Shigemoto R, Mercer JN, Surmeier DJ (2004) HCN2 and HCN1 channels govern the regularity of autonomous pacemaking and synaptic resetting in globus pallidus neurons. J Neurosci 24:9921-9932.

Chen J, Piper DR, Sanguinetti MC (2002) Voltage sensing and activation gating of HCN pacemaker channels. Trends Cardiovasc Med 12:42-45.

Chen S, Wang J, Siegelbaum SA (2001) Properties of hyperpolarization-activated pacemaker current defined by coassembly of HCN1 and HCN2 subunits and basal modulation by cyclic nucleotide. J Gen Physiol 117:491-504.

Chen X, Sirois JE, Lei Q, Talley EM, Lynch C, 3rd, Bayliss DA (2005) HCN subunit-specific and cAMP-modulated effects of anesthetics on neuronal pacemaker currents. J Neurosci 25:5803-5814.

Chen Y, Yu FH, Surmeier DJ, Scheuer T, Catterall WA (2006) Neuromodulation of Na+ channel slow inactivation via cAMP-dependent protein kinase and protein kinase C. Neuron 49:409-420.

Clark BA, Monsivais P, Branco T, London M, Hausser M (2005) The site of action potential initiation in cerebellar Purkinje neurons. Nat Neurosci 8:137-139.

Colbert CM, Johnston D (1996) Axonal action-potential initiation and Na+ channel densities in the soma and axon initial segment of subicular pyramidal neurons. J Neurosci 16:6676-6686.

Colbert CM, Pan E (2002) Ion channel properties underlying axonal action potential initiation in pyramidal neurons. Nat Neurosci 5:533-538.

Colbert CM, Magee JC, Hoffman DA, Johnston D (1997) Slow recovery from inactivation of Na+ channels underlies the activity-dependent attenuation of dendritic action potentials in hippocampal CA1 pyramidal neurons. J Neurosci 17:6512-6521.

Cooper AJ, Stanford IM (2000) Electrophysiological and morphological characteristics of three subtypes of rat globus pallidus neurone in vitro. J Physiol 527 Pt 2:291-304.

Costall B, Naylor RJ, Olley JE (1972) Catalepsy and circling behaviour after intracerebral injections of neuroleptic, cholinergic and anticholinergic agents into the caudate-putamen, globus pallidus and substantia nigra of rat brain. Neuropharmacology 11:645-663.

Cummins TR, Dib-Hajj SD, Herzog RI, Waxman SG (2005) Nav1.6 channels generate resurgent sodium currents in spinal sensory neurons. FEBS Lett 579:2166-2170.

D'Angelo E, Nieus T, Maffei A, Armano S, Rossi P, Taglietti V, Fontana A, Naldi G (2001) Theta-frequency bursting and resonance in cerebellar granule cells: experimental evidence and modeling of a slow k+-dependent mechanism. J Neurosci 21:759-770.

Dalle C, Eisenach JC (2005) Peripheral block of the hyperpolarization-activated cation current (Ih) reduces mechanical allodynia in animal models of postoperative and neuropathic pain. Reg Anesth Pain Med 30:243-248.

Datla KP, Curzon G (1996) Effect of p-chlorophenylalanine at moderate dosage on 5-HT and 5-HIAA concentrations in brain regions of control and p-chloroamphetamine treated rats. Neuropharmacology 35:315-320.

Dawson TM, Dawson VL (2003) Molecular pathways of neurodegeneration in Parkinson's disease. Science 302:819-822.

Day M, Carr DB, Ulrich S, Ilijic E, Tkatch T, Surmeier DJ (2005) Dendritic excitability of mouse frontal cortex pyramidal neurons is shaped by the interaction among HCN, Kir2, and Kleak channels. J Neurosci 25:8776-8787.

DeBoer P, Abercrombie ED, Heeringa M, Westerink BH (1993) Differential effect of systemic administration of bromocriptine and L-dopa on the release of acetylcholine from striatum of intact and 6-OHDA-treated rats. Brain Res 608:198-203.

DeLong MR (1971) Activity of pallidal neurons during movement. J Neurophysiol 34:414-427.

Di Chiara G, Morelli M, Consolo S (1994) Modulatory functions of neurotransmitters in the striatum: ACh/dopamine/NMDA interactions. Trends Neurosci 17:228-233.

Difiglia M, Pasik P, Pasik T (1982) A Golgi and ultrastructural study of the monkey globus pallidus. J Comp Neurol 212:53-75.

Ding J, Guzman JN, Tkatch T, Chen S, Goldberg JA, Ebert PJ, Levitt P, Wilson CJ, Hamm HE, Surmeier DJ (2006) RGS4-dependent attenuation of M4 autoreceptor function in striatal cholinergic interneurons following dopamine depletion. Nat Neurosci 9:832-842.

Do MT, Bean BP (2003) Subthreshold sodium currents and pacemaking of subthalamic neurons: modulation by slow inactivation. Neuron 39:109-120.

Do MT, Bean BP (2004) Sodium currents in subthalamic nucleus neurons from Nav1.6-null mice. J Neurophysiol.

El-Deredy W, Branston NM, Samuel M, Schrag A, Rothwell JC, Thomas DG, Quinn NP (2000) Firing patterns of pallidal cells in parkinsonian patients correlate with their pre-pallidotomy clinical scores. Neuroreport 11:3413-3418.

Ellerkmann RK, Riazanski V, Elger CE, Urban BW, Beck H (2001) Slow recovery from inactivation regulates the availability of voltage-dependent Na(+) channels in hippocampal granule cells, hilar neurons and basket cells. J Physiol 532:385-397.

Enomoto A, Han JM, Hsiao CF, Wu N, Chandler SH (2006) Participation of sodium currents in burst generation and control of membrane excitability in mesencephalic trigeminal neurons. J Neurosci 26:3412-3422.

Fan Y, Fricker D, Brager DH, Chen X, Lu HC, Chitwood RA, Johnston D (2005) Activity-dependent decrease of excitability in rat hippocampal neurons through increases in I(h). Nat Neurosci 8:1542-1551.

Ferre S, O'Connor WT, Svenningsson P, Bjorklund L, Lindberg J, Tinner B, Stromberg I, Goldstein M, Ogren SO, Ungerstedt U, Fredholm BB, Fuxe K (1996) Dopamine D1 receptor-mediated facilitation of GABAergic neurotransmission in the rat strioentopenduncular pathway and its modulation by adenosine A1 receptor-mediated mechanisms. Eur J Neurosci 8:1545-1553.

Filion M (1979) Effects of interruption of the nigrostriatal pathway and of dopaminergic agents on the spontaneous activity of globus pallidus neurons in the awake monkey. Brain Res 178:425-441.

Filion M, Tremblay L (1991) Abnormal spontaneous activity of globus pallidus neurons in monkeys with MPTP-induced parkinsonism. Brain Res 547:142-151.

Fohlmeister JF, Miller RF (1997) Mechanisms by which cell geometry controls repetitive impulse firing in retinal ganglion cells. J Neurophysiol 78:1948-1964.

Franz O, Liss B, Neu A, Roeper J (2000) Single-cell mRNA expression of HCN1 correlates with a fast gating phenotype of hyperpolarization-activated cyclic nucleotide-gated ion channels (Ih) in central neurons. Eur J Neurosci 12:2685-2693.

Galvan A, Floran B, Erlij D, Aceves J (2001) Intrapallidal dopamine restores motor deficits induced by 6-hydroxydopamine in the rat. J Neural Transm 108:153-166.

Gaykema RP, Zaborszky L (1996) Direct catecholaminergic-cholinergic interactions in the basal forebrain. II. Substantia nigra-ventral tegmental area projections to cholinergic neurons. J Comp Neurol 374:555-577.

Gerfen CR, Engber TM, Mahan LC, Susel Z, Chase TN, Monsma FJ, Jr., Sibley DR (1990) D1 and D2 dopamine receptor-regulated gene expression of striatonigral and striatopallidal neurons. Science 250:1429-1432.

Gill SS, Heywood P (1997) Bilateral dorsolateral subthalamotomy for advanced Parkinson's disease. Lancet 350:1224.

Goldberg JA, Wilson CJ (2005) Control of spontaneous firing patterns by the selective coupling of calcium currents to calcium-activated potassium currents in striatal cholinergic interneurons. J Neurosci 25:10230-10238.

Goldberg JA, Kats SS, Jaeger D (2003) Globus pallidus discharge is coincident with striatal activity during global slow wave activity in the rat. J Neurosci 23:10058-10063.

Goldin AL (1999) Diversity of mammalian voltage-gated sodium channels. Ann N Y Acad Sci 868:38-50.

Goldin AL (2001) Resurgence of sodium channel research. Annu Rev Physiol 63:871-894.

Gong S, Zheng C, Doughty ML, Losos K, Didkovsky N, Schambra UB, Nowak NJ, Joyner A, Leblanc G, Hatten ME, Heintz N (2003) A gene expression atlas of the central nervous system based on bacterial artificial chromosomes. Nature 425:917-925.

Grace AA, Bunney BS (1983a) Intracellular and extracellular electrophysiology of nigral dopaminergic neurons--1. Identification and characterization. Neuroscience 10:301-315.

Grace AA, Bunney BS (1983b) Intracellular and extracellular electrophysiology of nigral dopaminergic neurons--2. Action potential generating mechanisms and morphological correlates. Neuroscience 10:317-331.

Graybiel AM, Hirsch EC, Agid Y (1990) The nigrostriatal system in Parkinson's disease. Adv Neurol 53:17-29.

Graybiel AM, Aosaki T, Flaherty AW, Kimura M (1994) The basal ganglia and adaptive motor control. Science 265:1826-1831.

Grieco TM, Malhotra JD, Chen C, Isom LL, Raman IM (2005) Open-channel block by the cytoplasmic tail of sodium channel beta4 as a mechanism for resurgent sodium current. Neuron 45:233-244.

Grillner P, Mercuri NB (2002) Intrinsic membrane properties and synaptic inputs regulating the firing activity of the dopamine neurons. Behav Brain Res 130:149-169.

Hallworth NE, Wilson CJ, Bevan MD (2003) Apamin-sensitive small conductance calcium-activated potassium channels, through their selective coupling to voltage-gated calcium channels, are critical determinants of the precision, pace, and pattern of action potential generation in rat subthalamic nucleus neurons in vitro. J Neurosci 23:7525-7542.

Hanson JE, Smith Y, Jaeger D (2004) Sodium channels and dendritic spike initiation at excitatory synapses in globus pallidus neurons. J Neurosci 24:329-340.

Harris NC, Webb C, Greenfield SA (1989) A possible pacemaker mechanism in pars compacta neurons of the guinea-pig substantia nigra revealed by various ion channel blocking agents. Neuroscience 31:355-362.

Hashimoto T, Elder CM, Okun MS, Patrick SK, Vitek JL (2003) Stimulation of the subthalamic nucleus changes the firing pattern of pallidal neurons. J Neurosci 23:1916-1923.

Hassani OK, Mouroux M, Feger J (1996) Increased subthalamic neuronal activity after nigral dopaminergic lesion independent of disinhibition via the globus pallidus. Neuroscience 72:105-115.

Hauber W, Lutz S (1999) Dopamine D1 or D2 receptor blockade in the globus pallidus produces akinesia in the rat. Behav Brain Res 106:143-150.

Hausser M, Clark BA (1997) Tonic synaptic inhibition modulates neuronal output pattern and spatiotemporal synaptic integration. Neuron 19:665-678.

Heimer G, Rivlin-Etzion M, Bar-Gad I, Goldberg JA, Haber SN, Bergman H (2006) Dopamine replacement therapy does not restore the full spectrum of normal pallidal activity in the 1-methyl-4-phenyl-1,2,3,6-tetra-hydropyridine primate model of Parkinsonism. J Neurosci 26:8101-8114.

Hernandez-Lopez S, Tkatch T, Perez-Garci E, Galarraga E, Bargas J, Hamm H, Surmeier DJ (2000) D2 dopamine receptors in striatal medium spiny neurons reduce L-type Ca2+ currents and excitability via a novel PLC[beta]1-IP3-calcineurin-signaling cascade. J Neurosci 20:8987-8995.

Hille B (2001) Ion channels of excitable membranes, 3rd Edition. Sunderland, Mass.: Sinauer.

Hines ML, Carnevale NT (1997) The NEURON simulation environment. Neural Comput 9:1179-1209.

Hines ML, Carnevale NT (2001) NEURON: a tool for neuroscientists. Neuroscientist 7:123-135.

Hodgkin AL, Huxley AF (1952) A quantitative description of membrane current and its application to conduction and excitation in nerve. J Physiol 117:500-544.

Hoover BR, Marshall JF (1999) Population characteristics of preproenkephalin mRNA-containing neurons in the globus pallidus of the rat. Neurosci Lett 265:199-202.

Hoover BR, Marshall JF (2002) Further characterization of preproenkephalin mRNA-containing cells in the rodent globus pallidus. Neuroscience 111:111-125.

Hornykiewicz O (1966) Dopamine (3-hydroxytyramine) and brain function. Pharmacol Rev 18:925-964.

Hornykiewicz O (1976) Neurohumoral interactions and basal ganglia function and dysfunction. Res Publ Assoc Res Nerv Ment Dis 55:269-280.

Hornykiewicz O (1982) Imbalance of brain monoamines and clinical disorders. Prog Brain Res 55:419-429.

Hutchison WD, Lozano AM, Tasker RR, Lang AE, Dostrovsky JO (1997) Identification and characterization of neurons with tremor-frequency activity in human globus pallidus. Exp Brain Res 113:557-563.

Ingram SL, Williams JT (1996) Modulation of the hyperpolarization-activated current (Ih) by cyclic nucleotides in guinea-pig primary afferent neurons. J Physiol 492 (Pt 1):97-106.

Isom LL, Scheuer T, Brownstein AB, Ragsdale DS, Murphy BJ, Catterall WA (1995a) Functional co-expression of the beta 1 and type IIA alpha subunits of sodium channels in a mammalian cell line. J Biol Chem 270:3306-3312.

Isom LL, Ragsdale DS, De Jongh KS, Westenbroek RE, Reber BF, Scheuer T, Catterall WA (1995b) Structure and function of the beta 2 subunit of brain sodium channels, a transmembrane glycoprotein with a CAM motif. Cell 83:433-442.

Isom LL, De Jongh KS, Patton DE, Reber BF, Offord J, Charbonneau H, Walsh K, Goldin AL, Catterall WA (1992) Primary structure and functional expression of the beta 1 subunit of the rat brain sodium channel. Science 256:839-842.

Iwahori N, Mizuno N (1981) A Golgi study on the globus pallidus of the mouse. J Comp Neurol 197:29-43.

Jech R, Urgosik D, Tintera J, Nebuzelsky A, Krasensky J, Liscak R, Roth J, Ruzicka E (2001) Functional magnetic resonance imaging during deep brain stimulation: a pilot study in four patients with Parkinson's disease. Mov Disord 16:1126-1132.

Jiang M, Spicher K, Boulay G, Wang Y, Birnbaumer L (2001) Most central nervous system D2 dopamine receptors are coupled to their effectors by Go. Proc Natl Acad Sci U S A 98:3577-3582.

Jonas P (1989) Temperature dependence of gating current in myelinated nerve fibers. J Membr Biol 112:277-289.

Jung HY, Mickus T, Spruston N (1997) Prolonged sodium channel inactivation contributes to dendritic action potential attenuation in hippocampal pyramidal neurons. J Neurosci 17:6639-6646.

Khaliq ZM, Gouwens NW, Raman IM (2003) The contribution of resurgent sodium current to high-frequency firing in Purkinje neurons: an experimental and modeling study. J Neurosci 23:4899-4912.

Kita H (1994) Parvalbumin-immunopositive neurons in rat globus pallidus: a light and electron microscopic study. Brain Res 657:31-41.

Kita H, Kitai ST (1991) Intracellular study of rat globus pallidus neurons: membrane properties and responses to neostriatal, subthalamic and nigral stimulation. Brain Res 564:296-305.

Kita H, Kitai ST (1994) The morphology of globus pallidus projection neurons in the rat: an intracellular staining study. Brain Res 636:308-319.

Kita H, Kita T (2001) Number, origins, and chemical types of rat pallidostriatal projection neurons. J Comp Neurol 437:438-448.

Kita H, Tokuno H, Nambu A (1999) Monkey globus pallidus external segment neurons projecting to the neostriatum. Neuroreport 10:1467-1472.

Kitai ST, Kita H (1987) Anatomy and physiology of the subthalamic nucleus: a driving force of the basal ganglia. In: The basal ganglia II : structure and function : current concepts (Carpenter MB, Jayaraman A, eds), pp 357-373. New York: Plenum Press.

Koch WJ, Hawes BE, Inglese J, Luttrell LM, Lefkowitz RJ (1994) Cellular expression of the carboxyl terminus of a G protein-coupled receptor kinase attenuates G beta gamma-mediated signaling. J Biol Chem 269:6193-6197.

Koe BK, Weissman A (1966) p-Chlorophenylalanine: a specific depletor of brain serotonin. J Pharmacol Exp Ther 154:499-516.

Kohrman DC, Smith MR, Goldin AL, Harris J, Meisler MH (1996) A missense mutation in the sodium channel Scn8a is responsible for cerebellar ataxia in the mouse mutant jolting. J Neurosci 16:5993-5999.

Kohrman DC, Plummer NW, Schuster T, Jones JM, Jang W, Burgess DL, Galt J, Spear BT, Meisler MH (1995) Insertional mutation of the motor endplate disease (med) locus on mouse chromosome 15. Genomics 26:171-177.

Krzemien DM, Schaller KL, Levinson SR, Caldwell JH (2000) Immunolocalization of sodium channel isoform NaCh6 in the nervous system. J Comp Neurol 420:70-83.

Kuo CC, Bean BP (1994) Na+ channels must deactivate to recover from inactivation. Neuron 12:819-829.

Lapper SR, Bolam JP (1992) Input from the frontal cortex and the parafascicular nucleus to cholinergic interneurons in the dorsal striatum of the rat. Neuroscience 51:533-545.

Lazarewicz MT, Migliore M, Ascoli GA (2002) A new bursting model of CA3 pyramidal cell physiology suggests multiple locations for spike initiation. Biosystems 67:129-137.

Lee KH, Chang SY, Roberts DW, Kim U (2004) Neurotransmitter release from high-frequency stimulation of the subthalamic nucleus. J Neurosurg 101:511-517.

Lehmann J, Langer SZ (1983) The striatal cholinergic interneuron: synaptic target of dopaminergic terminals? Neuroscience 10:1105-1120.

Levey AI, Hersch SM, Rye DB, Sunahara RK, Niznik HB, Kitt CA, Price DL, Maggio R, Brann MR, Ciliax BJ, et al. (1993) Localization of D1 and D2 dopamine receptors in brain with subtype-specific antibodies. Proc Natl Acad Sci U S A 90:8861-8865.

Liang CL, Sinton CM, Sonsalla PK, German DC (1996) Midbrain dopaminergic neurons in the mouse that contain calbindin-D28k exhibit reduced vulnerability to MPTP-induced neurodegeneration. Neurodegeneration 5:313-318.

Limousin P, Pollak P, Benazzouz A, Hoffmann D, Broussolle E, Perret JE, Benabid AL (1995) Bilateral subthalamic nucleus stimulation for severe Parkinson's disease. Mov Disord 10:672-674.

Llinas R, Sugimori M (1980) Electrophysiological properties of in vitro Purkinje cell somata in mammalian cerebellar slices. J Physiol 305:171-195.

Lloyd K, Hornykiewicz O (1970) Parkinson's disease: activity of L-dopa decarboxylase in discrete brain regions. Science 170:1212-1213.

Lozano A, Hutchison W, Kiss Z, Tasker R, Davis K, Dostrovsky J (1996) Methods for microelectrode-guided posteroventral pallidotomy. J Neurosurg 84:194-202.

Lozano AM, Dostrovsky J, Chen R, Ashby P (2002) Deep brain stimulation for Parkinson's disease: disrupting the disruption. Lancet Neurol 1:225-231.

Ludwig A, Budde T, Stieber J, Moosmang S, Wahl C, Holthoff K, Langebartels A, Wotjak C, Munsch T, Zong X, Feil S, Feil R, Lancel M, Chien KR, Konnerth A, Pape HC, Biel M, Hofmann F (2003) Absence epilepsy and sinus dysrhythmia in mice lacking the pacemaker channel HCN2. Embo J 22:216-224.

Lujan R, Albasanz JL, Shigemoto R, Juiz JM (2005) Preferential localization of the hyperpolarization-activated cyclic nucleotide-gated cation channel subunit HCN1 in basket cell terminals of the rat cerebellum. Eur J Neurosci 21:2073-2082.

Lydiard RB, Fossom LH, Sparber SB (1975) Postnatal elevation of brain tyrosine hydroxylase activity, without concurrent increases in steady-state catecholamine levels, resulting from dl-alpha-methylparatyrosine administration during embryonic development. J Pharmacol Exp Ther 194:27-36.

MacLean JN, Zhang Y, Goeritz ML, Casey R, Oliva R, Guckenheimer J, Harris-Warrick RM (2005) Activity-independent coregulation of IA and Ih in rhythmically active neurons. J Neurophysiol 94:3601-3617.

Magarinos-Ascone C, Pazo JH, Macadar O, Buno W (2002) High-frequency stimulation of the subthalamic nucleus silences subthalamic neurons: a possible cellular mechanism in Parkinson's disease. Neuroscience 115:1109-1117.

Magill PJ, Bolam JP, Bevan MD (2000) Relationship of activity in the subthalamic nucleus-globus pallidus network to cortical electroencephalogram. J Neurosci 20:820-833.

Magistretti J, Alonso A (1999) Biophysical properties and slow voltage-dependent inactivation of a sustained sodium current in entorhinal cortex layer-II principal neurons: a whole-cell and single-channel study. J Gen Physiol 114:491-509.

Magistretti J, Castelli L, Forti L, D'Angelo E (2006) Kinetic and functional analysis of transient, persistent and resurgent sodium currents in rat cerebellar granule cells in situ: an electrophysiological and modelling study. J Physiol 573:83-106.

Magnin M, Morel A, Jeanmonod D (2000) Single-unit analysis of the pallidum, thalamus and subthalamic nucleus in parkinsonian patients. Neuroscience 96:549-564.

Mallet N, Ballion B, Le Moine C, Gonon F (2006) Cortical inputs and GABA interneurons imbalance projection neurons in the striatum of parkinsonian rats. J Neurosci 26:3875-3884.

Marshall JF, Henry BL, Billings LM, Hoover BR (2001) The role of the globus pallidus D2 subfamily of dopamine receptors in pallidal immediate early gene expression. Neuroscience 105:365-378.

Martina M, Jonas P (1997) Functional differences in Na+ channel gating between fast-spiking interneurones and principal neurones of rat hippocampus. J Physiol 505 (Pt 3):593-603.

Matsumoto N, Minamimoto T, Graybiel AM, Kimura M (2001) Neurons in the thalamic CM-Pf complex supply striatal neurons with information about behaviorally significant sensory events. J Neurophysiol 85:960-976.

Maurice N, Tkatch T, Meisler M, Sprunger LK, Surmeier DJ (2001) D1/D5 dopamine receptor activation differentially modulates rapidly inactivating and persistent sodium currents in prefrontal cortex pyramidal neurons. J Neurosci 21:2268-2277.

Maurice N, Mercer J, Chan CS, Hernandez-Lopez S, Held J, Tkatch T, Surmeier DJ (2004) D2 dopamine receptor-mediated modulation of voltage-dependent Na+ channels reduces autonomous activity in striatal cholinergic interneurons. J Neurosci 24:10289-10301.

Mayer ML, James MH, Russell RJ, Kelly JS, Pasternak CA (1986) Changes in excitability induced by herpes simplex viruses in rat dorsal root ganglion neurons. J Neurosci 6:391-402.

McIntyre CC, Savasta M, Kerkerian-Le Goff L, Vitek JL (2004a) Uncovering the mechanism(s) of action of deep brain stimulation: activation, inhibition, or both. Clin Neurophysiol 115:1239-1248.

McIntyre CC, Grill WM, Sherman DL, Thakor NV (2004b) Cellular effects of deep brain stimulation: model-based analysis of activation and inhibition. J Neurophysiol 91:1457-1469.

Mengod G, Villaro MT, Landwehrmeyer GB, Martinez-Mir MI, Niznik HB, Sunahara RK, Seeman P, O'Dowd BF, Probst A, Palacios JM (1992) Visualization of dopamine D1, D2 and D3 receptor mRNAs in human and rat brain. Neurochem Int 20 Suppl:33S-43S.

Mercuri NB, Bonci A, Calabresi P, Stratta F, Stefani A, Bernardi G (1994) Effects of dihydropyridine calcium antagonists on rat midbrain dopaminergic neurones. Br J Pharmacol 113:831-838.

Mickus T, Jung H, Spruston N (1999) Properties of slow, cumulative sodium channel inactivation in rat hippocampal CA1 pyramidal neurons. Biophys J 76:846-860.

Migliore M, Cook EP, Jaffe DB, Turner DA, Johnston D (1995) Computer simulations of morphologically reconstructed CA3 hippocampal neurons. J Neurophysiol 73:1157-1168.

Miller WC, DeLong M (1987) Altered tonic activity of neurons in the globus pallidus and subthalamic nucleus in the pramte MPTP model of parkinsonism. In: The basal ganglia II : structure and function : current concepts (Carpenter MB, Jayaraman A, eds), pp 415-427. New York: Plenum Press.

Miller WC, DeLong MR (1988) Parkinsonian symptomatology. An anatomical and physiological analysis. Ann N Y Acad Sci 515:287-302.

Nambu A, Llinas R (1994) Electrophysiology of globus pallidus neurons in vitro. J Neurophysiol 72:1127-1139.

Nambu A, Llinas R (1997) Morphology of globus pallidus neurons: its correlation with electrophysiology in guinea pig brain slices. J Comp Neurol 377:85-94.

Narahashi T, Deguchi T, Urakawa N, Ohkubo Y (1960) Stabilization and rectification of muscle fiber membrane by tetrodotoxin. Am J Physiol 198:934-938.

Nedergaard S, Flatman JA, Engberg I (1993) Nifedipine- and omega-conotoxin-sensitive Ca2+ conductances in guinea-pig substantia nigra pars compacta neurones. J Physiol 466:727-747.

Neuhoff H, Neu A, Liss B, Roeper J (2002) I(h) channels contribute to the different functional properties of identified dopaminergic subpopulations in the midbrain. J Neurosci 22:1290-1302.

Nini A, Feingold A, Slovin H, Bergman H (1995) Neurons in the globus pallidus do not show correlated activity in the normal monkey, but phase-locked oscillations appear in the MPTP model of parkinsonism. J Neurophysiol 74:1800-1805.

Nisenbaum ES, Wilson CJ (1995) Potassium currents responsible for inward and outward rectification in rat neostriatal spiny projection neurons. J Neurosci 15:4449-4463.

Nisenbaum LK, Crowley WR, Kitai ST (1996) Partial striatal dopamine depletion differentially affects striatal substance P and enkephalin messenger RNA expression. Brain Res Mol Brain Res 37:209-216.

Obeso JA, Olanow CW, Nutt JG (2000) Levodopa motor complications in Parkinson's disease. Trends Neurosci 23:S2-7.

Oertel WH, Mugnaini E (1984) Immunocytochemical studies of GABAergic neurons in rat basal ganglia and their relations to other neuronal systems. Neurosci Lett 47:233-238.

Olson PA, Tkatch T, Hernandez-Lopez S, Ulrich S, Ilijic E, Mugnaini E, Zhang H, Bezprozvanny I, Surmeier DJ (2005) G-protein-coupled receptor modulation of striatal CaV1.3 L-type Ca2+ channels is dependent on a Shank-binding domain. J Neurosci 25:1050-1062.

Palmer LM, Stuart GJ (2006) Site of action potential initiation in layer 5 pyramidal neurons. J Neurosci 26:1854-1863.

Pan HS, Walters JR (1988) Unilateral lesion of the nigrostriatal pathway decreases the firing rate and alters the firing pattern of globus pallidus neurons in the rat. Synapse 2:650-656.

Parent A, Sato F, Wu Y, Gauthier J, Levesque M, Parent M (2000) Organization of the basal ganglia: the importance of axonal collateralization. Trends Neurosci 23:S20-27.

Pennartz CM, Bierlaagh MA, Geurtsen AM (1997) Cellular mechanisms underlying spontaneous firing in rat suprachiasmatic nucleus: involvement of a slowly inactivating component of sodium current. J Neurophysiol 78:1811-1825.

Ping HX, Shepard PD (1996) Apamin-sensitive Ca(2+)-activated K+ channels regulate pacemaker activity in nigral dopamine neurons. Neuroreport 7:809-814.

Platzer J, Engel J, Schrott-Fischer A, Stephan K, Bova S, Chen H, Zheng H, Striessnig J (2000) Congenital deafness and sinoatrial node dysfunction in mice lacking class D L-type Ca2+ channels. Cell 102:89-97.

Plenz D, Kitai ST (1999) A basal ganglia pacemaker formed by the subthalamic nucleus and external globus pallidus. Nature 400:677-682.

Raman IM, Bean BP (1997) Resurgent sodium current and action potential formation in dissociated cerebellar Purkinje neurons. J Neurosci 17:4517-4526.

Raman IM, Bean BP (1999) Ionic currents underlying spontaneous action potentials in isolated cerebellar Purkinje neurons. J Neurosci 19:1663-1674.

Raman IM, Bean BP (2001) Inactivation and recovery of sodium currents in cerebellar Purkinje neurons: evidence for two mechanisms. Biophys J 80:729-737.

Raman IM, Gustafson AE, Padgett D (2000) Ionic currents and spontaneous firing in neurons isolated from the cerebellar nuclei. J Neurosci 20:9004-9016.

Raman IM, Sprunger LK, Meisler MH, Bean BP (1997) Altered subthreshold sodium currents and disrupted firing patterns in Purkinje neurons of Scn8a mutant mice. Neuron 19:881-891.

Raz A, Vaadia E, Bergman H (2000) Firing patterns and correlations of spontaneous discharge of pallidal neurons in the normal and the tremulous 1-methyl-4-phenyl-1,2,3,6-tetrahydropyridine vervet model of parkinsonism. J Neurosci 20:8559-8571.

Raz A, Feingold A, Zelanskaya V, Vaadia E, Bergman H (1996) Neuronal synchronization of tonically active neurons in the striatum of normal and parkinsonian primates. J Neurophysiol 76:2083-2088.

Raz A, Frechter-Mazar V, Feingold A, Abeles M, Vaadia E, Bergman H (2001) Activity of pallidal and striatal tonically active neurons is correlated in mptp-treated monkeys but not in normal monkeys. J Neurosci 21:RC128.

Reynolds JN, Hyland BI, Wickens JR (2004) Modulation of an afterhyperpolarization by the substantia nigra induces pauses in the tonic firing of striatal cholinergic interneurons. J Neurosci 24:9870-9877.

Robinson RB, Siegelbaum SA (2003) Hyperpolarization-activated cation currents: from molecules to physiological function. Annu Rev Physiol 65:453-480.

Rodriguez BM, Sigg D, Bezanilla F (1998) Voltage gating of Shaker K+ channels. The effect of temperature on ionic and gating currents. J Gen Physiol 112:223-242.

Rudy B, McBain CJ (2001) Kv3 channels: voltage-gated K+ channels designed for high-frequency repetitive firing. Trends Neurosci 24:517-526.

Ruskin DN, Marshall JF (1997) Differing influences of dopamine agonists and antagonists on Fos expression in identified populations of globus pallidus neurons. Neuroscience 81:79-92.

Ryan LJ, Clark KB (1992) Alteration of neuronal responses in the subthalamic nucleus following globus pallidus and neostriatal lesions in rats. Brain Res Bull 29:319-327.

Ryan LJ, Sanders DJ, Clark KB (1992) Auto- and cross-correlation analysis of subthalamic nucleus neuronal activity in neostriatal- and globus pallidal-lesioned rats. Brain Res 583:253-261.

Santoro B, Baram TZ (2003) The multiple personalities of h-channels. Trends Neurosci 26:550-554.

Santoro B, Chen S, Luthi A, Pavlidis P, Shumyatsky GP, Tibbs GR, Siegelbaum SA (2000) Molecular and functional heterogeneity of hyperpolarization-activated pacemaker channels in the mouse CNS. J Neurosci 20:5264-5275.

Schultz W (2002) Getting formal with dopamine and reward. Neuron 36:241-263.

Shah MM, Anderson AE, Leung V, Lin X, Johnston D (2004) Seizure-induced plasticity of h channels in entorhinal cortical layer III pyramidal neurons. Neuron 44:495-508.

Shen W, Hamilton SE, Nathanson NM, Surmeier DJ (2005) Cholinergic suppression of KCNQ channel currents enhances excitability of striatal medium spiny neurons. J Neurosci 25:7449-7458.

Smith MR, Smith RD, Plummer NW, Meisler MH, Goldin AL (1998) Functional analysis of the mouse Scn8a sodium channel. J Neurosci 18:6093-6102.

Smith RD, Goldin AL (1998) Functional analysis of the rat I sodium channel in xenopus oocytes. J Neurosci 18:811-820.

Smith Y, Lavoie B, Dumas J, Parent A (1989) Evidence for a distinct nigropallidal dopaminergic projection in the squirrel monkey. Brain Res 482:381-386.

Smith Y, Bennett BD, Bolam JP, Parent A, Sadikot AF (1994) Synaptic relationships between dopaminergic afferents and cortical or thalamic input in the sensorimotor territory of the striatum in monkey. J Comp Neurol 344:1-19.

Soares J, Kliem MA, Betarbet R, Greenamyre JT, Yamamoto B, Wichmann T (2004) Role of external pallidal segment in primate parkinsonism: comparison of the effects of 1-methyl-4-phenyl-1,2,3,6-tetrahydropyridine-induced parkinsonism and lesions of the external pallidal segment. J Neurosci 24:6417-6426.

Song WJ, Tkatch T, Baranauskas G, Ichinohe N, Kitai ST, Surmeier DJ (1998) Somatodendritic depolarization-activated potassium currents in rat neostriatal cholinergic interneurons are predominantly of the A type and attributable to coexpression of Kv4.2 and Kv4.1 subunits. J Neurosci 18:3124-3137.

Steigrad P, Tobler I, Waser PG, Borbely AA (1978) Effect of p-chlorophenylalanine on cerebral serotonin binding, serotonin concentration and motor activity in the rat. Naunyn Schmiedebergs Arch Pharmacol 305:143-148.

Steinman JL, Carlton SM, Haber B, Willis WD (1987) Differential effects of p-chlorophenylalanine on indoleamines in brainstem nuclei and spinal cord of rats. I. Biochemical and behavioral analysis. Brain Res 426:297-309.

Stoof JC, Drukarch B, de Boer P, Westerink BH, Groenewegen HJ (1992) Regulation of the activity of striatal cholinergic neurons by dopamine. Neuroscience 47:755-770.

Strauss U, Kole MH, Brauer AU, Pahnke J, Bajorat R, Rolfs A, Nitsch R, Deisz RA (2004) An impaired neocortical Ih is associated with enhanced excitability and absence epilepsy. Eur J Neurosci 19:3048-3058.

Stuart G, Hausser M (1994) Initiation and spread of sodium action potentials in cerebellar Purkinje cells. Neuron 13:703-712.

Stuart G, Schiller J, Sakmann B (1997) Action potential initiation and propagation in rat neocortical pyramidal neurons. J Physiol 505 (Pt 3):617-632.

Surmeier DJ, Song WJ, Yan Z (1996) Coordinated expression of dopamine receptors in neostriatal medium spiny neurons. J Neurosci 16:6579-6591.

Surmeier DJ, Mercer JN, Chan CS (2005) Autonomous pacemakers in the basal ganglia: who needs excitatory synapses anyway? Curr Opin Neurobiol 15:312-318.

Taddese A, Bean BP (2002) Subthreshold sodium current from rapidly inactivating sodium channels drives spontaneous firing of tuberomammillary neurons. Neuron 33:587-600.

Taha JM, Favre J, Baumann TK, Burchiel KJ (1996) Characteristics and somatotopic organization of kinesthetic cells in the globus pallidus of patients with Parkinson's disease. J Neurosurg 85:1005-1012.

Tai CH, Boraud T, Bezard E, Bioulac B, Gross C, Benazzouz A (2003) Electrophysiological and metabolic evidence that high-frequency stimulation of the subthalamic nucleus bridles neuronal activity in the subthalamic nucleus and the substantia nigra reticulata. Faseb J 17:1820-1830.

Takada M, Kang Y, Imanishi M (2001) Immunohistochemical localization of voltage-gated calcium channels in substantia nigra dopamine neurons. Eur J Neurosci 13:757-762.

Talley EM, Solorzano G, Lei Q, Kim D, Bayliss DA (2001) Cns distribution of members of the two-pore-domain (KCNK) potassium channel family. J Neurosci 21:7491-7505.

Tammaro P, Conti F, Moran O (2002) Modulation of sodium current in mammalian cells by an epilepsy-correlated beta 1-subunit mutation. Biochem Biophys Res Commun 291:1095-1101.

Terman D, Rubin JE, Yew AC, Wilson CJ (2002) Activity patterns in a model for the subthalamopallidal network of the basal ganglia. J Neurosci 22:2963-2976.

Tkatch T, Baranauskas G, Surmeier DJ (1998) Basal forebrain neurons adjacent to the globus pallidus co-express GABAergic and cholinergic marker mRNAs. Neuroreport 9:1935-1939.

Tkatch T, Baranauskas G, Surmeier DJ (2000) Kv4.2 mRNA abundance and A-type K(+) current amplitude are linearly related in basal ganglia and basal forebrain neurons. J Neurosci 20:579-588.

Tohyama I, Kameyama M, Kimura H (1988) Quantitative morphometric analysis of two types of serotonin-immunoreactive nerve fibres differentially responding to p-chlorophenylalanine treatment in the rat brain. Neuroscience 26:971-991.

Townsend C, Horn R (1997) Effect of alkali metal cations on slow inactivation of cardiac Na+ channels. J Gen Physiol 110:23-33.

Tseng KY, Kasanetz F, Kargieman L, Riquelme LA, Murer MG (2001) Cortical slow oscillatory activity is reflected in the membrane potential and spike trains of striatal neurons in rats with chronic nigrostriatal lesions. J Neurosci 21:6430-6439.

Tzoumaka E, Tischler AC, Sangameswaran L, Eglen RM, Hunter JC, Novakovic SD (2000) Differential distribution of the tetrodotoxin-sensitive rPN4/NaCh6/Scn8a sodium channel in the nervous system. J Neurosci Res 60:37-44.

Van Wart A, Matthews G (2006) Impaired firing and cell-specific compensation in neurons lacking nav1.6 sodium channels. J Neurosci 26:7172-7180.

van Welie I, van Hooft JA, Wadman WJ (2004) Homeostatic scaling of neuronal excitability by synaptic modulation of somatic hyperpolarization-activated Ih channels. Proc Natl Acad Sci U S A 101:5123-5128.

Vasilyev DV, Barish ME (2002) Postnatal development of the hyperpolarization-activated excitatory current Ih in mouse hippocampal pyramidal neurons. J Neurosci 22:8992-9004.

Vitek JL, Hashimoto T, Peoples J, DeLong MR, Bakay RA (2004) Acute stimulation in the external segment of the globus pallidus improves parkinsonian motor signs. Mov Disord 19:907-915.

Voorn P, van de Witte S, Tjon G, Jonker AJ (1999) Expression of enkephalin in pallido-striatal neurons. Ann N Y Acad Sci 877:671-675.

Wainger BJ, DeGennaro M, Santoro B, Siegelbaum SA, Tibbs GR (2001) Molecular mechanism of cAMP modulation of HCN pacemaker channels. Nature 411:805-810.

Walters JR, Bergstrom DA, Carlson JH, Chase TN, Braun AR (1987) D1 dopamine receptor activation required for postsynaptic expression of D2 agonist effects. Science 236:719-722.

Wang J, Chen S, Siegelbaum SA (2001) Regulation of hyperpolarization-activated HCN channel gating and cAMP modulation due to interactions of COOH terminus and core transmembrane regions. J Gen Physiol 118:237-250.

Wang J, Chen S, Nolan MF, Siegelbaum SA (2002) Activity-dependent regulation of HCN pacemaker channels by cyclic AMP: signaling through dynamic allosteric coupling. Neuron 36:451-461.

Watanabe K, Kimura M (1998) Dopamine receptor-mediated mechanisms involved in the expression of learned activity of primate striatal neurons. J Neurophysiol 79:2568-2580.

Wichmann T, DeLong MR (1999) Oscillations in the basal ganglia. Nature 400:621-622.

Wichmann T, DeLong MR (2003) Functional neuroanatomy of the basal ganglia in Parkinson's disease. Adv Neurol 91:9-18.

Wichmann T, Soares J (2006) Neuronal firing before and after burst discharges in the monkey Basal Ganglia is predictably patterned in the normal state and altered in parkinsonism. J Neurophysiol 95:2120-2133.

Wigmore MA, Lacey MG (2000) A Kv3-like persistent, outwardly rectifying, Cs+-permeable, K+ current in rat subthalamic nucleus neurones. J Physiol 527 Pt 3:493-506.

Wilson CJ (2005) The mechanism of intrinsic amplification of hyperpolarizations and spontaneous bursting in striatal cholinergic interneurons. Neuron 45:575-585.

Wilson CJ, Callaway JC (2000) Coupled oscillator model of the dopaminergic neuron of the substantia nigra. J Neurophysiol 83:3084-3100.

Wilson CJ, Chang HT, Kitai ST (1990) Firing patterns and synaptic potentials of identified giant aspiny interneurons in the rat neostriatum. J Neurosci 10:508-519.

Windels F, Carcenac C, Poupard A, Savasta M (2005) Pallidal origin of GABA release within the substantia nigra pars reticulata during high-frequency stimulation of the subthalamic nucleus. J Neurosci 25:5079-5086.

Windels F, Bruet N, Poupard A, Feuerstein C, Bertrand A, Savasta M (2003) Influence of the frequency parameter on extracellular glutamate and gamma-aminobutyric acid in substantia nigra and globus pallidus during electrical stimulation of subthalamic nucleus in rats. J Neurosci Res 72:259-267.

Windels F, Bruet N, Poupard A, Urbain N, Chouvet G, Feuerstein C, Savasta M (2000) Effects of high frequency stimulation of subthalamic nucleus on extracellular glutamate and GABA in substantia nigra and globus pallidus in the normal rat. Eur J Neurosci 12:4141-4146.

Wittmack EK, Rush AM, Craner MJ, Goldfarb M, Waxman SG, Dib-Hajj SD (2004) Fibroblast growth factor homologous factor 2B: association with Nav1.6 and selective colocalization at nodes of Ranvier of dorsal root axons. J Neurosci 24:6765-6775.

Wolfart J, Roeper J (2002) Selective coupling of T-type calcium channels to SK potassium channels prevents intrinsic bursting in dopaminergic midbrain neurons. J Neurosci 22:3404-3413.

Wolfart J, Neuhoff H, Franz O, Roeper J (2001) Differential expression of the small-conductance, calcium-activated potassium channel SK3 is critical for pacemaker control in dopaminergic midbrain neurons. J Neurosci 21:3443-3456.

Wooten GF (1990) Parkinsonism. In: The Neurobiology of disease (Pearlman AL, Collins RC, eds), pp 454-468. New York: Oxford University Press.

Wu YR, Levy R, Ashby P, Tasker RR, Dostrovsky JO (2001) Does stimulation of the GPi control dyskinesia by activating inhibitory axons? Mov Disord 16:208-216.

Xu W, Lipscombe D (2001) Neuronal Ca(V)1.3alpha(1) L-type channels activate at relatively hyperpolarized membrane potentials and are incompletely inhibited by dihydropyridines. J Neurosci 21:5944-5951.

Yan Z, Surmeier DJ (1997) D5 dopamine receptors enhance Zn2+-sensitive GABA(A) currents in striatal cholinergic interneurons through a PKA/PP1 cascade. Neuron 19:1115-1126.

Yan Z, Song WJ, Surmeier J (1997) D2 dopamine receptors reduce N-type Ca2+ currents in rat neostriatal cholinergic interneurons through a membrane-delimited, protein-kinase-C-insensitive pathway. J Neurophysiol 77:1003-1015.

Yelnik J, Francois C, Percheron G, Tande D (1996) A spatial and quantitative study of the striatopallidal connection in the monkey. Neuroreport 7:985-988.

Yu FH, Westenbroek RE, Silos-Santiago I, McCormick KA, Lawson D, Ge P, Ferriera H, Lilly J, DiStefano PS, Catterall WA, Scheuer T, Curtis R (2003) Sodium channel beta4, a new disulfide-linked auxiliary subunit with similarity to beta2. J Neurosci 23:7577-7585.

Yung WH, Hausser MA, Jack JJ (1991) Electrophysiology of dopaminergic and non-dopaminergic neurones of the guinea-pig substantia nigra pars compacta in vitro. J Physiol 436:643-667.

Jeff N Mercer

INFORMATION

date of birth August 2, 1977
place of birth Portland, OR
503.523.9439 *cell : pager* 312.249.1180

ADDRESS

733 W. Bittersweet Pl., apt. 2W
Chicago, IL 60613
mercer@md.northwestern.edu *e-mail*

EDUCATION

Northwestern University, Chicago, IL	M.D./ Ph.D. (Neurosciences)	Expected 2008
Rice University, Houston, TX	B.A. (Biology)	1995-1999

SCIENTIFIC EXPERIENCE

2001-2006 Graduate Student with Dr. D. James Surmeier, Department of Physiology, Northwestern University. *Thesis: Regulation of autonomous pacemaking and high frequency firing in the basal ganglia*.

1998-1999 Senior Honors Student with Dr. Richard Gomer, Department of Biochemistry and Cell Biology, Rice University. *Senior Honors Project: Differential Protein Expression in Dictyostelium Development*.

1997-1998 Summer Student with Dr. Jan Christian, Department of Cell Biology and Development, Oregon Health Sciences University. *The Role of Smad Proteins in the BMP Signal Transduction Pathway.*

AWARDS AND HONORS

Graduated *magna cum laude*, Rice University, 1999.
2nd Place Poster, Senior Research Poster Session, Rice University, 1999.
American Heart Association Fellowship, Oregon Health Sciences University, 1998.

SOCIETIES AND MEMBERSHIPS

American Medical Student Association
American College of Surgeons
Society for Neuroscience

PUBLICATIONS

Mercer JN*, Chan CS*, Surmeier DJ (2006) Intrinsic Silencing of Globus Pallidus Neurons in a Parkinson's Disease Model Mediated by Diminished HCN Channel Activity. *In preparation.* *contributed equally to the project

Mercer JN, Chan CS, Tkatch T, Surmeier DJ (2006) Resurgent Nav1.6 sodium channel gating is critical to pacemaking and fast spiking in globus pallidus neurons. *In preparation.*

Chan CS, Guzman-Lucero JN, Ilijic E, Mercer JN, Rick C, Tkatch T, Surmeier DJ (2006) Rejuvenation of substantia nigra dopaminergic neurons confers protection from the mitochondrial toxin rotenone. *In preparation.*

Surmeier DJ, Mercer JN, Chan CS (2005) Autonomous Pacemakers In The Basal Ganglia: Who Needs Excitatory Synapses Anyway? *Curr Op Of Neurobiol.* 15:1-7.

Maurice N, Mercer J, Chan CS, Hernandez-Lopez S, Held J, Tkatch T, Surmeier DJ (2004) D_2 Dependent Receptor-Mediated Modulation Of Voltage-Dependent Na^+ Channels Reduces Autonomous Activity In Striatal Cholinergic Interneurons. *J Neurosci* 24(46):10289-10301.

Chan CS, Shigemoto R, Mercer JN, Surmeier DJ (2004) HCN2 and HCN1 Channels Govern the Regularity of Autonomous Pacemaking and Synaptic Resetting in Globus Pallidus Neurons. *J Neurosci* 24(44):9921-9932.

ABSTRACTS

Mercer JN, Surmeier DJ (2004) D_2 Dopamine Receptor Activation Suppresses Transient and Persistent Sodium Currents in Striatal Medium Spiny Neurons. *Soc Neurosci Abstr* 753.26.

Mercer JN, Chan CS, Surmeier DJ (2003) Sodium channels in neurons of the globus pallidus. *Soc Neurosci Abstr* 706.12.

PRESENTATIONS

Sept. 2006	"Regulation of autonomous pacemaking and high frequency firing in neurons of the globus pallidus." Thesis defense seminar, Northwestern University.
Aug. 2005	"D_2 Dopamine Receptor Activation Suppresses Transient And Persistent Sodium Currents In Striatal Medium Spiny Neurons." MSTP Retreat Poster Session, Northwestern University.
Mar. 2005	Modeling of intrinsic pacemaking in globus pallidus neurons." Physiology Dept. Student Talks, Northwestern University.
Oct. 2004	"D_2 Dopamine Receptor Activation Suppresses Transient And Persistent Sodium Currents In Striatal Medium Spiny Neurons." Poster Session, Society for Neuroscience Annual Convention.
July 2004	"Using NEURON to understand the importance of Na^+ channel biophysics." Motor Systems Day Talk, Northwestern University.
Nov. 2003	"Sodium Channels in Neurons of the Globus Pallidus." Poster Session, Society for Neuroscience Annual Convention.
Aug. 2003	"Sodium Channels in Neurons of the external Globus Pallidus." MSTP Retreat Presentations. Northwestern University.
July 2003	"Sodium Channels in Neurons of the external Globus Pallidus." MD/PhD Student Conference Poster Session.
July 2003	"Sodium Channels in Neurons of the external Globus Pallidus." Motor Systems Day Talk, Northwestern University.
Aug. 2002	"Biophysical Properties of Sodium Channels in Neurons of the Globus Pallidus." MSTP Retreat Poster Session, Northwestern University.
May 1999	"The differential expression of Discoidin I in developing Dictyostelium." Poster Session, Rice University.
May 1999	"The method of action used by Smad7, an antagonist of the BMP-4 signal." Poster Session, Rice University.

TEACHING EXPERIENCE

Spring 03-06 Teaching Assistant, Membrane Excitability Lab. Dr Phil Hockberger, Director.
Fall 2002 Teaching Assistant, Neuro Lab. Dr. Tracy Hodgson, Director.
Fall 1999 Teaching Assistant. Introductory Biology. Dr. Michael Gustin, Director.
Spring 1998 Teaching Assistant. Introductory Biology Lab. Dr. David Caprette, Director.

NATIONAL SCIENTIFIC MEETINGS

Society for Neuroscience, Annual Convention, San Diego, CA 2004

NEURON Simulator Meeting, Chicago, IL 2004

Society for Neuroscience, Annual Convention, New Orleans, LA 2003

MD/PhD Student Conference, Snowmass, CO 2003

Society for Neuroscience, Annual Convention, Orlando, FL 2002

Society for Neuroscience, Annual Convention, San Diego, CA 2001.